



**HAL**  
open science

# Etude des instabilités dans les puits activés par gas-lift

Laure Sinegre

► **To cite this version:**

Laure Sinegre. Etude des instabilités dans les puits activés par gas-lift. Mathematics [math]. École Nationale Supérieure des Mines de Paris, 2006. English. NNT : . pastel-00001938

**HAL Id: pastel-00001938**

**<https://pastel.hal.science/pastel-00001938>**

Submitted on 6 Nov 2006

**HAL** is a multi-disciplinary open access archive for the deposit and dissemination of scientific research documents, whether they are published or not. The documents may come from teaching and research institutions in France or abroad, or from public or private research centers.

L'archive ouverte pluridisciplinaire **HAL**, est destinée au dépôt et à la diffusion de documents scientifiques de niveau recherche, publiés ou non, émanant des établissements d'enseignement et de recherche français ou étrangers, des laboratoires publics ou privés.





LAURE SINÈGRE

---

**DYNAMIC STUDY OF  
UNSTABLE PHENOMENA  
STEPPING IN GAS-LIFT  
ACTIVATED WELLS**

---

LAURE SINÈGRE

École Nationale Supérieure des Mines de Paris, Centre Automatique et  
Systèmes, 60, Bd. Saint-Michel, 75272 Paris Cedex 06, France.

*E-mail* : `sinegre@cas.ensmp.fr`

---

***Key words and phrases.*** — Process control, dynamic systems, limit cycles, switching system, gas-lifted Well, density-wave, stabilization, distributed parameters model.

**Mots clés.** — Contrôle de procédés, systèmes dynamiques, cycle limite, système à switch, puits activés en gas-lift, density-wave, stabilisation, modèles à paramètres distribués.

---

*28th September 2006*

**DYNAMIC STUDY OF UNSTABLE  
PHENOMENA STEPPING IN GAS-LIFT  
ACTIVATED WELLS**

LAURE SINÈGRE

**Abstract.** — Gas-lifted wells often present unstable behaviors that cannot be described by hydrostatic laws. In this thesis, we aim at analyzing the well dynamics, especially when its production is irregular. We end up by designing control solutions.

We begin with a brief description of the gas-lift activation technique. The negative impact of instabilities on oil production is underlined. Two main mechanisms are at birth of the unstable behaviors. On-site real time records serve as illustrative examples. We explain the first mechanism, well referenced in the literature, thanks to mass balances equations. Analyzing the vector field properties allows us to interpret the observed phenomenon as a limit cycle. Then, we expose the main contribution of this thesis. It lies in the description and analysis of the second mechanism. We show that the instability arises from out-of-phase effects induced by the propagation delay in the well. A distributed parameter model is used. Then, we gather our results and present a complete and compact model of the well dynamics. This model is a first order stable system interconnected with a distributed parameters system. Thanks to the small gain theorem, the instabilities root-causes appear as two possibly positive feedback loops. This model inspires the design of control solutions that suit the physical structure of the well. Moreover, these solutions fit with the operational constraints. Realistic simulation results illustrate the efficiency of our strategies. Some of the solutions have been tested on line on a production site. Some of the obtained results are presented.

## ***Résumé* (Étude des instabilités dans les puits activés par gas-lift)**

Les puits pétroliers activés par gas-lift sont souvent sujet à des comportements instables qui ne peuvent être décrits par les lois de l'hydrostatique. L'objectif du travail présenté dans ce mémoire est l'analyse de la dynamique de ces puits, en particulier lorsqu'ils produisent par à-coups. Elle aboutit à la conception de solutions de contrôle adaptées.

Nous commençons par décrire brièvement les principes de l'activation des puits par gas-lift et soulignons l'impact très négatif des instabilités sur les volumes de pétrole produits. Il existe deux principaux mécanismes susceptibles d'engendrer ces productions par à-coups. Nous les mettons en évidence à partir d'enregistrements temps-réel issus de sites de production. Le premier mécanisme, connu dans la littérature, est expliqué grâce à des bilans de masses. Nous montrons, grâce à une analyse des propriétés du champ de vecteurs, que ce phénomène s'interprète géométriquement comme un cycle limite. La principale contribution de ce mémoire consiste en la description et l'analyse du second mécanisme, très mal connu auparavant. Nous montrons que le retard lié aux temps de propagation des fluides dans le puits induit le déphasage à l'origine de cette instabilité. L'étude de ces deux instabilités se poursuit par la présentation d'un modèle complet et compact de la dynamique du puits. Il s'agit de l'interconnection d'un système du premier ordre stable avec un système à paramètres distribués. Il permet d'attribuer, grâce au théorème des petits gains, la cause des instabilités observées à deux boucles de rétroaction potentiellement positives. Ce modèle nous permet de développer des solutions de contrôle, inspirées de la structure physique du puits et respectant les contraintes opérationnelles. L'efficacité de ces stratégies est illustrée par des résultats de simulations réalistes. Une partie des solutions a également été testée, en ligne, sur site de production. Certains résultats obtenus, très encourageants, sont présentés.



## REMERCIEMENTS

Je remercie chaleureusement Rodolphe Sepulchre, président du jury, Jean-Pierre Richard et Bjarne Foss, rapporteurs de ma thèse.

Je tiens à remercier Pierre Lemétayer. Mine de savoir et d'expérience, il a soutenu le projet depuis le début. Sans sa conviction et sa ténacité jamais les tests sur site de production n'auraient pu avoir lieu. Je remercie également tout le personnel du site de production pour sa disponibilité. Je remercie Valérie Larrose-Martinez qui a très bien su gérer ma délicate situation administrative et m'a ainsi évité bien des tracasseries. Merci à ceux qui ont permis à cette thèse d'exister, Marc Souche et Yves Guénard.

Un grand merci à Mme Le Gallic dont l'efficacité et la gentillesse m'ont été, à maintes reprises, d'un grand secours. Je remercie François Chaplais, Pierre Rouchon, Philippe Martin et Laurent Praly pour l'intérêt qu'ils ont porté à ce travail. Enfin bon courage à mes compagnons de route, Erwan, David, Mazyar et Silvère.

Merci à ceux, et tout particulièrement Jonathan, qui ont supporté sans broncher mes moments de découragement, mes sautes d'humeur et mille et une présentations sur le gas-lift.

Je souhaite remercier mon directeur de thèse, Nicolas Petit, qui m'a suivie pendant ces cinq dernières années. Enfin suivie... poussée plutôt, guidée surtout. Merci de m'avoir fait confiance. Merci d'avoir toujours été là. Je vais regretter votre enthousiasme pour les clés à molette, les grands scientifiques, les engins volants, le théorème des petits gains et les baklavas.



# CONTENTS

<b>Remerciements</b> .....	vii
<b>Introduction</b> .....	3
<b>1. Process description and problematic</b>	
<i>Description du procédé et problématique</i> .....	13
1.1. Operations description .....	14
1.2. Operating conditions and efficiency .....	18
<b>2. A dynamical system approach to the study of instabilities</b>	
<i>Une approche dynamique de l'analyse des instabilités</i> ..	25
2.1. The casing-heading instability .....	26
2.2. The Density wave instability .....	45
2.3. Global study of unstable phenomena .....	65
<b>3. Control solutions</b>	
<i>Solutions de contrôle</i> .....	79
3.1. State of the art .....	81
3.2. Controlling the tubing dynamics using gas inlet as input ..	84

3.3. Controlling the tubing dynamics using the production choke as input .....	90
3.4. Controlling the well dynamics using production choke as input .....	98
<b>Conclusion</b> .....	105
<b>A. OLGA<sup>®</sup>2000 simulations settings</b> .....	111
<b>B. Nomenclature</b> .....	113
<b>List of figures</b> .....	117
<b>Bibliography</b> .....	123

## INTRODUCTION

**Contexte.** — *Le pétrole est une ressource stratégique. Énergie essentielle dans de nombreux secteurs tels que les transports et l'industrie, il représente un enjeu à la fois économique et géopolitique. La crise actuelle du marché de l'énergie, la troisième du genre, apparaît propice aux développements technologiques. La croissance de la demande en Chine et en Inde, conjuguée à la montée des nationalismes pétroliers (tels qu'au Venezuela et en Bolivie, par exemple) entraîne une tension accrue sur le marché du pétrole. Le prix du baril a doublé pour atteindre plus de soixante dollars en moins de deux ans. Cette flambée est alimentée par le spectre du manque de réserves et par les tensions géopolitiques. Ce contexte est très favorable aux développements technologiques. D'un côté il est nécessaire de produire plus et mieux. De l'autre le prix du baril augmentant, les budgets alloués aux projets à long terme sont conséquents car les investissements sont plus facilement rentabilisés.*

**Ordres de grandeurs.** — *Si les variations du prix de l'or noir et les conséquences économiques qu'elles induisent paraissent familières, son extraction et le fonctionnement des installations restent mystérieux sous bien des aspects. Les formes sous lesquelles le pétrole se présente varient beaucoup d'un champ à l'autre, la profondeur à laquelle il faut forer ou la quantité de barils produits aussi. Il est donc assez difficile de définir des ordres de grandeurs généraux. On peut néanmoins dire qu'un puits*

typique a une profondeur d'un à deux kilomètres et un diamètre de l'ordre d'une dizaine de centimètres, que les pressions et les températures en jeu au niveau du réservoir sont de l'ordre d'une ou deux centaines de bars pour l'un et d'une centaine de degrés pour l'autre et qu'un réservoir est supposé contenir quelques milliards de barils de pétrole. Un puits peut produire jusqu'à plusieurs centaines de barils par jour et un champ consiste généralement en plusieurs centaines de puits. Pour se faire une idée correcte des enjeux il faut également savoir qu'une grande partie des réserves estimées de pétrole se trouve en mer à plusieurs kilomètres de profondeur et dans des régions parfois hostiles ou difficiles d'accès, comme en mer du Nord ou en Alaska par exemple. Il faut également insister sur les disparités. En effet le champ d'Elgin Franklin en mer du Nord est caractérisé par un réservoir à plus de 1000 bar et 200 °C et est donc très loin des ordres de grandeurs moyens.

**Activation de la production.** — Au début de la production d'un puits la pression du réservoir suffit fréquemment à propulser les hydrocarbures jusqu'à la surface. C'est une phase de production dite "naturelle" qui, suivant les caractéristiques du réservoir, peut durer de quelques à de nombreuses années. Malheureusement en expulsant les effluents vers la surface, le réservoir tend à se dépressuriser jusqu'à n'être plus capable de contrebalancer le poids de la colonne de liquide dans le puits. Il faut alors recourir à des moyens de production alternatifs, appelés moyens d'activation. Leur but peut être de maintenir le réservoir sous pression ou de tenter de diminuer le poids de la colonne liquide.

**Gas-lift.** — Parmi les moyens les plus fréquemment utilisés on trouve l'activation par pompe. Il peut s'agir de ce que l'on appelle des "têtes de cheval" à cause de leur forme particulière. On trouve également l'activation par gas-lift. Le gaz est injecté au fond du puits, il peut alors être utilisé pour pousser le liquide ou pour s'y mêler de façon à diminuer la masse volumique moyenne. Au total, cette activation par gas-lift concerne plus de 53% des puits produisant significativement, c'est-à-dire plus de dix barils par jour (chiffres issus de [41, p6]). Dans ce mémoire, nous nous intéressons exclusivement à ce mode de production.

**Évolution du puits.** — *La plupart du temps, il est possible d'estimer l'évolution de la production d'un champ de pétrole. Dans un premier temps, la productivité augmente jusqu'à atteindre son maximum. S'en suit une longue période de baisse. On représente cette évolution sous la forme d'une courbe appelée "courbe de déclin". Il est également important de noter que moins des deux tiers des réserves estimées ont été produites quand un champ est abandonné. Augmenter ce taux, c'est-à-dire augmenter la productivité des champs dit "matures" est un enjeu très important.*

**Combattre le déclin de la production.** — *Il existe différents moyens pour essayer de freiner ce déclin. La plupart concentrent leurs efforts sur le réservoir et font en sorte de pallier la dégradation progressive des conditions de production. On peut par exemple réinjecter de l'eau pour maintenir le réservoir sous pression ou traiter chimiquement la zone de roche située à proximité du puits pour favoriser une meilleure circulation des effluents. Nous nous intéressons ici aux moyens de continuer à produire malgré la dégradation des conditions de production. Recourir à l'activation par gas-lift implique une complexification du mode opératoire qui dans des conditions défavorables (pression faible au niveau du réservoir, aspiration du puits faible, peu de gaz disponible) conduit à une production dégradée. Le développement actuel de l'utilisation de capteurs et de vannes contrôlables sur les puits ouvre un vaste champ d'opportunités dans le domaine de l'optimisation de la production. On peut aujourd'hui trouver des capteurs distribués de température, des débitmètres polyphasiques et des jauges qui, placés en fond de puits, permettent l'accès à des mesures (en temps réel ou avec retard) telles que la pression et la température. Les puits équipés de telles technologies sont appelés "smart wells" (pour plus de détails voir [45]). L'accès direct aux mesures et la compatibilité des actionneurs avec les contraintes temps-réel permettent de développer des solutions de contrôle et d'améliorer la conduite des puits sans modifier le mode opératoire. Le but de cette thèse est d'exposer l'analyse et le développement de lois de commande qui garantissent de produire plus, en terme de quantité et mieux, en terme de régularité du débit.*

**Organisation du manuscrit.** — Dans le Chapitre 1 nous détaillons le procédé de production d'huile dans le cas de l'activation par gas-lift. Les puits ainsi activés se composent de deux parties : un tuyau central, le tubing, dans lequel s'écoule ce qui provient du réservoir et autour un volume annulaire, le casing. Le casing contient le gaz pressurisé prêt à rentrer dans le tubing. Notre but est de mettre en évidence le nombre très important de contraintes et d'objectifs souvent antagonistes qui président au choix des conditions opératoires. Nous nous restreignons dans un premier temps à l'étude d'un puits isolé et aux contraintes qui interviennent dans l'optimisation de son mode de production. Cette étude s'appuie en particulier sur une relation statique (courbe de réponse) obtenue, entre autres, grâce à la loi de Bernoulli. Ensuite nous changeons d'échelle et nous montrons que de nombreuses contraintes apparaissent lorsque l'on considère un ensemble de puits interconnectés. Ainsi, la production serait globalement améliorée si les puits ne se perturbaient pas mutuellement. La nature des interconnexions est détaillée en prenant en compte les réseaux de gaz et de production et le réservoir. Cependant, la difficulté du problème d'optimisation n'est pas la seule cause de manques à produire car les puits sont généralement prisonniers d'instabilités (au sens des systèmes dynamiques). Nous détaillons enfin les préjudices causés par ces phénomènes, tels que les diminutions notables de la production moyenne et les dommages sur les équipements.

Dans le Chapitre 2, nous présentons notre principale contribution. Elle consiste en la modélisation et l'analyse de stabilité de ces phénomènes d'instabilités. Nous commençons par présenter deux modes de production instables observés depuis de nombreuses années sur différents sites de production. Il s'agit du "casing-heading" et de la "density-wave", aussi appelée parfois "tubing-heading". La même démarche est appliquée pour chacun de ces deux phénomènes. Après avoir rappelé les résultats de la littérature, nous donnons une description phénoménologique illustrée par des données issues de site de production ou de simulations réalistes. Des modèles adaptés à la réalisation de lois de commande et à l'analyse des propriétés mathématiques sont proposés. Dans le cas du casing-heading

nous utilisons une réduction d'un modèle emprunté à [3], ce qui nous permet d'interpréter les oscillations observées comme le cycle limite d'un système dynamique à deux dimensions. L'impact sur la stabilité de différents paramètres physiques est étudié. La density-wave est un phénomène dont l'existence ne fut démontrée qu'en 2003, dans [23] et qui est souvent mal interprété car confondu avec d'autres causes d'oscillations dans le tubing. Pour lever toute ambiguïté, nous donnons une définition simple, illustrée par des données issues de site de production. La caractéristique de cette instabilité est qu'elle peut être étudiée en ne considérant que la partie tubing du puits. En considérant seulement la propagation dans le tubing, on déduit l'existence d'un invariant de Riemann et finalement nous modélisons ce phénomène sous forme d'un modèle à paramètres distribués. Nous étudions ensuite sa stabilité sous la forme d'une équation à retards distribués. Après avoir effectué cette analyse mathématique, nous mettons en évidence les correspondances existant entre les formules obtenues et les règles opératoires en vigueur sur les sites. Nous évaluons ensuite la possibilité de simplifier encore le modèle présenté. Nous prouvons qu'en envisageant quelques hypothèses apparemment raisonnables le modèle perd sa pertinence physique et ne peut plus représenter la density-wave. Enfin, forts de la connaissance acquise sur chacun des deux phénomènes nous proposons un modèle global. Comme le puits est représenté par l'interconnexion de ses deux parties : le tubing et le casing, le modèle proposé est le bouclage d'un système à paramètres distribués et d'un système du premier ordre stable. Les deux régimes instables s'interprètent alors comme deux boucles de rétroaction positives qui interviennent pour l'une au niveau de l'interconnexion et pour l'autre au niveau du système à paramètres distribués.

Dans le Chapitre 3, nous utilisons les modèles proposés pour mettre au point des solutions de contrôle. Dans un premier temps, nous donnons un bref aperçu de l'état de l'art des techniques de contrôle des puits activés en gas-lift. Ensuite, nous nous intéressons au problème qui consiste à stabiliser le tubing. Des simulations montrent qu'une première solution boucle ouverte donne de bons résultats. Cela nous permet de valider la pertinence du modèle à paramètres distribués proposés au Chapitre 2.

*Des solutions de contrôle en meilleur accord avec les contraintes opérationnelles sont ensuite proposées. La convergence du système bouclé avec contrôleur de type PI est prouvée en utilisant la démarche qui a permis de réaliser l'étude de stabilité au Chapitre 2. Un observateur permet de reconstruire les variables qui ne sont pas directement disponibles. L'efficacité du contrôleur est illustrée par de nombreuses simulations réalistes.*

*Une grande partie de ce qui est ici proposé a été présentée lors de conférences nationales et internationales. Ainsi le Chapitre 2 reprend des éléments des publications [36], [39] et de [38] tandis que le Chapitre 3 correspond en partie à [37] et [35].*

**Context.** — Oil is a required source of energy in modern societies. In particular, transportation and numerous manufacturing industries are in great need of petroleum derived products. Therefore, it represents a key to economic and geopolitics issues. The late crisis in the gas price has spurred a great interest in technological developments. The economic growth of China and India (among others), and the rise of petroleum nationalisms (e.g. Venezuela and Bolivia) have pushed the oil price up. Over the last two years, crude oil price has increased by more than 100%. Shortages of oil are feared. In this context, technology is seen as a possibility to increase the production rates and the quality of the product. This situation also enables formerly too costly projects to be considered again. For example, it is now economically efficient to produce oil from the bituminous sands of Canada.

**Scales.** — Generally the oil production technology is quite sophisticated. Operating conditions significantly vary between fields. In particular, depth and total available quantity highly depend on the considered region. However, it is possible to sketch a typical scenario with a well depth ranging from 1 km to 2 km, a well radius of several inches, pressures and temperatures around hundred of bars and hundreds of degrees,

with a reservoir containing several billions of barrels of oil. A single well can produce up to several hundreds of barrels per day. A field is composed of several hundreds of wells. A vast part of estimated reserves are offshore, several kilometers deep under the sea level, often in hostile regions that can be difficult to reach (e.g. North Sea, or Alaska). Finally, let us note that there are exceptions with extreme values, e.g. the Elgin Franklin field in the North Sea has a 1000 bar reservoir pressure with a 200 degrees temperature.

**Production activation.** — At the early stages of the life of a well, the reservoir pressure is usually sufficient to push the oil up to the surface facilities. This so-called “natural” production phase may last several years. Unfortunately, the reservoir pressure tends to decrease over time and, eventually, a point is reached when the pressure difference between the reservoir and the surface is not sufficient to make oil naturally flow. Then, it is necessary to use *activation* methods, either to keep the reservoir pressure above a certain level, or to lighten the liquid column in the well.

**Gas-lift.** — Among these methods, the most generally considered are pumping, e.g. using “horse-heads” as can be seen in numerous terrestrial fields, and *gas-lift*. In this last method, gas is injected at the bottom of the well, it can be used to push the liquid or to mix with it in order to lower the average density of the mixture being produced. It appears that this technique is used on more than 53 % of the wells that produce more than 10 barrels per day (as mentioned in [41, p.6]). This method is the subject of our study.

**Production decline.** — Most of the time, it is possible to estimate the future evolution of the production of a well. After a short period, productivity stops rising, reaches a maximum, and start decreasing. This decrease can last for years (e.g. in the USA more than eight oil fields have been producing during more than a century). This trend is usually represented in a plot called “decline curve”. An important fact is that more than a third of estimated reserves are left when the field is

shut down. The emerging “mature fields” projects led by numerous oil companies aim at reducing the rate of left-over oil in reservoirs.

**Fighting the production decline.** — Several tentative solutions are considered. A large number of them deal with the reservoir. It is sought to artificially maintain the operating conditions at a satisfactory level. A prime example is to inject pressurized water into the reservoir, another solution is to chemically treat the surroundings of the bottom of the well (draw-down zone) to speed up liquid flow. Here, we focus on means of producing despite the operating conditions progressive decline. gas-lift activation implies serious complexification of operating modes. As will appear in details later on in this report, in difficult situations (low reservoir pressure, little gas availability), production can be negatively impacted. Recent development of sensors embedded in the well and of remotely controlled chokes has opened new perspectives of production optimization. A large variety of sensors can be considered, among which are distributed temperature sensors, polyphasic flow meters and gages which can be placed at the bottom of the well to provide pressure and temperature measurements. Such sensors and actuators equipped wells are called “smart wells” (for more details see [45]). These technologies enable real-time feedback control strategies that can yield productivity increases. The subject of this report is the mathematical analysis and control design for such wells. We propose a physics-based approach and develop control oriented low-dimensional models. Thanks to this, simple cascaded controllers are designed and shown to be compatible with the above-mentioned technology.

The report is organized as follows.

**Report organisation.** — In Chapter 1, we detail the process of oil production with gas-lift activation techniques. In these techniques the well is composed of two connected parts: the *tubing* (production pipe) and the *casing* (a buffer volume for the gas entering the tubing). Our goal here is to stress the numerous objectives and constraints defining the operating conditions. In particular, looking at a single generic well, we explain selection rules for optimal gas-lift operations. This results in a static model (response-curve) derived (among others) from Bernoulli’s

law. Then, we show that the interconnection of wells results in an important constraint and conclude that, on overall, more oil could be produced if the wells were not negatively interacting with each other. The role of gas and oil networks, and of reservoir is detailed. Yet, the most important issues that should be addressed to increase the production are *instabilities* (in the usual sense of dynamical systems). We explain how these malicious phenomena directly impact on production. The observed sluggish flows result in noticeable average productivity losses, and can cause serious facilities damages.

In Chapter 2, we present our main contribution which is the modeling and stability analysis of these instabilities. First, we focus on two specific oscillating modes long-time observed by production specialists. These are the “*casing-heading*” and the “*density-wave*” (a.k.a. “*tubing-heading*”). In the two cases, we propose an overview of state-of-the-art knowledge. Then, we write a sequential presentation of the phenomenon. These description are presented along with on-site data or simulations. Control-oriented models are proposed. In the casing-heading case, we use a reduction of the model proposed in [3], in order to study the observed oscillations as a limit cycle of a two-dimensional dynamical system. A discussion on the role of various physical parameters with respect to stability is given. In the density-wave case, we propose a new model for this phenomenon which existence was first demonstrated in [23]. It is often misinterpreted and confused with various oscillations occurring in the tubing. We illustrate our definition with field data. Then, we derive a distributed parameter model. This instability can be studied from a tubing local point of view. We analyse stability of this model under the form of a delay equation obtained by considering a Riemann invariant. After performing a mathematical analysis, we draw parallels between obtained formulas and well-established operations rules. Interestingly, we show that the presented model can not be simplified further without losing its physical relevance. We prove that an apparently reasonable simplifying assumption completely prevents the density-wave. Finally, we propose a global model that allows understanding of the two discussed instabilities. In this model, we consider the well as the interconnection of a casing

and a tubing. It consists of the feedback connection of a distributed parameters system and a stable first order system. It appears that both unstable regimes stem from positive feedback loops. These take place at the interconnection level and inside the distributed subsystem.

In Chapter 3, we propose control solutions derived from the proposed modeling. First, we recall state-of-the-art control techniques for gas-lifted wells. Then, we address the control problem of stabilizing the tubing subsystem. A first open-loop solution is shown to be efficient in simulation. It stresses the relevance of the distributed parameters model proposed in Chapter 2. More realistic control solutions are addressed next. Following along the lines of the stability analysis of Chapter 2, we prove convergence of the closed loop system with a PI controller. To reconstruct unavailable variables, we filter measurements through an observer. Realistic simulations prove the relevance of the proposed controller.

A large part of the material presented here has appeared at international conferences. Publications [36], [39] and [38] refer to Chapter 2, and publication [37] and [35] refer to Chapter 3.

# CHAPTER 1

## PROCESS DESCRIPTION AND PROBLEMATIC

### *DESCRIPTION DU PROCÉDÉ ET PROBLÉMATIQUE*

*Dans ce chapitre nous détaillons le procédé de production d'hydrocarbure. Nous nous intéressons plus particulièrement à la technique d'activation par gas-lift. Après un certain temps, les puits ne sont plus capables de produire de façon dite "naturelle". Il est nécessaire de leur fournir de l'énergie, soit seulement pour amorcer la production, soit de façon continue pendant toute la durée de l'exploitation, on a alors recours à des moyens d'activation. Dans la Section 1.1, nous décrivons les éléments du processus de production, du réservoir aux tuyaux d'export d'huile et de gaz. Ensuite nous expliquons les principes de l'activation par gas-lift. La production doit atteindre certains objectifs tout en respectant de nombreuses contraintes, c'est ainsi que sont définis les conditions d'exploitation. Il faut en particulier tenir compte des conditions opératoires optimales pour chaque puits mais également des effets induits par leur interconnexion. Ce compromis est présenté dans la Section 1.2. La complexité des opérations est amplifiée par la présence d'instabilités. Nous en donnons l'illustration à l'aide de données provenant d'un site d'exploitation.*

In this Chapter, we detail the process of oil production with the gas-lift activation techniques. In Section 1.1, we give an overview of a typical oil production process, which goes from the reservoir to the export pipes.

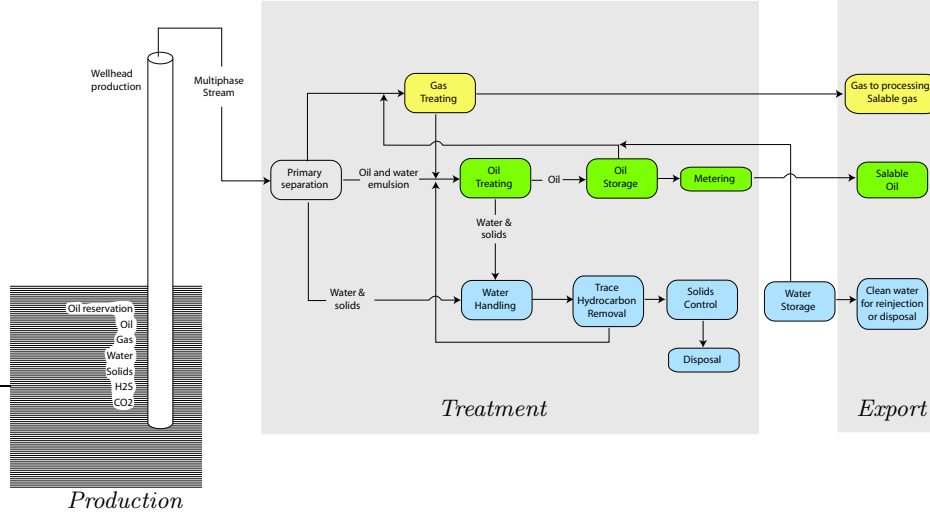


FIGURE 1.1. Typical oil production process system (schematic borrowed from [29]).

Then, we explain the principles of the gas-lift activation at the well scale. In Section 1.2, we stress the numerous objectives and constraints defining the operating conditions and we show an on-site example of an unstable production regime.

## 1.1. Operations description

We describe the different period of a well life. In particular, we focus on the stage where the well is not able to “naturally” produce anymore and where it requires some help from activations techniques. We detail some of these techniques. We also describe a typical oil production process. Then we give a precise description of the continuous gas-lift activation technique.

**1.1.1. Artificial lifting.** — Figure 1.1 shows a typical oil production process system. Effluents from the reservoir are produced by the wells. Then, they go through the treatment process which mainly consists in a phases separation. At last salable oil and gas are sent for export.

In the early stages of their lives, most wells flow naturally to the surface and are thus called flowing wells. This assumes that the pressure in the reservoir is sufficient to overcome the pressure gradient of the oil column. When this assumption fails wells die.

Two causes can lead to such situations: either the pressure in the reservoir becomes too low, or the pressure gradient in the well sharply rises over time. The pressure in the reservoir naturally decreases when the produced fluids are not replaced. This phenomenon is referred to as reservoir depletion. In the meantime, total pressure losses in the column usually tend to raise: density of the fluids increases and less gas is produced.

Artificial lifting methods are needed. They enable production from already dead wells or help to increase productivity of flowing wells. There exist two artificial lift methods: one solution is to artificially increase the pressure at the bottom of the well, another mean is to artificially decrease the pressure gradient in the well.

In the first solution, method pumps are used. Their injection point below the liquid level and, therefore, these pumps increase the well upstream pressure. Periodic injection of compressed gas below the liquid level in the well can also be considered. The expansion energy of the gas is used to push the liquid up to the surface. Another solution is the continuous gas-lift activation method. Here, the idea is to continuously inject high pressure gas at the bottom of the well. Gas mixes with the fluids from the reservoir and the overall density of the liquid flowing in the well decreases. Both methods belongs to the gas-lift activation method family. They use the same hardware, although they rely on two completely different principles. In the first case, the flow is composed of a succession of slugs of liquid pushed by bubbles of gas, whereas, in the second case, the flow should be composed of an homogeneous mix of liquid and gas. More details on this subject can be found in [41] and [11].

Gas-lift activation techniques can be used during the whole life of a well, from the time it start to die out to its actual closing. Usually, the continuous gas-lift method is used first and then, when reservoir pressure and liquid flow rates eventually drop below a critical point,

intermittent gas injection is preferred. Main advantages of gas-lift over other activation methods are as follows (see [1] for more details) :

- In contrast to most other artificial methods, gas-lifting offers a high degree of flexibility. In practice, this means that any gas-lift installation can be easily modified to accommodate possibly extremely large changes in production rates
- In fields where wells produce substantial amount of gas from the reservoir, gas-lifting is technically and economically very attractive
- Compared to other techniques, the required surface wellhead equipment is not obtrusive and is little space demanding.
- gas-lift techniques can be used during the entire productive time of the well until it is fully depleted.

Two of the main disadvantages are:

- Induced high separator pressures are very detrimental to the operation of any kind of gas-lift installations
- Gas-lifting is usually less energy efficient than the other kinds of artificial lift methods

More than 53% of the wells producing more than 10 bpd are gas-lift activated. Our work focuses on this technique, and, more precisely, on the continuous gas-lift activation. This a prime solution considered to improve wells production (in the following, intermittent techniques are omitted).

**1.1.2. Continuous gas-lift activation.** — A gas-lifted well schematic is presented in Figure 1.2. High pressure gas is injected at the wellhead (point A in Figure 1.2) and flows down in the annular space, located between the drilling part called casing (B) and the production pipe called tubing (D). Then, it enters the production pipe at the bottom of the well (point C in Figure 1.2) and mixes with the fluids produced from the reservoir. The resulting mixture flows up to the surface. Equipment usually consists of a flow control valve for the gas injection at the surface (A), a simple orifice for the gas injection at the bottom of the well and production choke at the wellhead (E). This choke is actuated<sup>(1)</sup>. On some

---

<sup>(1)</sup>This is a very general case.

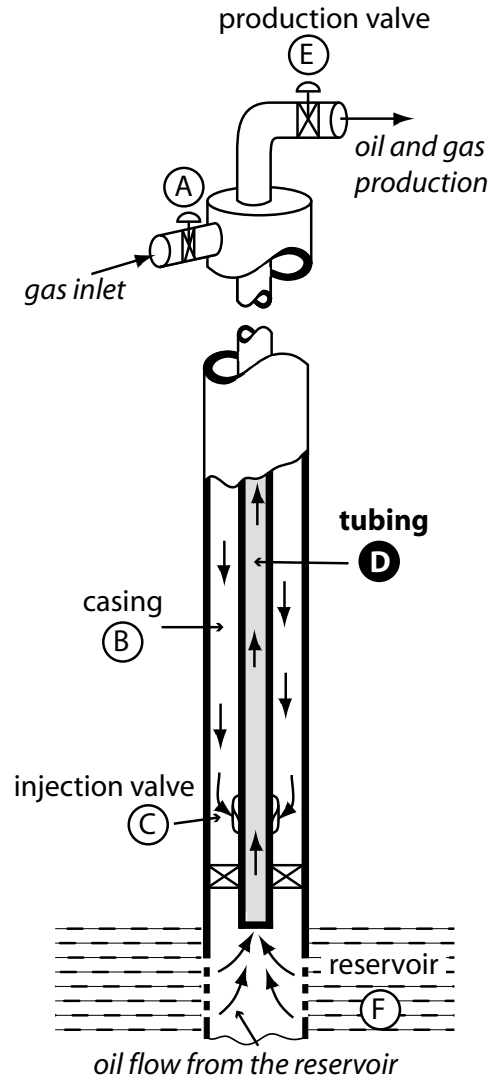


FIGURE 1.2. Scheme of a gas-lift activated well.

wells, unloading valves are installed between the casing and the tubing. They have predefined pressure operating ranges and are normally only open at the well start up. Usually, only wellhead measurements (e.g. tubing pressure and casing pressure) are available.

## 1.2. Operating conditions and efficiency

Here, we explain the selection rules that define the optimal gas-lift operating conditions for a single generic well. Then we show that numerous interconnexions between wells prevent them from being operated at their optimal conditions. Moreover field operations are all the more difficult that solving this highly coupled optimal problem is not the only issue, preventing wells from being unstable has also to be addressed.

**1.2.1. Normal operating conditions.** — At the single well scale, the main idea is to derive from Bernoulli’s law the response curve, a static equation giving the oil production with respect to the gas injection flow rate. Defining a linear cost function depending on oil price and gas cost let us compute the optimal gas-lift injection. At the multi-well scale, we give some insights of the constraints arising from the interconnexions between wells.

*1.2.1.1. At the single well scale.* — Given a particular gas-lifted well and a hardware configuration, one can set-up the production rate by acting upon two parameters (inputs),  $u$  the production choke opening and  $q_{gi}$  the gas injection rate. We now detail the impact of those two parameters on the production. A nomenclature is given in Table 1. A natural objective is to maximize the oil production while minimizing the need of gas.

*1.2.1.1.1. Gas injection impact.* — To study the effect of a gas injection rate variation, we assume that the production choke opening is constant. From the Bernoulli equation, one can derive that the pressure gradient in the tubing has a steady state value

$$(1) \quad p_r - p_s = \Delta p_{drawdown} + \Delta p_{choke} + \Delta p_{gravity} + \Delta p_{friction}$$

Parameters  $\Delta p_{drawdown}$ ,  $\Delta p_{choke}$ ,  $\Delta p_{gravity}$  and  $\Delta p_{friction}$  represent pressure gradients in the tubing due to the draw down, the production choke, gravity and friction respectively. These four terms depend on  $q_{gi}$  and  $q_{lp}$  (the injected gas flow rate and the produced liquid flow rate respectively). Therefore, from equation (1),  $q_{lp}$  one can predict the amount of oil produced for a given gas injection rate  $q_{gi}$ . When gas injection is low, the two dominant terms are  $\Delta p_{drawdown}$  and  $\Delta p_{gravity}$ . Then, equation (1)

reduces to

$$p_r - p_s = \Delta p_{drawdown}(q_{lp}) + \Delta p_{gravity}(q_{lp}, q_{gi})$$

where  $p_r$  and  $p_s$  are the reservoir pressure and the well downstream pressure, respectively. By the implicit function theorem, this defines  $\phi$  such that  $q_{lp} = \phi(q_{gi})$ , and we have

$$\phi'(q_{gi}) = -\frac{\partial_{q_{gi}} \Delta p_{gravity}}{\partial_{l_p} \Delta p_{drawdown} + \partial_{l_p} \Delta p_{gravity}}$$

with the obvious notations  $\partial_{q_{gi}} = \frac{\partial}{\partial q_{gi}}$  and  $\partial_{l_p} = \frac{\partial}{\partial q_{lp}}$ . The pressure gradient due to gravity effect ( $\Delta p_{gravity}$ ) decreases with the gas injection rate and increases with the liquid flow rate. The pressure gradient in the draw-down zone ( $\Delta p_{drawdown}$ ) increases with the liquid flow rate from the reservoir. Therefore, for low amount of gas injection rate

$$\phi' > 0$$

When large gas injection rate are considered the two predominant terms in equation (1) are  $\Delta p_{drawdown}$  and  $\Delta p_{friction}$ . Then equation (1) reduces to

$$p_r - p_s = \Delta p_{drawdown}(q_{lp}) + \Delta p_{friction}(q_{lp}, q_{gi})$$

One finds

$$\phi'(q_{gi}) = -\frac{\partial_{q_{gi}} \Delta p_{friction}}{\partial_{l_p} \Delta p_{drawdown} + \partial_{l_p} \Delta p_{friction}} < 0$$

since, under these conditions, the pressure gradient due to frictions effects increases with the gas injection rate and with the liquid flow rate

In summary, at low gas flow rate, injecting more gas tends to raise the liquid production, but at high flow rate, it decreases it. In between these two regions there is a (possibly non unique, though unique in practice) gas-lift optimal point where  $\phi' = 0$ .

*1.2.1.1.2. Choking impact.* — In a first approximation, it is usually assumed that choking mainly affects the pressure gradient in the production choke. Denoting  $u$  the choke opening and assuming  $q_{gi}$  constant, we define  $\psi$  such that  $q_{lp} = \psi(u)$ . From equation (1), one finds that

$$\psi'(u) = -\frac{\partial_u \Delta p_{choke}}{\partial_{l_p} \Delta p_{gravity} + \partial_{l_p} \Delta p_{drawdown} + \partial_{l_p} \Delta p_{friction} + \partial_{l_p} \Delta p_{choke}} > 0$$

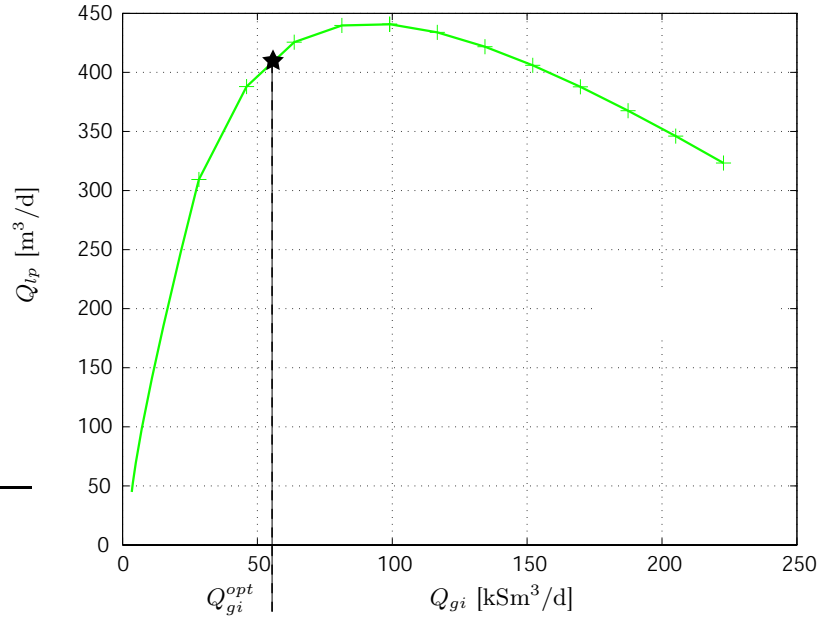


FIGURE 1.3. Performance curve (liquid production  $Q_{lp}$  with respect to gas injection flow rate  $Q_{gi}$ ) derived from OLGA<sup>®</sup>2000 simulations (numerical set up given in Appendix A, Table 1). The black star shows the optimum gas-lift injection  $Q_{gi}^{opt}$  for given economic conditions.

since all pressure gradients increase with the liquid flow rate, and because the gradient in the production choke decreases with the opening  $u$ .

Therefore, wells ought to be operated at maximum production choke opening.

*1.2.1.1.3. Performance curve and economic considerations.* — Thanks to the formulas presented in the two previous paragraphs one can get an idea of the shape of a typical performance curve, i.e. the function expressing the oil production with respect to the gas injection rate and to the production choke opening. More detailed computations can be found in [11], where different methods based on the energy balance equation are given such as the more widely accepted procedure by Poettman and Carpenter.

Figure 1.3 shows a typical performance curve derived from OLGA<sup>®</sup>2000 simulations. OLGA<sup>®</sup>2000 is a Transient Multiphase Flow Simulator. A realistic dynamic oil-gas model is used along with semi-implicit numerical solver (see [32] for details). A complete numerical set-up is given in Appendix A, Table 1. This curve possesses a gas injection for which the liquid production reaches an optimum. Assuming that an infinite amount of gas is available, the optimal gas injection can be defined as follows. It correspond to the operating point at which injecting more or less gas will lead to less profit. Profit is defined as the price of oil times the oil produced minus the price of gas times the amount of gas used. Therefore, optimal gas injection is the one at which the derivative of the performance curve equals the cost of the used gas divided by the production profit. Usually, it is slightly less than the point cancelling the derivative of the performance curve.

*1.2.1.2. At the multi-well scale.* — We have been focusing on single wells. Yet, one also has to take into account constraints that arise from the coupling between the wells. A single well sees the rest of its networks through the following parameters (see Figure 1.4 for a complete view of the system)

- the gas availability,
- the pressure of the gas network,
- the pressure of the reservoir,
- the pressure downstream the production choke.

In facts, each of the three pressures correspond to a separate network. The amount of gas available is upper bounded by the number and the capacities of compressors on the network. The pressure at the upstream of the production choke must match the surface equipments constraints (e.g. it must be higher than a defined limit allowing the flow in the export pipe).

Bottom hole pressure variations create a local gradient in the reservoir that propagates in a way depending on the physical properties of the geological formation. Presence of faults, change of porosity and/or permeability create convoluted transient gradients that affect the reservoir pressure at the bottom of the neighbor wells.

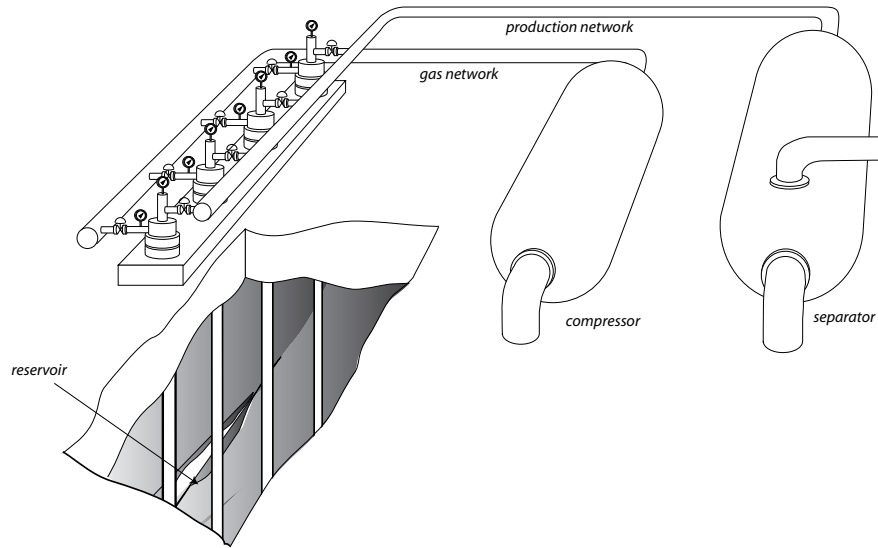


FIGURE 1.4. Schematic of an onshore installation. Wells are linked together through three networks: the gas network, the production network and the reservoir

Well production is globally optimized on the basis of technical constraints and economical and strategic objectives. Constraints such as safety, production rules, reservoir extraction policy (maximum flow rate per well, production quotas etc...), well-bore formation interface and capacity have to be taken into account. The optimal operating points for a set of wells is often different from the set of optimal operating points for each well. In practice, these constraints are handled by a team of engineers based on geophysical parameter computations.

**1.2.2. Unstable operations conditions and their cost.** — As we have seen it, finding optimal operating points can imply numerous constraints. Yet, a very important problem is usually forgotten and underestimated. Wells are often not at steady state. They are often locked in oscillating modes, called headings, which correspond to regular and/or irregular changes in flow parameters (pressures and fluid rates) occurring in the system. Figure 1.5 shows an on-site example of well instabilities.

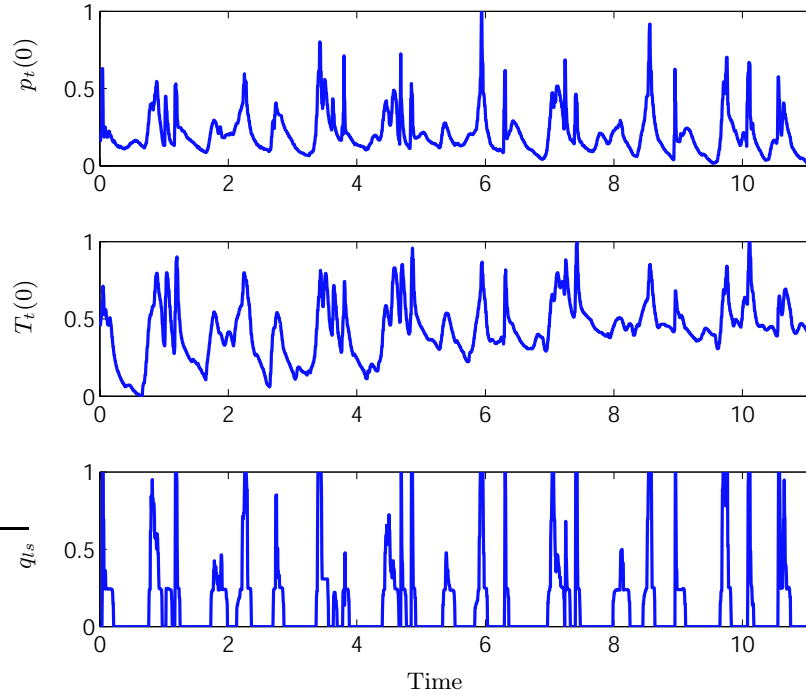


FIGURE 1.5. Well instabilities example. Wellhead pressure, temperature and oil flow from the separator are represented. An almost periodic regime appears while oil production is intermittent. Scales are omitted for confidentiality reasons (courtesy of TOTAL).

There is a slug production as can be seen on the oil flow from the separator (the oil flowing from the well could not be measured). The phenomenon seems periodic even though any absolutely repeated pattern cannot be clearly seen.

*1.2.2.1. At single well scale.* — The average amount of oil produced in unstable conditions is much lower than predicted.

Finally, let us recall that operating in unstable conditions sharply increases the risk of severe reservoir damage and troubles in the draw-down zone.

*1.2.2.2. Instabilities propagation.* — As described in Section 1.2.1.2 a well is part of a highly coupled system of wells, surface installations and

reservoirs linked by a network of pipes. In particular, each time a well becomes unstable, there is a risk for the other wells to be contaminated. In normal situations, because the pressure of the separator is often controlled, the slugs can be absorbed and do not lead to changes of the downstream pressures of the other wells. Yet, these margins are very thin and if the pressure in the export pipe (see Figure ??) is close to the separator pressure, a decentralized controllers structure is not able to cope with the change of flow inlet. The separator pressure sharply increases which, in turn, destabilizes the other wells. To overcome this, predefined safety rules (e.g. to shut down a well when its downstream pressure is above a certain constant) are used. Keeping a majority of wells quite stable is often preferred to producing from all wells. This non optimal strategy is very frequent in practice.

Similarly, wellhead casing variations should not propagate upstream in the gas network because gas flow controller aims at guaranteeing a constant gas injection however the upstream or downstream pressures may vary. Yet, if the upstream pressure in the gas network is close to the wellhead pressure in the casing, the gas control valve cannot absorb the oscillations anymore.

Finally, the reservoir can also be seen as a network through which instabilities (cyclic changes of pressure and flow rates) can propagate. This last point should not be overlooked.

In summary, instabilities have a very high cost. Not only do they lower a single well productivity, but also they propagate and cause shut downs, safety alarms trigger, compressor failures and eventually negatively impact on the productivity of the whole field.

## CHAPTER 2

### A DYNAMICAL SYSTEM APPROACH TO THE STUDY OF INSTABILITIES

#### UNE APPROCHE DYNAMIQUE DE L'ANALYSE DES INSTABILITÉS

*Dans ce chapitre nous présentons notre contribution principale : la modélisation et l'analyse de la stabilité des deux instabilités les plus répandus pour les puits activés en gas-lift. Dans un premier temps nous nous intéressons à l'instabilité la plus référencée dans la littérature : le casing-heading. Dans la Section 2.1 nous décrivons ce phénomène et nous en expliquons le mécanisme. Grâce à une réduction du modèle présenté par [3] nous montrons que le casing-heading peut être interprété comme le cycle limite d'un modèle à deux dimensions. Nous en donnons une preuve mathématique en nous plaçant dans un cadre relativement général non Lipschitz. En résumé, le casing-heading apparaît résulter du couplage entre les deux parties qui composent le puits.*

*Une idée simple pour éradiquer ce phénomène pourrait être de faire en sorte que les deux parties du puits se comportent de façon indépendantes. Un tel découplage est techniquement réalisable. Malheureusement, dans le système ainsi découplé il peut apparaître un autre type d'instabilité : la density-wave. Ce phénomène résulte de la propagation d'une succession de bouchons liquides et de bulles de gaz dans le puits. Son étude nécessite une modélisation spécifique sous la forme d'un modèle à paramètres distribués, que nous présentons dans la Section 2.2. L'analyse de la stabilité de ce système dynamique nous permet d'interpréter la density-wave comme une bifurcation.*

*Le puits peut donc être modélisé par la combinaison des modèles présentés aux Sections 2.1 et 2.2. Il est l'interconnexion d'un modèle à paramètres distribués avec un système dynamique du premier ordre.*

*La stabilité est alors étudiée dans la Section 2.3 grâce au théorème des petits gains. Nous nous intéressons particulièrement à l'évolution du comportement du puits lorsque certains paramètres évoluent. Les résultats obtenus sont en accord avec les règles utilisées généralement sur site (et vont d'ailleurs au-delà).*

In this chapter lies our main contribution: the modeling and the stability analysis of the two main unstable phenomena occurring on gas-lifted wells. In Section 2.1, we focus on the so-called casing-heading instability. This is the best-known unstable mechanism. We give a reduction of the model proposed in [3] in order to analyse the casing-heading as a limit cycle of a two-dimensional model with switches. In Section 2.2, we describe the density-wave instability. The propagation in tubing is modeled as a distributed parameters model, which let us analyse its stability. At last, in Section 2.3, we propose a complete model for the well as the connexion of a stable first order model (the casing) and a distributed parameters model (the tubing). Stability analysis is performed thanks to the small gain theorem. Well known operating rules are shown to be in accordance with the stability properties of the model.

### 2.1. The casing-heading instability

In this first section, we focus on the best-known and best understood of the unstable phenomena: the casing-heading instability. [9] lists three types of headings that can be encountered. They are classified according to where the free gas cyclically builds up and discharges: tubing heading, formation heading and casing heading. This location-dependent terminology tends to be replaced by a terminology where instabilities are described by classes of mechanisms. Casing heading is the only one that has kept its name, because not only has it been described for a long time but its mechanism has also been understood in details.

In this section, we first describe this phenomenon, then we recall the finite-dimensional modeling of [24]. Thanks to this model, we derive a

complete description of the known oscillating mode under the form of a limit cycle of a 2D model with switches. Mathematical proof is given with relatively few hypotheses on the model properties. This stresses what, in the physical structure of the well, leads to the casing-heading phenomenon.

**2.1.1. Casing-heading description.** — This cyclic phenomenon has been described in many publications such as [43], [42] and [26]. Originally, its sequence was divided into 4 phases in [43] and in seven in [26]. Figure 2.2 shows an example of casing-headings obtained with the OLGA<sup>®</sup>2000 simulator. We choose to describe casing-heading as a four stages phenomenon (shown in Figure 2.2). One should report to Figure 2.1 for an illustration of the terms involved in the following description, notations are given in Appendix B, Table 1.

1. Starting with a *downhole annulus pressure* that is lower than the *bottom-hole pressure*, there is no gas flow through the gas *injection valve* into the *tubing*. As the gas flow rate at the surface is kept constant the pressure in the *casing* builds up.
2. After some time, the annulus pressure exceeds the downstream pressure in the tubing. Gas is injected into the tubing. The injected gas lowers the tubing gradient. The bottom-hole pressure begins to decrease. Simultaneously, *the production rate* and the *wellhead tubing pressure* begin to increase.
3. Gas now flows from the annulus into the tubing at an increasing rate. Because insufficient gas can be supplied, the pressure in the casing sharply decreases. Oil and gas are produced through the production choke at a high rate. Wellhead tubing pressure reaches a maximum and the bottom-hole pressure reaches its minimum.
4. With decreasing annulus pressure, the gas flow rate entering the tubing drops. Therefore, the gradient in the tubing gets heavier, and the bottom-hole pressure starts to increase again. The production rate and the wellhead pressure decrease again. The bottom-hole pressure equals the annulus pressure, the gas injection in the tubing stops. The whole system reaches Phase 1 of the description

h

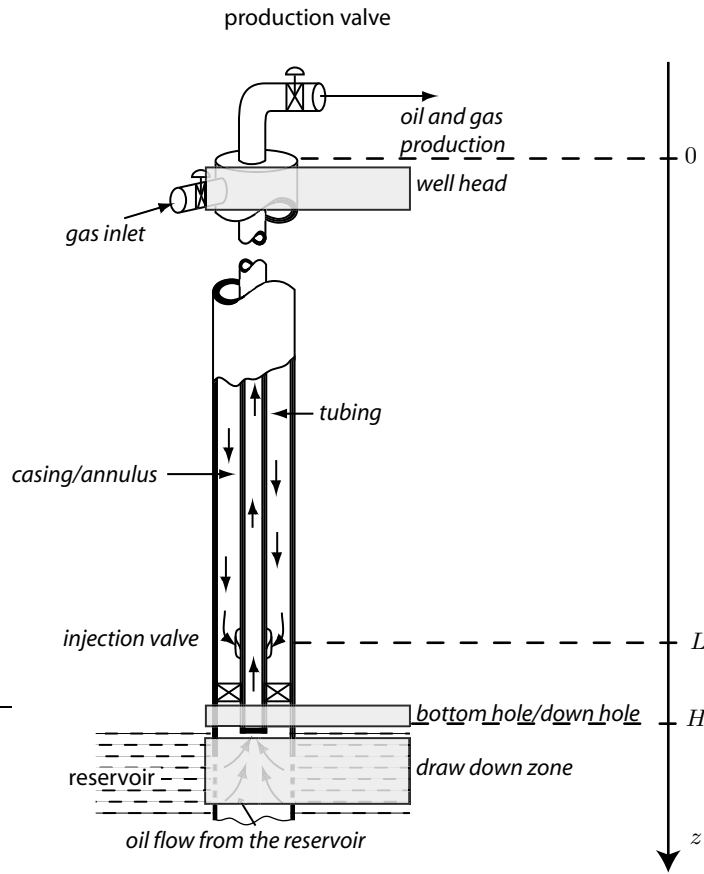
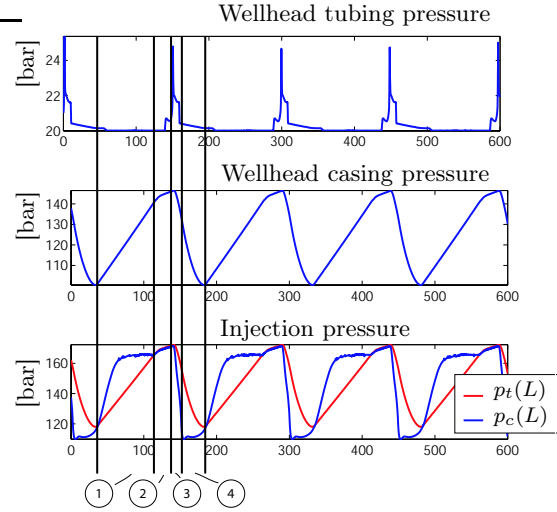
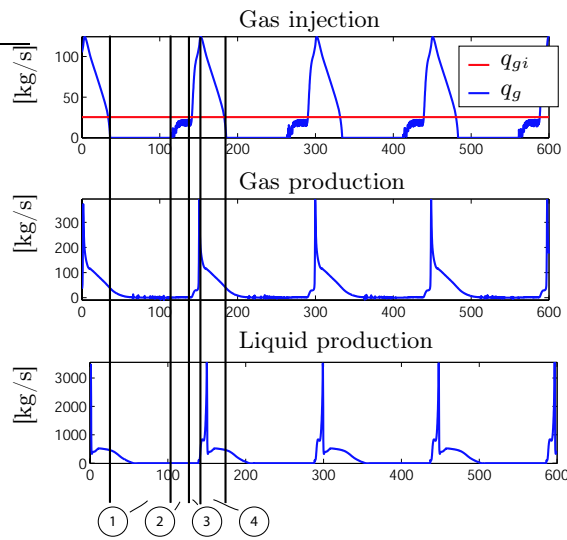


FIGURE 2.1. Schematic of the well. Zones of consideration (well head zone, bottom hole zone) appear in gray.

**2.1.2. Modeling.** — Different types of models have been developed to represent this instability. For example in [43], a complete and very detailed model is presented. It not only takes into account the one dimensional propagation in the production pipe, but also the shape of the bubble of gas entering the tubing and the liquid film fall-back. The results of this very precise modeling are compared with measurements obtained from a laboratory-scaled experiments. The aim of such a fine mathematical description is to predict the well behavior so that optimal operations set point can be designed. Such an approach relies on the idea



(a) Pressure



(b) Flow rate

FIGURE 2.2. Unstable well behavior, casing heading, obtained with  $q_{gi} = 0.2\text{kg/s}$  simulated with OLGA<sup>®</sup>2000 (numerical set up given in Appendix A, 2). The four main stages of the phenomenon are highlighted.

that it is possible to prevent instabilities by a better design of installations. Here, we aim at showing that it is possible, thanks to feedback control laws based on a better understanding of the physical mechanism, to alleviate instabilities while operating in the same conditions.

For control and mathematical analysis purposes, we seek the simplest model capturing the well dynamics. In [18], [19] and [3], the following three balance ordinary differential equations model is shown to accurately represent the casing-heading dynamics

$$(2) \quad \begin{cases} \dot{m}_1 = q_{gi} - q_g \\ \dot{m}_2 = q_g - q_{gp} \\ \dot{m}_3 = q_l - q_{lp} \end{cases}$$

Where  $m_1$  and  $m_2$  are the masses of gas in the casing and in the tubing, respectively, and  $m_3$  is the mass of liquid in the tubing. Respectively,  $q_{gi}$ ,  $q_g$  and  $q_{gp}$  represent the flow rates of gas at the wellhead, into the tubing at the injection depth, and the flow rate of gas produced through the production choke.  $q_l$  and  $q_{lp}$  represent the flow rate of liquid coming from the reservoir and produced at the wellhead. All those flow rates are described by the following laws

$$\begin{aligned} q_{gi} &= \text{constant flow rate of gas} \\ q_g &= C_g \sqrt{\rho_c(L) \max\{0, p_c(L) - p_t(L)\}} \\ q_{pc} &= C_{pc} \sqrt{\rho_m(0) \max\{0, p_t(0) - p_s\}} \Psi \\ q_{gp} &= \frac{m_2}{m_2 + m_3} q_{pc} \\ q_{gl} &= \frac{m_3}{m_2 + m_3} q_{pc} \\ q_r &= PI(p_r - p_t(H)) \end{aligned}$$

$C_g$ ,  $C_{pc}$  and  $PI$  are constants.  $\Psi$  is the production choke opening, it ranges from 0 to 1.  $H$  is the well depth and  $L$  the injection depth. Notice that the liquid flow rate from the reservoir is proportional to the term  $p_r - p_t(0)$ , (usually referred to as draw-down). This constant  $PI$  characterizes the reservoir response and stands for Productivity Index.  $p_c(L)$ ,  $p_t(L)$  represent the pressures at the injection depth on the two

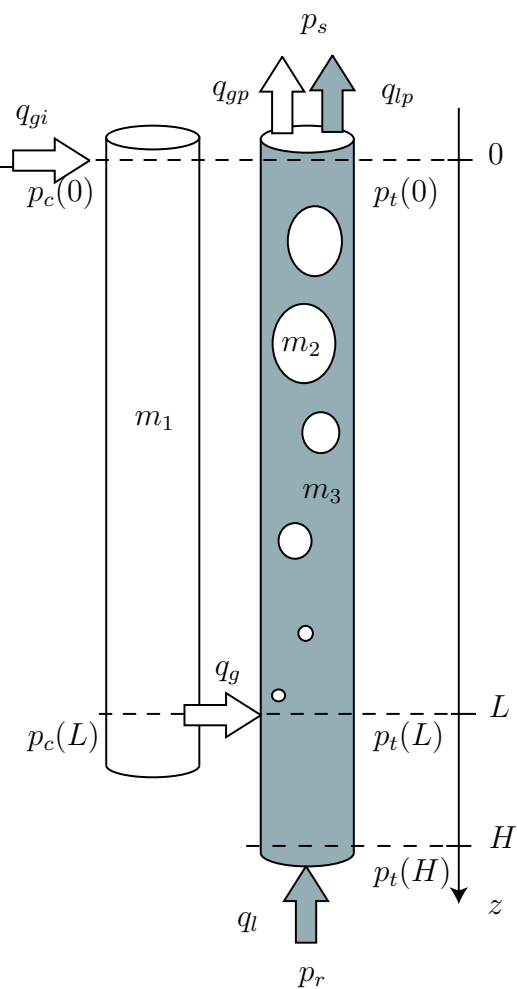
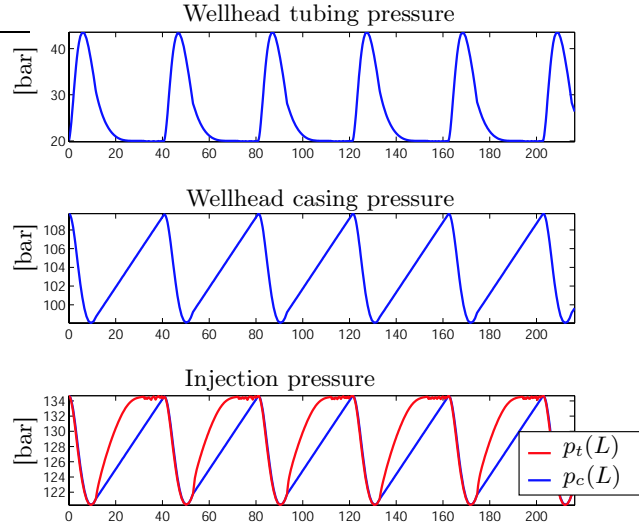


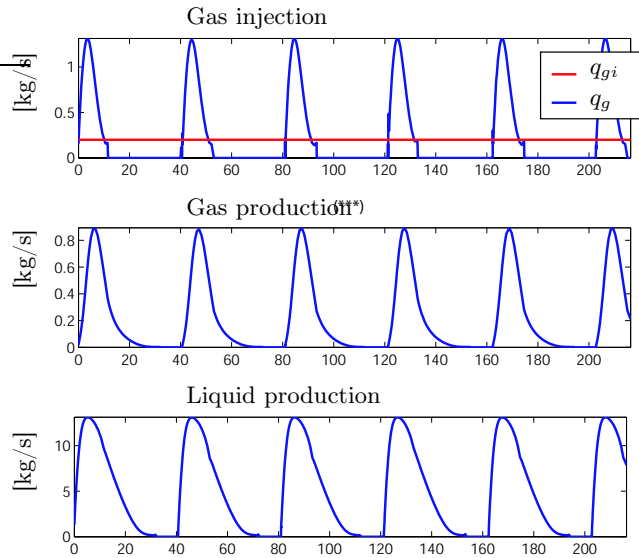
FIGURE 2.3. Scheme of the well and notations used in equation (2) (the casing and the tubing part have been artificially separated to improve readability).

sides of the valve.  $p_c(L)$  is the upstream pressure in the casing, and  $p_t(L)$  is the downstream pressure in the tubing.  $\rho_c(L)$  is the gas density in the casing at the injection depth.  $p_t(0)$  is the pressure in the tubing at the wellhead and  $p_s$  the pressure in the separator.

**2.1.3. Stability study.** — With the exception of the part located between the bottom-hole and the gas injection point which is filled with



(a) Pressure



(b) Flow rate

FIGURE 2.4. Unstable well behavior, casing heading, obtained with  $q_{gi} = 0.2\text{kg/s}$  simulated with equation (2)

liquid, we assume that the flow in the tubing is homogeneous. Using the ideal gas law and following [3], densities can be computed as follows

$$\rho_c(L) = \frac{M}{RT_c} p_c(L)$$

$$\rho_m(0) = \frac{m_2 + m_3 - \rho_l(H - L)S_t}{LS_t}$$

We also get the pressure expressions from the following equations

$$(3) \quad p_c(L) = \left( \frac{RT_c}{V_c M} + \frac{gL_c}{V_c} \right) m_1$$

$$(4) \quad p_t(0) = \frac{RT_t}{M} \frac{m_2}{HS_t - \nu_0 m_3}$$

$$p_t(L) = p_t(0) + \frac{g}{S_t} (m_2 + m_3 - \rho_l(H - L)S_t)$$

$$p_t(H) = p_t(L) + \rho_l g(H - L)$$

$M$ ,  $R$ ,  $g$  represent the molar mass of the gas, the ideal law constant and the gravity respectively.  $S_t$ ,  $L_c$ ,  $V_c$  are the tubing section, the casing length and the casing volume. The casing and tubing temperatures are denoted  $T_c$  and  $T_t$  respectively.

Equation (4) giving  $p_c(L)$  is a first order approximation of an atmospheric model.

Figure 2.4 shows an unstable behavior of the casing heading type simulated for  $q_{gi} = 0.2\text{kg/s}$  with equation (2). As in Figure 2.2 we see that there is a first phase with no injection. Then injection begins as the annular pressure builds up to the tubing pressure. Oil and gas are produced at the well head. At last the casing can not face the gas demand and the annular pressure decreases. Gas injection and liquid production stop. Model (2) capture the main dynamics of the casing heading phenomenon.

This model allows us to give here some insights on the well stability (this point will be developed further in Section 2.3). Figure 2.5 and 2.6 illustrate the stability. One sees that for low values of the gas injection rate the well will be unstable. Roots crossing the imaginary axis are at birth of this instability (see Figure 2.6).

**2.1.4. Casing-heading as a limit cycle.** — We now show that the casing-heading phenomenon can be depicted as the limit cycle of a two-dimensional model with switches. This study has been published in the

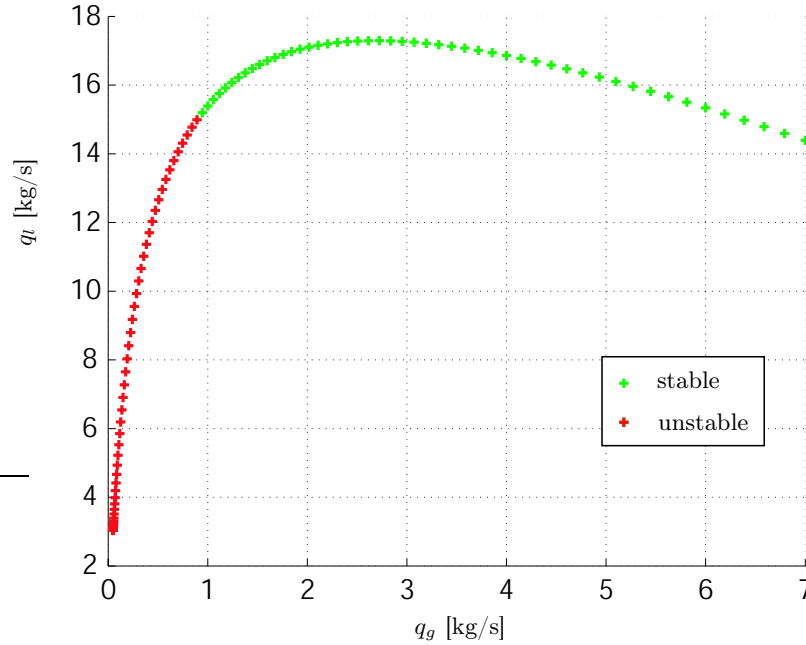


FIGURE 2.5. Performance curve corresponding to the model (2) with gas injection rate  $q_g$  ranging from 0.01 to 7 kg/s and a liquid production from 3 to 17kg/s. Stable equilibrium points are represented in green and unstable in red.

IFAC world congress in Praha (see [36]). The proof is given for a system of the form (2) under a limited set of hypotheses on the flow rate.

Studies reveal that, around a casing-heading set-point, the system is well modeled by a two dimensional approximation (the masses of oil and gas in the tubing are highly correlated). This representation is handy to interpret the casing-heading oscillations as a limit cycle. Our contribution is to explain the observed planar limit cycle (e.g Figure 2.2 for a sample OLGA<sup>®</sup>2000 well simulation) through the Poincaré-Bendixon theorem. This system is related to other work on hybrid systems, such as the two-tank system addressed in [22], or the generalization of the Poincaré-Bendixon theorem to planar hybrid systems by [33]. Yet, several specific issues have to be addressed here. The model includes two switching curves. These model the flow rate through the two valves (A and E on Figure 1.2). According to classic Saint-Venant laws (refer to [2]) the flow rate is non

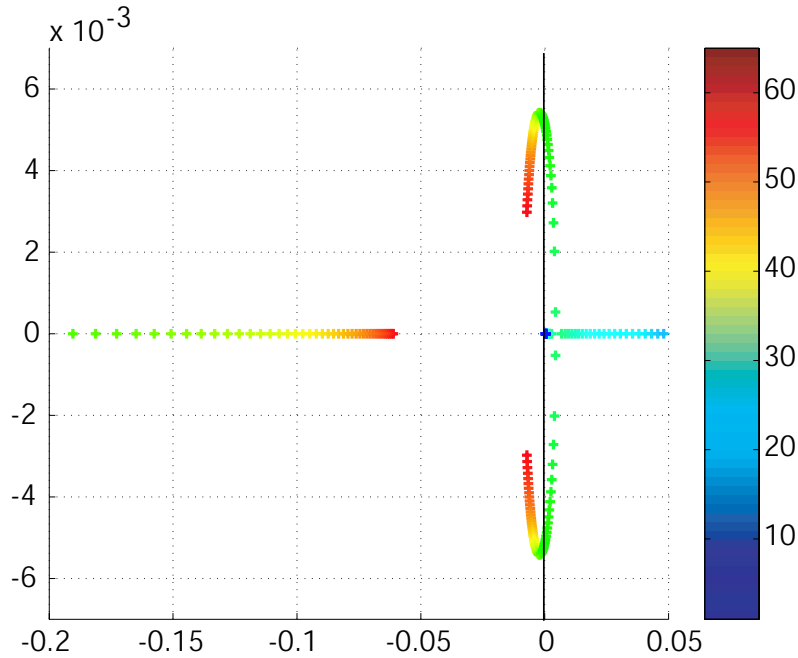


FIGURE 2.6. Roots of model (2) are represented in the complex plane for gas injection ranging from 0.01 to 7 kg/s. Color axis goes from 0 to 100% of the gas injection range.

differentially smooth around zero. The model is thus non differentially smooth across the switching curves. Therefore, proving existence and uniqueness of the trajectories requires special care and does not directly derive from a Lipschitz-continuity assumption.

#### 2.1.4.1. Dynamics definition and hypotheses. —

*Physical hypotheses.* — We assume that during the casing-heading phases the oil mass is proportional to the gas mass in the tubing. Therefore, we only need two ordinary differential equations to describe the system. For sake of simplicity, we denote  $x = m_1$  and  $y = m_2$ .

We represent the behavior of the well around an unstable set point by the following dynamics over  $[\underline{x}, \bar{x}] \times [\underline{y}, \bar{y}] \subset \mathbb{R}^+ \times \mathbb{R}^+$

$$(5) \quad \begin{pmatrix} \dot{x} \\ \dot{y} \end{pmatrix} = \begin{pmatrix} \varepsilon q_{gi}(x) - q_g(x, y) \\ q_g(x, y) - \mu q_{gp}(y) \end{pmatrix}$$

We note  $\mathcal{X} \triangleq [\underline{x}, \bar{x}]$ ,  $\mathcal{Y} \triangleq [\underline{y}, \bar{y}]$ ,  $X \triangleq (x, y)^t$  and

$$\dot{X} = F(X) = (F_1(x), F_2(x))^T.$$

The positive parameters  $\varepsilon$  and  $\mu$  stand for the openings of valves A and E.  $\phi(\cdot, X_0)$  denote the solution of equation (5) with  $X_0$  as initial condition.

*Mathematical hypotheses and physical justifications.* — We assume that both  $q_g$  and  $q_{gp}$  vanish over their definition intervals. Let  $\partial\mathcal{F}_g^o$  and  $\partial\mathcal{F}_{gp}^o$  be the boundaries of the sets  $q_g^{-1}(0)$  and  $q_{gp}^{-1}(0)$ . We assume the following hypotheses hold.

**(H1)** :  $q_{gi} : \mathbb{R} \rightarrow \mathbb{R}$  is  $C^1$ , strictly decreasing and does not vanish.

**(H2)** :  $q_g = g_g \circ \tau_g$

–  $\tau_g : \mathbb{R}^2 \rightarrow \mathbb{R}$ , is  $C^2$ , and strictly increasing w.r.t  $x$  and  $y$ .

–  $g_g : \mathbb{R} \rightarrow \mathbb{R}^+$ , is  $C^0$ , strictly increasing over  $\mathbb{R}^+$ ,  $C^1$  over  $\mathbb{R}/\{0\}$ , and non Lipschitz at 0.  $g_g(0) = 0$ .  $g'_g$  is decreasing over  $\mathbb{R}^+ \setminus \{0\}$ .  $g'_g \sim t^\lambda$  with  $-1/2 < \lambda < 0$ .

**(H3)** :  $q_{gp} = g_{gp} \circ \tau_{gp}$

–  $\tau_{gp} : \mathbb{R}^2 \rightarrow \mathbb{R}$ , is  $C^1$ , strictly increasing w.r.t.  $y$ , and does not depend on  $x$ .

–  $g_{gp} : \mathbb{R} \rightarrow \mathbb{R}^+$ , is  $C^0$ , strictly increasing over  $\mathbb{R}^+$  and  $C^1$  over  $\mathbb{R}/\{0\}$ , non Lipschitz at 0.  $g_{gp}(0) = 0$ .

**(H4)** :  $\tau_g$  and  $\tau_{gp}$  vanish over  $\mathcal{X} \times \mathcal{Y}$ . We define  $\partial\mathcal{F}_g^o \triangleq \tau_g^{-1}(0)$  and  $\partial\mathcal{F}_{gp}^o \triangleq \tau_{gp}^{-1}(0)$ .

In order to construct a polygon  $\mathcal{P}$  such as defined later on in Section 2.1.5.1, we need some further assumptions.

**(H5)** :  $\forall x \in \mathcal{X}, \dot{y}(x, \bar{y}) < 0$

**(H6)** :  $\dot{x}(\bar{x}, y_{gp}) < 0$

**(H7)** :  $\forall x \in \mathcal{X}, \tau_g(x, \underline{y}) \leq 0$

**(H8)** :  $\forall y \in \mathcal{Y}, \tau_g(\underline{x}, y) \leq 0$

where, thanks to the continuity of  $q_{gp}$ ,  $y_{gp} \triangleq \max\{y/q_{gp}(y) = 0\}$ .

One last assumption **(H9)** is that a constant  $K$ , uniquely defined later on (equation (20)) in Section 2.1.6.3 by the functions above, is not zero.

*Existence conditions of a limit cycle.* — Let  $\Omega(\phi)$  be the limit set of  $\phi$ . According to the Poincaré-Bendixon theorem as expressed in [31], the fact that  $\Omega(\phi)$  contains no critical point combined to the uniqueness of

the solution of equation (5) is sufficient to guarantee the existence of a limit cycle. On the other hand, exhibiting a positive invariant set containing no stable equilibrium implies that  $\Omega(\phi)$  contains no critical point. Therefore we can simply check that

- there exists a positive invariant set (this is shown in Section 2.1.5),
- given a particular initial condition the solution is uniquely defined (this is addressed in Section 2.1.6).

### 2.1.5. Positive invariance. —

*2.1.5.1. Some useful lemmas.* — Let  $\mathcal{P}$  be a polygon  $((P_i)_{i \in [1, N]}$  its vertices) such that

$$(6) \quad \forall i \in [1, N], \exists \lambda \text{ such that } \overrightarrow{P_i P_{i+1}} = \lambda F(P_i)$$

Classically,  $\mathcal{P}$  is a positive invariant set if and only if

$$(7) \quad \forall X_0 \in \partial \mathcal{P}, \exists t > 0 \text{ s.t. } \forall \epsilon \in [0, t] : \phi(\epsilon, X_0) \in \mathcal{P}$$

**Lemma 1.** — *Assume that  $F$  is  $C^n$  on a neighborhood of  $X_0$ , with  $X_0 \in [P_i, P_{i+1}]$ . Define  $u = \frac{P_1 \times P_2}{\|P_1 \times P_2\|}$ . If there exists  $k \in [1, n]$  s.t.*

$$\begin{cases} F(P_i) \times \frac{d^j \phi}{dt^j}(0, X_0) \cdot u = 0, j = 1..k-1 \\ F(P_i) \times \frac{d^k \phi}{dt^k}(0, X_0) \cdot u > 0 \end{cases}$$

then condition (7) holds.

*Proof.* — A sufficient condition for condition (7) to be satisfied is that

$$\overrightarrow{P_i P_{i+1}} \times \overrightarrow{P_i \phi(\epsilon, X_0)} \cdot u > 0$$

This is equivalent to

$$(8) \quad A(\epsilon, X_0) = F(P_i) \times \overrightarrow{X_0 \phi(\epsilon, X_0)} \cdot u > 0$$

Since  $F$  is  $C^n$  on a neighborhood of  $X_0$ , an expansion of  $A(\cdot, X_0)$  is

$$A(\epsilon, X_0) = \epsilon^{k-1} (F(P_i) \times \frac{d^k \phi}{dt^k}(0, X_0) \cdot u + o(1))$$

Therefore  $A(\cdot, X_0)$  is strictly positive and condition (7) is satisfied.  $\square$

Similarly one can prove that

**Lemma 2.** — Let  $X_0 \in [P_i, P_{i+1}]$  and  $(j, l) \in \{(1, 2); (2, 1)\}$ . Assume that  $F_j(P_i) = 0$ . If  $F_l$  is continuous around  $X_0$  and  $F_j$  is  $C^1$ , a sufficient condition leading to (7) is

$$(9) \quad \left. \begin{array}{l} (-1)^j \dot{x}_l(P_i) \dot{x}_j(X_0) > 0 \text{ or} \\ \left\{ \begin{array}{l} \dot{x}_l(P_i) \dot{x}_j(X_0) = 0 \\ (-1)^j \dot{x}_l(P_i) \ddot{x}_j(X_0) > 0 \end{array} \right\} \end{array} \right\}$$

**Corollary 1.** — If  $F_j(P_i) = 0$  and if  $F_j$  and  $F_l$  are only  $C^0$ , a more restrictive condition is

$$(-1)^j \dot{x}_l(P_i) \dot{x}_j(X_0) > 0$$

*2.1.5.2. Positive invariant set candidate.* — Two curves play a key role in the construction of the candidate rectangle  $\mathcal{P} = (P_1 P_2 P_3 P_4)$ . These are the set  $\{(x, y) / \dot{x} = 0\}$  and the set  $\{(x, y) / \dot{y} = 0\}$ . We show that this rectangle, which is illustrated in Figure 2.7, satisfies equation (6).

*Construction of  $P_1, P_2$  and  $P_3$ .* — Let  $\psi$  be defined by

$$\psi(x) \triangleq \varepsilon q_{gi}(x) - q_g(x, y_{gp})$$

From (H6) and (H8),  $\psi(\underline{x}) > 0$  and  $\psi(\bar{x}) < 0$ . Since  $\psi$  is continuous, increasing, we can uniquely define

$$x_1 = \max\{x / \psi(x) = 0\}$$

We note  $P_1 \triangleq (x_1, y_{gp})$ . At that point, both  $\dot{x}$  and  $q_{gp}$  vanish. Further, similar arguments relying on (H5), and (H2)-(H8) respectively, uniquely define  $P_2 \triangleq (x_1, y_2)$  with  $y_2 \triangleq \min\{y / \dot{y}(x_1, y) = 0\}$  and  $P_3 \triangleq (x_3, y_2)$  with  $x_3 \triangleq \max\{x / \dot{x}(x, y_2) = 0\}$ .

*Construction of  $P_4$ .* — Let  $P_4 \triangleq (x_3, y_{gp})$ .  $[P_3, P_4]$  is tangent to the field at  $P_3$ . Further,  $[P_4, P_1]$  is tangent to the field at  $P_4$ . This arises from the following argument. Since  $q_g$  is cancelling at  $(\underline{x}, y_{gp})$  and strictly positive at  $P_1$ , we can choose  $\varepsilon$  parameter in equation (5) such that  $[P_4, P_1] \cap \partial \mathcal{F}_g^o \neq \emptyset$ . Therefore  $q_g(P_4) = 0$ . As a consequence,  $\dot{x}(P_4) > 0$  and  $\dot{y}(P_4) = 0$ .

2.1.5.3. *Intersections with switching lines.* — Let  $X_g^2 \triangleq (x_g, y_{gp})$  with  $x_g = \max\{x/(x, y_{gp}) \in [P_4, P_1] \cap \partial\mathcal{F}_g^o\}$ . Remembering that  $q_g(P_3) = \varepsilon q_{gi}(P_3) > 0$ , we conclude  $[P_3, P_4] \cap \partial\mathcal{F}_g^o \neq \emptyset$ . We note  $X_g^1 \triangleq (x^3, y_g)$  with  $y_g \triangleq \max\{y/(x^3, y) \in [P_3, P_4] \cap \partial\mathcal{F}_g^o\}$ .

2.1.5.4. *Positive invariance.* — Let  $X_0$  be a point on the side of the rectangle. We want to prove that the trajectory  $\phi(\cdot, X_0) = (\phi_x, \phi_y)^t$  starting at  $X_0$  remains inside  $\mathcal{P}$  for  $t > 0$ . We assume that trajectories are uniquely defined, this is proven at Section 2.1.6.

*Using Lemma 2 at points where  $F_2$  is not  $C^1$ .* — Let  $X_0 \in [P_1, P_2]$ .  $F_1$  vanishes at  $P_1$ , so  $F_1$  being  $C^1$  and  $F_2$  only continuous around  $X_0$  will complete the list of hypotheses needed to apply Lemma 2.  $F_2$  is continuous by definition and  $F_1$  is  $C^1$ , because  $\forall X_0 \in [P_1, P_2]$

$$q_g(X_0) \leq q_g(P_1) = \varepsilon q_{gi}(P_1) > 0$$

Therefore, checking condition (9) of Lemma 2 will prove that the trajectory starting at  $X_0$  goes inside ( $\mathcal{P}$ ). If  $X_0 \in ]P_1, P_2]$  the condition rewrites  $-\dot{y}(P_1)\dot{x}(X_0) > 0$ . As  $-q_g$  is decreasing w.r.t.  $y$ ,  $\dot{x}(X_0) < 0$ . Adding that  $\dot{y}(P_1) > 0$  ensures that the condition holds. If  $X_0 = P_1$  the condition rewrites  $-\dot{y}(P_1)\ddot{x}(X_0) > 0$ . As  $\ddot{x}(X_0) = -\partial_y q_g(X_0)\dot{y}(X_0) < 0$  this condition holds. Following along the same lines it is easy to check that Lemma 2 can be applied at every point of  $\partial\mathcal{P}$  except  $X_g^1$  and  $[P_4, P_1]$ . At these points the  $C^1$  condition is not verified. Notice also that at each vertex two conditions have to be verified, one for each side.

*Using Corollary 1 at points where  $F_1$  and  $F_2$  are only  $C^0$ .* — When  $X_0$  is an element of  $X_g^1 \cup ]X_g^2, P_1]$  none of  $F$  coordinates vanish, therefore we can simply use the fact that  $F$  is continuous to apply Corollary 1. So for  $X_0 = X_g^1$  the condition is  $-\dot{x}_2(P_3)\dot{x}_1(X_0) > 0$  which is easily checked. At  $X_0 \in ]X_g^2, P_1]$  the condition is  $\dot{x}_1(P_4)\dot{x}_2(X_0) > 0$ .

*A proof by contradiction when  $X_0 \in [P_4, X_g^2]$ .* — Neither Lemma 2 ( $F_2$  is not  $C^1$ ) nor Corollary 1 ( $\dot{y}(X_0) = 0$ ) can be used here. Yet, we can prove that a solution starting at  $X_0$  cannot go below  $y = y^{gp}$ . Assume

that there exists  $t_2$  such that  $\phi_y(t_2) < x_2^{gp}$ , define  $t_1$  such that

$$(10) \quad \begin{cases} \forall t \in ]t_1, t_2], \phi_y(t) < x_2^{gp} \\ \phi_y(t_1) = x_2^{gp} \end{cases}$$

Referring to the mean value theorem  $\phi_y(t_2) = \phi_y(t_1) + (t_2 - t_1)\phi'_y(t_c)$  with  $t_c \in [t_1, t_2]$ .  $\phi'_y(t_c) = 0$  implies  $\phi_y(t_2) = \phi_y(t_1)$  which contradicts (10). Finally, as the trajectory starting at  $X_0 \in \partial\mathcal{P}$  satisfies condition (7),  $\mathcal{P}$  defines a positive invariant set.

**2.1.6. Existence and uniqueness of the trajectories.** — The first hypothesis required by the Poincaré-Bendixon theorem is the existence and forward uniqueness of the solutions. Existence of a solution of (5) starting at  $X_0 \in \mathcal{X} \times \mathcal{Y}$  follows from the continuity of  $F$ . Uniqueness of a solution of (5) starting at  $X_0 \in (\mathcal{X} \times \mathcal{Y}) / (\partial\mathcal{F}_g^o \cup \partial\mathcal{F}_{gp}^o)$  follows from the differentiable continuity of  $F$  around  $X_0$ .

*2.1.6.1. Decoupling.* — Consider  $X_0 \in [P_4, X_g^2[ \subset \partial\mathcal{F}_{gp}^o$ .  $q_g$  is null at  $P_1$  and increasing with respect to  $x$ , so it cancels over  $[P_4, X_g^2]$ . In a neighborhood of any point of this segment the system is decoupled. At this point the system writes

$$\begin{cases} \dot{x}(X_0) = \varepsilon q_{gi}(x_0) \\ \dot{y}(X_0) = -\mu q_{gp}(y_0) \end{cases}$$

Both right hand sides are decreasing functions because  $q_{gp}$  is increasing and  $q_{gi}$  is decreasing. Thus the solution starting at  $X_0$  is unique (see [10]).

Let  $X_0 \in \partial\mathcal{F}_g^o$ , such that  $F(X_0) \cdot \nabla\tau_g(X_0) < 0$ . Let  $\phi$  be a solution starting at  $X_0$ .  $F$  being continuous and bounded in a neighborhood of  $X_0$ , we can define  $T > 0$  such that  $\forall t < T$ ,  $X_0\phi(t) \cdot \nabla\tau_g(X_0) > 0$ . Therefore the solutions of (5) are the solutions of the decoupled system

$$\begin{cases} \dot{x} = \varepsilon q_{gi}(x) \\ \dot{y} = -\mu q_{gp}(y) \end{cases}$$

Each equation has a unique solution, so there exists a unique solution starting at  $X_0$ .

$$(14) \quad \begin{cases} \dot{z} = \partial_x \tau_g(\xi(y, z), y)(\varepsilon q_{gi}(\xi(y, z)) - g_g(z)) + \partial_y \tau_g(\xi(y, z), y)(g_g(z) - \mu q_{gp}(y)) \\ \dot{y} = g_g(z) - \mu q_{gp}(y) \end{cases}$$

2.1.6.2. *Transversality argument.* — Let

$$X_0 \in \{X \in \partial \mathcal{F}_g^o / F(X) \cdot \nabla \tau_g(X) > 0\} \cup [X_g^2, P_1]$$

Rewriting dynamics (5) in the  $(y, z)$  coordinates, with  $z = \tau_g(x, y)$ , yields

$$(11) \quad \begin{cases} \dot{z} = F(\xi(y, z), y) \cdot \nabla \tau_g(\xi(y, z), y) \\ \dot{y} = g_g(z) - \mu q_{gp}(y) \end{cases}$$

where  $\xi$  is a  $C^2$  function defined from the implicit function theorem applied to  $z = \tau_g(\xi(y, z), y)$ . The decoupling argument does not hold anymore, but we can use the transversality property at 0,  $\dot{z}$  is strictly positive, therefore  $\exists \alpha^-, \alpha^+, T \in \mathbb{R}^+ \setminus \{0\}$  such that  $\forall t \in [0, T]$

$$(12) \quad z_0 + \alpha^- t \leq z(t) \leq z_0 + \alpha^+ t$$

When  $y_0 = \underline{y}$  and  $z_0 \neq 0$ ,  $\dot{y}(0)$  is strictly positive which allow us to define  $\beta^-, \beta^+, T \in \mathbb{R}^+ \setminus \{0\}$

$$(13) \quad y_0 + \beta^- t \leq y(t) \leq y_0 + \beta^+ t$$

Now, consider two distinct solutions  $(y_1, z_1)$  and  $(y_2, z_2)$ , let  $e_y \triangleq y_2 - y_1$  and  $e_z \triangleq z_2 - z_1$ . The key of the proof is to use equation (12) to define an upper-bound to  $|e| = |(e_y, e_z)|$ . From (12) and (13) we deduce that  $\forall t \in ]0, T[$   $y(t) > y_0$  and  $z(t) > 0$ . Therefore the solution of (11) starting at that point is unique. In the case of  $(y_0, z_0) = (\underline{y}, 0)$  this property still holds. The two solutions  $(y_1, z_1)$  and  $(y_2, z_2)$  cannot split but at  $t = 0$ . Furthermore we define  $T'$  such that  $e_y, e_z$  and their derivatives remain positive over  $]0, T'[$ . The dynamics rewrites as equation (14). We replace the  $C^1$  functions  $\partial_x \tau_g, \partial_y \tau_g$  and  $q_{gi}$  by their first order expansion around  $X_0$  in the first equation of (14)

$$(15) \quad \dot{z} = A - Bg_g(z) - C\mu q_{gp}(y) + Dz + Ey + R(y, z)$$

With  $A > 0$ ,  $C > 0$  and

$$(16) \quad \lim_{(y,z) \rightarrow (y_0,0)} \frac{R(y,z)}{|(y,z) - (y_0,0)|} = 0$$

Using the mean value theorem, we can define  $(y_c, y'_c, y''_c) \in [y_1, y_2]$  and  $(z_c, z'_c, z''_c) \in [z_1, z_2]$  such that the dynamics of  $e$  is

$$(17) \quad \begin{cases} \dot{e}_y = -\mu w'_{gp}(y_c)e_y + g'_g(z_c)e_z \\ \dot{e}_z = (-C\mu w'_{gp}(y'_c) + E + \partial_y R(y''_c, z_2))e_y \\ \quad + (-Bg'_g(z'_c) + D + \partial_z R(y_1, z''_c))e_z \end{cases}$$

Recalling (16) one can define  $T'$ ,  $k$  and  $k'$  such that over  $]0, T']$

$$\dot{e}_z \leq (-C\mu w'_{gp}(y'_c) + kE)e_y + (-Bg'_g(z'_c) + k'D)e_z$$

To define the upper-bound of (17), we recall the transversality argument.  $g'_g$  being monotonous, we deduce

$$(18) \quad \begin{cases} 0 \leq \dot{e}_y \leq g'_g(z_0 + \alpha^\pm t)e_z \\ 0 \leq \dot{e}_z \leq kEe_y + (-Bg'_g(z_0 + \alpha^\pm t) + k'D)e_z \end{cases}$$

Notice that for  $z_0 > 0$  we do not need the linear bounds of (12) to derive a proper upper-bound in (18). Yet, for  $z_0 = 0$  the upper-bound goes to infinity, therefore we use that  $\dot{z}(0)$  is not zero. Remark also that this kind of hypothesis is not required for  $\dot{y}$ . Integrating between  $s$  and  $t$  ( $t < \min(t', t'')$  and  $s > 0$ ) gives

$$e(t) \leq \int_s^t A(u)e(u)du + e(s)$$

with  $A(t) = \begin{pmatrix} 0 & g'_g(z_0 + \alpha^\pm t) \\ kE & (-Bg'_g(z_0 + \alpha^\pm t) + k'D) \end{pmatrix}$

Using  $|A| = \sum_{i,j=1}^2 |a_{ij}|$  we deduce

$$|e(t)| \leq \int_s^t |A(u)||e(u)|du + |e(s)|$$

Therefore, the Gronwall inequality theorem([10]) yields

$$(19) \quad |e(t)| \leq |e(s)| \exp\left(\int_s^t |A(u)|du\right)$$

As the exponential term is bounded, the limit of the right-hand side of equation (19) is also 0 when  $s$  goes to 0 which concludes the proof.

*2.1.6.3. Non transverse case.* — Define  $X_0$  such that  $X_0 \in \partial\mathcal{F}_g^o$  and  $F(X_0) \cdot \nabla\tau_g(X_0) = 0$ . The initial conditions of equation (11) become  $\dot{z}(0) = z(0) = 0$ ,  $\dot{y}(0) < 0$  and  $y(0) > y_{gp}$ . In inequality (12),  $\dot{z}(0) = 0$  yields  $\alpha^\pm = 0$ . The upper-bound  $|A(u)|$  goes to infinity as  $u$  goes to zero. System (18) does not give further result. Yet, using  $y \sim y_0 + \dot{y}(0)t$ , equation (15) yields

$$\dot{z} \sim Kt - Bg_g(z)$$

with

$$(20) \quad K = (E - C\mu w'_{gp}(y_0))$$

The role of assumption (H9) appears here as a substitute to the transversality property of Section 2.1.6.2. It implies that when the field is tangent to the switching curve there exists a non vanishing higher order forcing term (which actually arises from the coupling of the  $y$  dynamics onto the  $z$  dynamics). Using L'Hospital's rule, we find that  $Kt$  is the predominant term. Thus, for a given  $K$ , the solutions are positive or negative exclusively. Therefore, if  $K < 0$  we use the decoupling argument to conclude to uniqueness. If  $K > 0$  we use  $z \sim Kt^2/2$  instead. As  $t \mapsto g'_g(t^2)$  is integrable around 0 the exponential term of the right-hand side of equation (19) is bounded, therefore letting  $s$  go to zero yields  $e(t) = 0$ .

*2.1.6.4. Conclusion.* — Away from  $\partial\mathcal{F}_g^o \cup \partial\mathcal{F}_{gp}^o$  uniqueness follows from the differentiable continuity of  $F$ . Points at which the field points toward the  $\tau_g < 0$  zone were studied in Section 2.1.6.1 where a decoupling argument was used. Otherwise, when available, transversality was used (see Section 2.1.6.2). Finally, the case of a field tangential to  $\partial\mathcal{F}_g^o$  was addressed in Section 2.1.6.3. All cases being addressed, uniqueness is proven.

**2.1.7. A case study.** — While appearing as a limit case of our result (see (H2)), square roots are often used for valve modeling. Uniqueness proof follows along the exact same lines except for the final points addressed in Section 2.1.6.3. Instructively, an alternative study leads to the

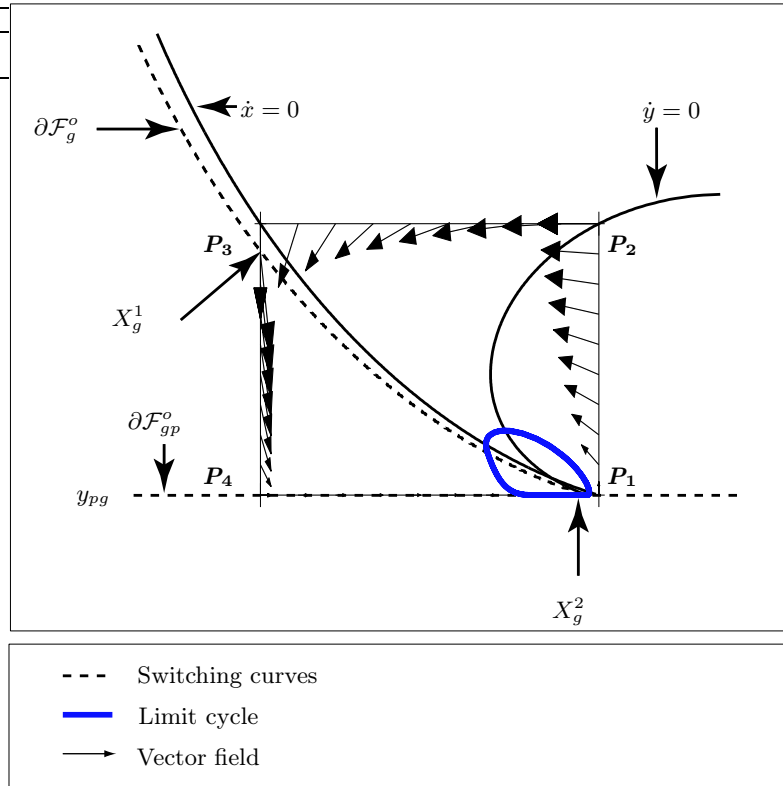


FIGURE 2.7. Limit cycle (in blue) and positive invariant set (rectangle  $P_1P_2P_3P_4$ ) for the sample problem. Switching curves  $\partial\mathcal{F}_g^o$  and  $\partial\mathcal{F}_{gp}^o$  are represented.

conclusion. Let  $\mathcal{X} = \mathcal{Y} \triangleq [5/4 - \sqrt{13/8}, 5/4]$ ,  $\varepsilon = 0.1$  and  $\mu = 2$ . Let

$$\begin{aligned}
 q_{gi}(x, y) &\triangleq \sqrt{2-x} \\
 \tau_g(x, y) &\triangleq 13/8 - (x - 5/4)^2 - (y - 5/4)^2 \\
 \tau_{gp}(x, y) &\triangleq y^{\frac{3}{2}}
 \end{aligned}$$

with  $g_g = g_{gp} \triangleq \sqrt{\max(0, \cdot)}$ . Equilibrium points are unstable with positive real part complex conjugate poles. Hypotheses (H1), (H2), (H3), (H4) are verified. Let us check hypotheses (H5), (H6), (H7) and (H8) (with  $y_{gp} = 0$ )

$$(H5) : \forall x \in \mathcal{X}, \dot{y}(x, \frac{5}{4}) = \sqrt{\frac{13}{8} - (x - \frac{5}{4})^2} - 2(\frac{5}{4})^{\frac{3}{4}} < 0$$

$$(H6) : \dot{x}(5/4, 0) = 0.1\sqrt{3}/2 - 1/4 < 0$$

$$(H7) : \forall x \in \mathcal{X}, \tau_g \left( x, \frac{5}{4} - \sqrt{\frac{13}{8}} \right) = -(x - \frac{5}{4})^2 \leq 0$$

$$(H8) : \forall y \in \mathcal{Y}, \tau_g \left( \frac{5}{4} - \sqrt{\frac{13}{8}}, y \right) = -(y - \frac{5}{4})^2 \leq 0$$

These hypotheses are also verified. Yet,  $\alpha = 1/2$ , thus we substitute Section 2.1.6.3 with the following study. Around  $X_0 = (y_0, 0)$  where the field is tangent to  $\partial\mathcal{F}_g^o$  we have,  $y \sim y_0 + \dot{y}(0)t$  ( $\dot{y}(0) < 0$ ). Equation (15) now yields

$$\dot{z} \sim -B\sqrt{z} + Kt$$

With  $B = -1.93$  and  $K = (E - C\mu 3/4 y_0^{-1/4})\dot{y}(0) = 0.503$ . Using L'Hospital's rule we compute:  $z(t) \sim at^2$ , with  $a = 1.38$ . As  $|e(s)| = o(s^2)$ , equation (16) becomes

$$|e(t)| \leq o(1)e^{b(t-s) + (2 - \frac{1-B}{2\sqrt{a}})\ln \frac{t}{s}}$$

As  $2 - (1 - B)/(2\sqrt{a}) = 0.757$ , letting  $s$  go to 0 implies that  $e(t) = 0$ . Uniqueness is proven. Figure 2.7 shows the construction of the positive invariant set and the limit cycle.

## 2.2. The Density wave instability

As predicted in Section 2.1, the casing-heading takes its origin from the coupling of the tubing and casing dynamics through the gas-lift injection. A simple idea to alleviate this phenomena is to keep the gas injection critical, i.e. independent from the downstream pressure variations. This decoupling can be achieved thanks to a hardware upgrade (new gas-lift gas design). In [42], it is advocated that such newly developed gas-lift valves ensure constant gas flow rate (at constant pressure in the casing) even when tubing pressure is only 10% less than casing pressure. The laterally asymmetric internal geometry of the nozzle-Venturi creates an injection valve that reaches critical flow velocity with pressure differential of only 10%. In [20], engineers from PDVSA report an interesting case study on the installation of such NOVA valves on gas-lift wells. The authors present interesting results in the case of simultaneous variations of casing and tubing pressures. Yet, this technology does not address all possibly encountered cases. Cases where only significant

tubing pressure variations are observed remain unsolved. In [15], some “slugging problem in Brage wells” that “is not casing heading” is also reported. This problem has not been solved by the use of Venturi-type gas-lift valve.

This underlines that, even with a constant gas-lift injection, the dynamics of the well can be unstable. This instability cannot be predicted by the model described by equation (2). The main assumption we have used for its derivation is though very common. It states that the pressure gradient reaches its steady state instantaneously. This is what is also implicitly assumed in [8], [9], [5] and [4]. Yet, this assumption prevents us from representing instabilities characterized by a fluctuation of the gas/liquid ratio in the tubing, such as the one which has been pointed out in [20] and [15]: the density-wave. In this instability, which existence was first demonstrated in [23], oscillations are confined in the tubing while the gas injection rate is constant. Out-of-phase effects between the well influx and the total pressure drop along the tubing are usually reported at the birth of this phenomenon. Figure 2.8 shows an example of a density-wave occurring on a well. This phenomenon is highly periodic, a repeated pattern can be clearly recognized. The observed cycle undoubtedly discards the hypothesis of casing-heading. The pressure at the casing head is almost constant.

In this section, we propose an interpretation of the observed oscillations in the tubing of gas-lifted wells. A distributed parameter model is derived for the propagation of pressure (system (35)). It describes the dynamics as a transport phenomenon with state dependent boundary condition. This equation is shown to be equivalent to a saturated linear delay model (equation (37)) involving the gas fraction. Analysis of the underlying characteristic equation is performed (for unsaturated solutions) and show that the critical parameter is the amount of injected gas. This is consistent with state-of-the-art and suggests a simple control strategy which is developed in Section 3.2.

In Section 2.2.1, we detail the observed density-wave oscillating phenomenon. In Section 2.2.2, we derive a reference distributed delay model for the density propagation in the tubing. Main assumptions and the use of Riemann invariant are explicitated along with boundary conditions.

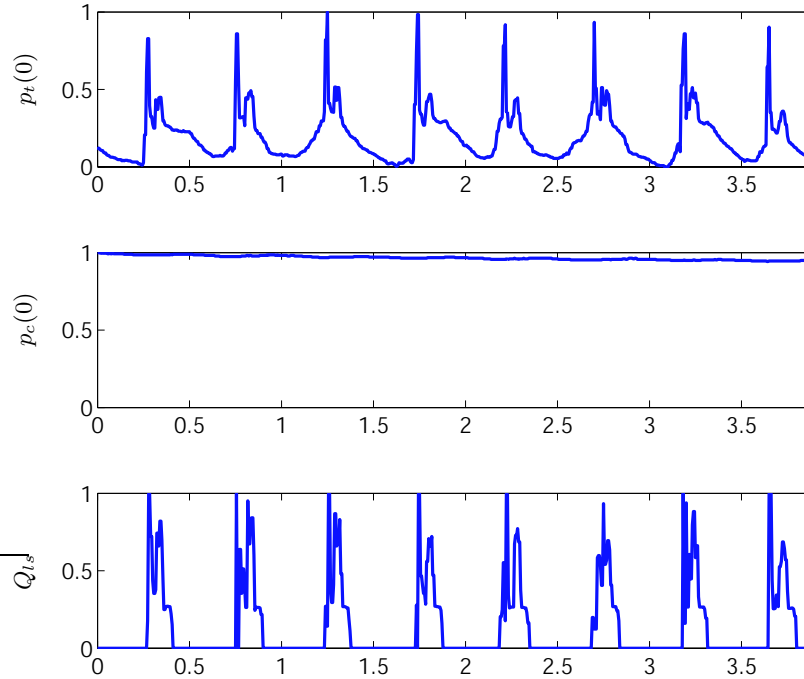


FIGURE 2.8. Density wave occurring on a well. Casing-head and tubing-head pressures (respectively  $p_c(0)$  and  $p_t(0)$ ) are represented as well as oil flow from the separator ( $Q_{ls}$ ). Notice that the casinghead pressure is almost constant, which demonstrates that the gas injection is constant. Scales are omitted for confidentiality reasons (courtesy of TOTAL).

In Section 2.2.3, stability analysis of the corresponding characteristic equations is performed. Comparisons with OLGA<sup>®</sup>2000 are conducted and stress the role of the amount of injected gas. This study has been published in the Conference on Decision and Control, 2005, in Seville (see [39]).

**2.2.1. Density-wave description.** — Figure 2.9 shows an example of density wave instability simulated with the transient multiphase flow simulator OLGA<sup>®</sup>2000. Typically, the depth of the well is 2500 m and the reservoir pressure is 150 bar. Oil production has an oscillating behavior consisting of 3 phases.

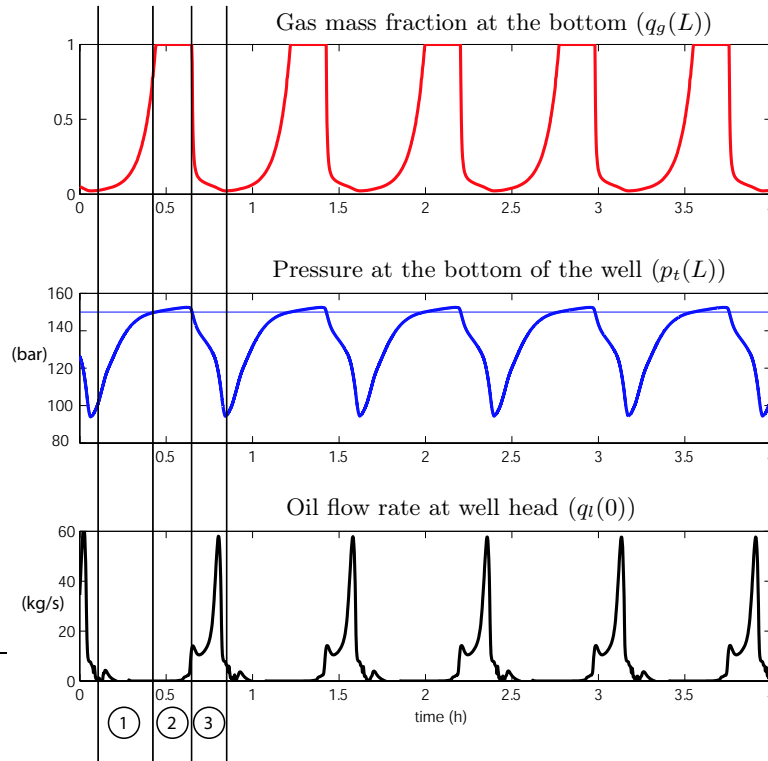


FIGURE 2.9. Density wave simulated with OLGA<sup>®</sup>2000 (numerical set up is given in Appendix A, Table 3).

1. There is no oil production at the surface but  $p_L$ , the pressure at the bottom of the well, is less than the reservoir pressure. Oil enters the pipe, letting  $p_t(L)$  get closer to 150 bar. This is the self regulating mechanism of the well: the more is produced from the reservoir, the greater  $p_t(L)$  becomes and eventually the less is produced.  $p_t(L)$  is going to reach a constant which, in this case, is greater than 150 bar.
2. This phase is characterized by zero oil production at the surface and from the reservoir (saturation of the oil flow rate at the bottom of the well). The gas mass fraction, which is close to 0 in phase 1, gets to a strictly positive constant in phase 2. Finally, the oil produced from the reservoir in phase 1 reaches the surface creating a pressure drop in the well.

3. The pressure  $p_L$  decreases below 150 bar, oil flow rate at the bottom of the well increases and brings the fall of the gas mass fraction.

In words, the density wave can be interpreted as the propagation of the mass fraction at the bottom of the well which is a result of a switching boundary condition. We now propose a mathematical model.

**2.2.2. Proposed Model.** — We propose to study the density wave instability as a two phases flow problem in an one-dimensional vertical pipe filled with a mixture of liquid and gas (see Figure 2.10). The pressure at both ends  $p_r$ , the reservoir pressure and  $p_s$ , the pressure downstream the production choke are considered constant. Liquid flows (oil and water) enter the pipe at the bottom. The flow rate is given by the difference of pressure between the bottom of the pipe and the reservoir. The gas injection rate is considered constant (its value can be arbitrary updated for control purposes). Notations are given in Table 1. Thanks to the choice of the slip velocity law (following [17]), we demonstrate the existence of a Riemann invariant, the gas mass fraction, which we denote  $x$  in the following . This lets the evolution of the distributed variables be summarized by the evolution of a single variable: this gas mass fraction,  $x$ , or equivalently by the evolution of the pressure at the bottom of the pipe,  $p_L(t)$ . Therefore the well is represented by two equivalent modelings. For sake of simplicity, depending on the studied cases, we switch from one to the other modeling.

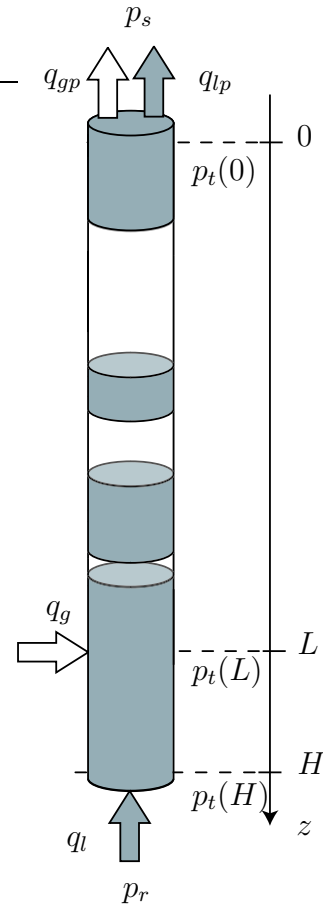


FIGURE 2.10. Scheme of the tubing.

Therefore the well is represented by two equivalent modelings. For sake of simplicity, depending on the studied cases, we switch from one to the other modeling.

2.2.2.1. *Physics reduction.* — We first summarize the main assumptions which are used in the following:

(H'1) : We consider that the friction term in Bernoulli's equation can be neglected in comparison with the gravity term.

(H'2) : The gas velocity is assumed to be constant.

(H'3) : The productivity index is assumed to be also constant, which means that the effluents mass flow rate from the reservoir is proportional to the difference of pressure between the bottom of the well and the reservoir.

(H'4) : The gas volume fraction is close to the gas mass fraction. This assumption arises from the fact that in the density-wave case, at a given depth in the tubing pipe, the mixture is either composed almost only by oil or almost only by gas.

(H'5) : The slip velocity is defined by

$$v_g - v_l = \frac{v_\infty}{r_l}$$

as in [17]. Where  $r_l$  is the oil volume fraction and  $v_g$  and  $v_l$  the gas and oil velocities.

*Pressure law.* — Using Bernoulli's law we get

$$(21) \quad p(t, z) = p_s + \int_0^z \rho_m(t, \zeta) g d\zeta$$

In (21), using assumption (H'1), we have neglected the friction term, it is consistent with the observed low flow rates for density wave instability (see [23]). Density of the mixture is given by

$$1/\rho_m = x/\rho_g + (1-x)/\rho_l$$

To work with a linear expression of  $\rho_m$ , we use assumption (H'4) and we get that

$$(22) \quad \rho_m \sim x\rho_g + (1-x)\rho_l$$

This approximation is quite false for medium values of  $x$  but since we are working with values of  $x$  close to 0 or 1 this assumption is valid. Further, in the derivation of the gas density, gas is considered perfect and the temperature  $T$  is constant. Besides, we assume that the pressure gradient between the injection point and the wellhead is constant and

computed from boundary condition. Notice that  $p_t(\cdot, H) = p_t(\cdot, L) + \rho_l g(H - L)$ . Therefore, we denote  $\bar{p}_r = p_r - \rho_l g(H - L)$  the appearing reservoir pressure. The pressure gradient is thus assumed to be equal to  $\frac{\bar{p}_r - p_s}{L}$ . Simulations have shown that this simplification improves the numerical tractability while saving the oscillatory behavior. Using the expressions in (22) and after substitution in (21), we get

$$(23) \quad p(t, z) = p_s + \rho_l g z + \int_0^z x(t, \zeta) g \left( \frac{(L - \zeta)p_s + \zeta \bar{p}_r}{LRT_t} - \rho_l \right) d\zeta$$

*Slip velocity and Riemann invariant.* — We use assumption (H'5) to define the slip velocity law. Mass conservation laws write

$$(24) \quad \frac{\partial \rho_g r_g}{\partial t} + \frac{\partial \Phi_g}{\partial z} = 0$$

$$(25) \quad \frac{\partial \rho_l r_l}{\partial t} + \frac{\partial \Phi_l}{\partial z} = 0$$

where  $\Phi_g$  and  $\Phi_l$  are respectively the gas and oil mass flux and  $r_g$  the gas volume fraction. Since

$$(26) \quad x = \frac{r_g \rho_g}{r_g \rho_g + r_l \rho_l}$$

one can combine (24), (25) and (26), to obtain

$$\frac{\partial x}{\partial t} + v_g \frac{\partial x}{\partial z} = 0$$

This proves that  $x$  is a Riemann invariant (see [13]). For sake of simplicity we use assumption (H'2) and assume that  $v_g$  is constant. On real wells it is not as simple and we shall discuss the implications of this hypothesis in Section 3.2.1.3. This implies

$$x(t, z) = x \left( t - \frac{L - z}{v_g}, L \right) = x^L \left( t - \frac{L - z}{v_g} \right)$$

Therefore, knowing bottom well gas mass fraction  $t \mapsto x^L(t)$ , we get the profile  $(t, z) \mapsto x(t, z)$  in the tubing. Replacing this expression in equation (23) and denoting  $p_L(t) = P(t, L)$ , we find

$$(27) \quad p(t, L) = p_L^* + \int_{t-\delta}^t k(t - \zeta) x^L(\zeta) d\zeta$$

with

$$(28) \quad \delta = L/v_g$$

$$(29) \quad p_L^* = p_s + \rho_l g L$$

and

$$(30) \quad [0, \delta] \ni t \mapsto k(t) \triangleq V_g g \left( \frac{tp_s + (\delta - t)p_r}{\delta RT_t} - \rho_l \right) < 0$$

Notice that  $k$  is a strictly decreasing affine function.

*Boundary condition.* — Classically, (see [11]), the oil rate  $q_l$  is given at the reservoir boundary by the constant Productivity Index (PI, see assumption (H'3)) through

$$(31) \quad \begin{aligned} q_l(t, H) &= PI \max(p_r - p_t(t, H), 0) \\ &= PI \max(\bar{p}_r - p_t(t, L), 0) \end{aligned}$$

By definition,

$$(32) \quad x^L(t) = \frac{1}{1 + PI/q_g \max(\bar{p}_r - p_L(t), 0)}$$

We want to simplify this last expression in the case of large  $PI$ . On one hand, as  $\bar{p}_r - p_t(L)$  begins to be positive,  $x^L$  goes to zero. Let  $\beta$  denote a threshold parameter. In particular  $x^L < \beta$  is equivalent to  $p_t(L) < \bar{p}_r - \frac{q_g}{PI}(1/\beta - 1)$ . We denote

$$(33) \quad \lambda \triangleq \frac{1}{PI}(1/\beta - 1)$$

On the other hand, when  $p_t(L) > \bar{p}_r$ ,  $x^L = 1$ . Therefore, we consider  $x^L$  as constant, equal to 1 when  $\bar{p}_L > \bar{p}_r$  and equal to 0 when  $p_t(L) < \bar{p}_r - \lambda q_g$ . Finally, the considered expression of  $x^L$  reduces to

$$(34) \quad x^L = h(X), \quad X \triangleq 1 - \frac{\bar{p}_r - p_t(L)}{\lambda q_g}$$

with

$$h(\cdot) = \max(\min(1, \cdot), 0)$$

equation (34) is the definition we use instead of equation (32) from now on.

2.2.2.2. *Density-wave as a distributed delay model.* — We now gather equations (27) and (34), and consider an initial condition  $[-\delta, 0] \ni t \mapsto \phi(t) \in \mathbb{R}$ . The following model represents the density wave phenomenon by the evolution of the pressure at the bottom of the well  $p_L$

$$(35) \quad \begin{cases} p_t(t, L) = p_L^* + \int_{t-\delta}^t k(t-\zeta)h\left(1 - \frac{\bar{p}_r - p_t(\zeta, L)}{\lambda q_g(\zeta)}\right) d\zeta \\ p_t(t, L) = \phi(t), t \in [-\delta, 0] \end{cases}$$

where  $\delta$  is the transport delay defined in (28),  $p_L^*$ , given in (29), is the pressure at the bottom of the pipe when it is full of oil and  $p_r$  is the pressure of the reservoir.  $k$  is an affine function, given in (30). It depends on the considered fluids.  $q_g$  considered is one of the control variable.

2.2.2.3. *Simulation results.* — Figure 2.11 shows the simulations results of (35). When  $p_r = 150$  bar and  $\lambda q_g = 10$  bar, we get an oscillating trajectory which presents similarities with Figure 2.9. Indeed, the periodic behavior consist of 3 phases. Alternatively, out of phase switches of  $h(X(t))$  and  $h(X(t-\delta))$  result in 4 slope changes of  $p_L$ . These reproduce the 3 phases observed in Figure 2.9: oil production from the reservoir (zone 1), followed by a pressure buildup (zone 2), and an eventual pressure drop (zone 3).

2.2.2.4. *Reference model for stability analysis.* — Model (35) is used in Section 3.2.1.1 to design a stabilizing control law  $\lambda q_g$ . To study stability, it is equivalent (but more convenient) to consider  $X$  as defined in equation (34). It follows from (35) that

$$(36) \quad X(t) = 1 - \frac{\bar{p}_r - p_L^*}{\lambda q_g} + \frac{1}{\lambda q_g} \int_{t-\delta}^t k(t-\tau)h(X(\zeta))d\zeta$$

By derivation (assuming  $\lambda q_g$  constant), we get

$$(37) \quad \lambda q_g \dot{X}(t) = k(0)h(X(t)) - k(\delta)h(X(t-\zeta)) + k'(0) \int_{t-\zeta}^t h(X(\zeta))d\zeta$$

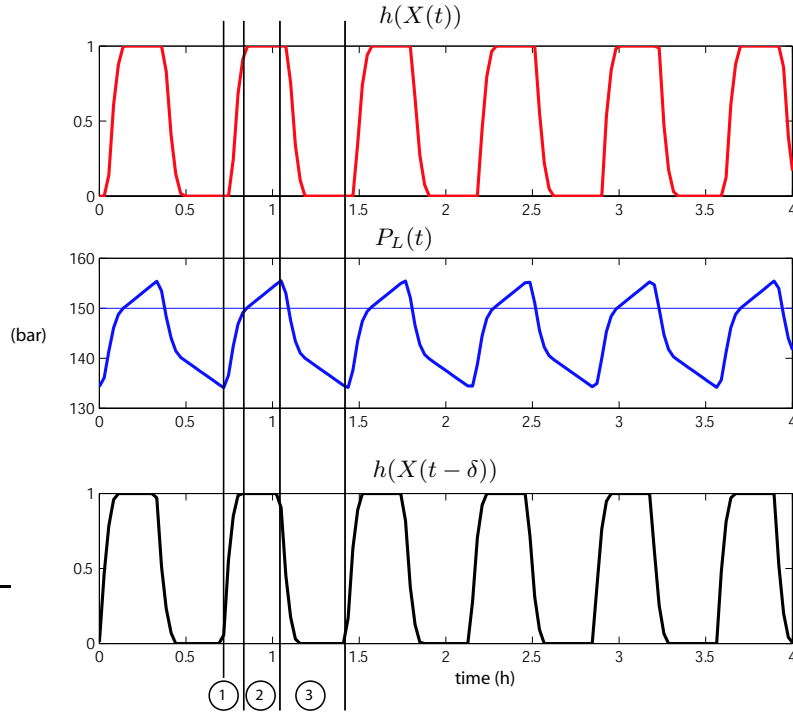


FIGURE 2.11. Density wave simulated with equation (35). The reservoir pressure  $P_r$  is 150 bar and  $\lambda q_g$  is set at 10 bar.

We consider system (37) with an initial condition  $\phi$ , defined and continuous over  $[-\delta, 0]$ , satisfying

$$\phi(0) = 1 - \frac{\bar{p}_r - p_L^*}{\lambda q_g} + \frac{1}{\lambda q_g} \int_{0-\delta}^0 k(t - \zeta) h(\phi(\zeta)) d\zeta$$

For this class of initial conditions, equations (36) and (37) have the same solutions.

**2.2.3. Stability.** — We first study the stability of the trivial solution of the following saturation-free model derived from equation (37). We denote

$$(38) \quad \tau \triangleq \delta / \lambda q_g$$

and  $\mathcal{C}$  the (Banach) space of continuous function mapping the interval  $[-\tau, 0]$  into  $\mathbb{R}$ . We define  $x_t \in \mathcal{C}$  as

$$[-\tau, 0] \ni \theta \mapsto x_t(\theta) = x(t + \theta)$$

By derivation and time scaling, equation (37) rewrites under the form

$$(39) \quad \begin{cases} \dot{x}(t) = f(x_t) \text{ for } t \geq 0 \\ x(t) = \phi(t) \text{ for } t \in [-\tau, 0] \end{cases}$$

with  $\phi \in \mathcal{C}$  and  $f : \mathcal{C} \rightarrow \mathbb{R}$  defined as

$$(40) \quad f(x_t) = ax(t) + bx(t - \tau) + \frac{c}{\tau} \int_{t-\tau}^t x(\zeta) d\zeta$$

with  $a + b + c = 0$ ,  $b > 0$ ,  $c < 0$  and  $b + c > 0$  (by equation (30)). Referring to the formulation used in [21], one can rewrite equation (39) as

$$(41) \quad f(x_t) = \int_{-\tau}^0 d(\eta(\theta))x_t(\theta)$$

with

$$\begin{cases} \eta(\theta) = (c/\tau)\theta, & \theta \in ]-\tau, 0[ \\ \eta(0) = a \\ \eta(-\tau) = -(c + b) \end{cases}$$

As  $\eta$  is continuous on  $]-\tau, 0[$  and has bounded variation on  $[-\tau, 0]$ , given any  $\phi \in \mathcal{C}$ , there exists a unique function  $x_t$ , continuous, that satisfies system (39). We now study stability of (39) through the solutions of its characteristic equation. As will appear, stability depends on  $\tau$ .

*2.2.3.1. Characteristics equation solutions.* — The characteristic equation associated with (39) writes

$$(42) \quad s = a + be^{-s\tau} + \frac{c}{s\tau}(1 - e^{-s\tau})$$

This equation is well defined by continuity at 0 and for all  $\tau \geq 0$ , 0 is an isolated solution. Referring to the necessary condition expressed in [40], as, for all  $\tau \geq 0$

$$\det(\eta(-\tau) - \eta(0)) = -(a + b + c) = 0 \leq 0,$$

the trivial solution is not asymptotically stable.

In the following, we characterize the location of the non zero roots when  $\tau$  increases. In Proposition 1, we exhibit a family  $(\tau_k)_{k \in \mathbb{N}}$  at which two roots simultaneously hit the imaginary axis. Then, we show that, for small  $\tau$ , roots are lying on the left half plane (Proposition 2). Further, proving that the roots cross the imaginary axis from left to right, we conclude towards the existence of  $\tau^* > 0$  (Proposition 3) such that

- for  $\tau \in [0, \tau^*[$ , all roots except 0 have strictly negative real part
- for  $\tau > \tau^*$ , there is at least one root with strictly positive real part.

**Proposition 1.** — *Consider the following system*

$$(43) \quad \dot{x}(t) = ax(t) + bx(t - \tau) + \frac{c}{\tau} \int_{t-\tau}^t x(\zeta) d\zeta$$

with  $a + b + c = 0$ ,  $b > 0$ ,  $c < 0$ ,  $b + c > 0$  and  $\tau > 0$ . Let  $\gamma = c/b$ . There exists  $(\tau_k, \omega_k)_{k \in \mathbb{N}} \in \mathbb{R}^+ \times \mathbb{R}^+$  such that, for  $\tau = \tau_k$ , besides 0 which is always a solution, the pure imaginary roots of the characteristic equation of (43) are  $\pm j\omega_k$ . This family  $(\tau_k, \omega_k)$  is defined by

$$(44) \quad \begin{cases} \cos(\omega_k \tau_k) = 1 + \frac{\gamma \sigma_k}{\sigma_k - (2 + \gamma)} \\ \omega_k \sin(\omega_k \tau_k) = \frac{c \sigma_k (2 + \gamma)}{\sigma_k - (2 + \gamma)} \\ \omega_k^2 = b^2 (2 + \gamma)^2 \left( \frac{-\gamma}{2 + \gamma} \frac{\sigma_k}{\sigma_k - 2} \right) \end{cases}$$

with  $\sigma_k = (2b + c)\tau_k + 2 > 3 + \gamma$ .

*Proof.* — We are now looking for pure imaginary roots of equation (42). If there exists  $\tau \geq 0$  such that  $j\omega$  is solution then  $-j\omega$  is also a solution. Therefore, we restrict our study to  $(\tau, \omega) \in \mathbb{R}^+ \times \mathbb{R}^+ \setminus \{0\}$ . Equation (42) yields

$$(45) \quad \begin{cases} b \cos(\omega\tau) + \frac{c}{\tau\omega} \sin(\omega\tau) = b + c \\ \frac{c}{\tau\omega} \cos(\omega\tau) - b \sin(\omega\tau) = \omega + \frac{c}{\tau\omega} \end{cases}$$

This implies

$$(46) \quad \omega^2 = -\frac{c}{\tau} (2b\tau + c\tau + 2)$$

By construction,  $\gamma \in ]-1, 0[$ . Note  $\sigma = (2b + c)\tau + 2 \geq 0$ . Equation (45) leads to

$$(47) \quad \cos\left(\sqrt{-\frac{\gamma}{2+\gamma}\sigma(\sigma-2)}\right) = 1 + \frac{\gamma\sigma}{(\sigma-2)-\gamma}$$

$$(48) \quad \sin\left(\sqrt{-\frac{\gamma}{2+\gamma}\sigma(\sigma-2)}\right) = \frac{1}{\omega} \frac{c\sigma(2+\gamma)}{\sigma-2-\tau} < 0$$

We derive from inequality (48) that

$$\sigma \in \bigcup_{k \in \mathbb{N}} \left[ 1 + \sqrt{1 + \frac{2+\gamma}{-\gamma}(2k+1)^2\pi^2}, 1 + \sqrt{1 + \frac{2+\gamma}{-\gamma}4k^2\pi^2} \right]$$

Right hand side of equation (47) approaches  $0 < 1 + \gamma < 1$  as  $\sigma$  goes to infinity. The left hand side is oscillating thanks to the cos function and equation (47) has an infinite number of solutions. Among these, we keep those compatible with equation (48) and gather them in  $(\sigma_i)_{i \in \mathbb{N}}$ , an increasing sequence. By construction,

$$\lim_{i \rightarrow \infty} \sigma_i = +\infty$$

and

$$\sigma_i \sim_{i \rightarrow \infty} \sqrt{\frac{2+\gamma}{-\gamma}} 2i\pi$$

Further, for all  $k \in \mathbb{N}$

$$1 + \sqrt{1 + \frac{2+\gamma}{-\gamma}(2k+1)^2\pi^2} > 1 + \sqrt{1 + \pi^2} > 3 + \gamma$$

The set  $(\sigma_i)_{i \in \mathbb{N}}$  is thus bounded by below as follows

$$(49) \quad \forall k \in \mathbb{N}, \quad \sigma_k > 3 + \gamma$$

This set defines a family of solutions of equation (45),  $(\tau_k, \omega_k)_{k \in \mathbb{N}}$  using equation (46), defined by

$$\begin{aligned} \tau_k &= \frac{\sigma_k - 2}{2b + c} \\ \omega_k^2 &= b^2(2 + \gamma)^2 \left( \frac{-\gamma}{2 + \gamma} \frac{\sigma_k}{\sigma_k - 2} \right) \end{aligned}$$

□

**Lemma 3.** — Define  $s(\tau)$  a non zero root of the characteristic equation (42). For all  $\alpha > -1$ ,  $\beta > 0$  and  $\tau_\alpha > 0$  there exists  $\tau \leq \tau_\alpha$  such that

$$|s(\tau)| > \beta\tau^\alpha$$

*Proof.* — By contradiction, assume that one can find  $(\alpha, \tau_\alpha, \beta)$  ( $\alpha > -1$ ,  $\beta > 0$  and  $\tau_\alpha > 0$ ) such that for all  $\tau \leq \tau_\alpha$

$$|s| \leq \beta\tau^\alpha$$

Thus,  $|s\tau| \rightarrow 0$  as  $\tau \rightarrow 0$ . A second order development of (42) yields

$$\frac{1}{\tau} = -b - \frac{c}{2} + \left(\frac{b}{2} + \frac{c}{6}\right) s\tau + o(s\tau)$$

The right hand side of this development goes to  $-b - c/2$  as  $\tau \rightarrow 0$  and the left hand side to  $+\infty$ . This cannot be. Therefore, the assumption is false. This concludes the proof.  $\square$

**Lemma 4.** — Define  $s$  a non zero root of the characteristic equation (42). For all  $\tau_r$ , there exists  $\tau \leq \tau_r$  such that

$$\mathbf{Re}(s(\tau)) < 0$$

*Proof.* — Assume that there exists  $\tau_r$  such that for all  $\tau \leq \tau_r$

$$\mathbf{Re}(s(\tau)) \geq 0$$

It follows that  $|e^{-s\tau}| \leq 1$  and that  $|\frac{1-e^{-s\tau}}{s\tau}| \leq 1$ . Using equation (42) we get

$$|s(\tau)| \leq |a| + |b| + |c|$$

which is in contradiction with Lemma 3.  $\square$

**Proposition 2.** — There exists  $\underline{\tau} > 0$  such that for all  $\tau \leq \underline{\tau}$  the roots of the characteristic equation (42) that are not zero are strictly lying on the left half plane.

*Proof.* — Consider a non zero root. From Proposition 1, we know that, for  $\tau < \tau_1$ , it does not intersect the imaginary axis. Further, we know, from Lemma 4, that there exists  $\tau < \tau_1$  such that the root lies on the left half plane. Since the real part of the root is continuous with respect to  $\tau$  (by the implicit function theorem), the root cannot go to the right part

without crossing the imaginary axis. This implies that, for all  $\tau < \tau_1$  the root is in the left half plane. Finally, for all  $\tau \in [0, \tau_1[$ , all roots except 0 have strictly negative real part. This concludes the proof.  $\square$

**Proposition 3.** — *There exists  $\tau^*$  such that for all  $\tau \in [0, \tau^*[$  the characteristic equation (42) has one root at 0 and all other roots strictly in the left part of the complex plane. For all  $\tau > \tau^*$ , there exists at least one root lying strictly on the right half plane.*

*Proof.* — Let  $\tau$  be positive. As proven in Proposition 2, for small  $\tau$  all roots except 0 lie in the left half plane. To know whether these roots become unstable or come back to the left hand side, we compute  $\text{Re} \frac{\partial s}{\partial \tau} \Big|_{s=\pm j\omega_k}$ . We use equations (44) and after some computations we get

$$\frac{\partial s}{\partial \tau} \Big|_{s=j\omega} = \frac{-b\omega^2 e^{-j\omega\tau} + \frac{c}{\tau^2}(1 - e^{-j\omega\tau}) - \frac{cj\omega}{\tau} e^{-j\omega\tau}}{-2j\omega - b - c + be^{-j\omega\tau} - bj\omega\tau e^{-j\omega\tau} + ce^{-j\omega\tau}}$$

and

$$\text{Re} \frac{\partial s}{\partial \tau} \Big|_{s=\pm j\omega_k} = -\frac{\gamma b^2 (2 + \gamma)^3 (\sigma_k - 3 - \gamma)}{(\sigma_k^2 + (2\gamma^2 - 2 + 5\gamma)\sigma_k - 2\gamma(3 + \gamma)^2)(\sigma_k - 2)}$$

From (49) and noticing that  $\sigma_k^2 + (2\gamma^2 - 2 + 5\gamma)\sigma_k - 2\gamma(3 + \gamma)^2 > 0$  for  $\sigma_k > 2$ , we have

$$\text{Re} \frac{\partial s}{\partial \tau} \Big|_{s=\pm j\omega_k} > 0$$

Therefore, after crossing the imaginary axis the roots always go to the right half plane. Thus simply,  $\tau^* = \tau_1 = \frac{\sigma_1 - 2}{2b + c}$ .  $\square$

**2.2.3.2. Conclusion.** — Parameter  $\tau$  has a direct impact on the roots location of the characteristic equation. Increasing the time delay  $\tau$  or letting the roots be unstable are equivalent. Recalling  $\tau = \frac{\delta}{\lambda q_g}$ , this last remark means that there exists a minimal gas injection rate that guarantees stability of the roots. Study of the characteristic equation is a key to the interpretation of the observed oscillating behavior. Depending on  $\lambda q_g$  trajectories of model (37) behave as follows. Unstable solutions of the model (37), which, initially match with unstable solutions of a linear system of type (40), finally reach saturation yielding behaviors depicted in Figure 2.11. Stable solutions remain bounded and if the

initial condition is well chosen (e.g. constant) they do not reach the saturation.

#### 2.2.4. Physical interpretation: the role of the gas expansion.

— We now give some physical insights on equation (40). The three parameters of this equation are closely related with the difference of gas and oil density between the top and the bottom of the well. More precisely, we demonstrate that without the gas density gradient in the tubing, i.e. the gas expansion, the density wave would not exist.

Coefficients  $a$ ,  $b$  and  $c$  of the characteristic equation (42) express in term of physical parameters. Recalling (30),

$$\begin{aligned} a &= k(0) = v_g g \left( \frac{p_r}{RT_t} - \rho_l \right) \\ b &= -k(\delta) = v_g g \left( \rho_l - \frac{p_s}{RT_t} \right) \\ c &= \delta k'(0) = v_g g \left( \frac{p_s}{RT_t} - \frac{p_r}{RT_t} \right) \end{aligned}$$

We notice that the key parameters of equation (42) all are proportional to difference of densities. This implies, from the analysis presented in Section 2.2.3 that stability depends on difference of densities between oil and gas and on the gas expansion.

We now show the key role played by the gas expansion term. Let us completely ignore it. This means that  $\rho_g(0) \sim \rho_g(H)$  or equivalently that  $a = b$  and  $c = 0$ . In these circumstances, the dynamics of the gas mass fraction at the bottom of the well is described by

$$(50) \quad x(t) = x_0 - a \int_{t-\tau}^t h(x(\theta)) d\theta$$

Where  $a$ ,  $x_0$  and  $\tau$  are strictly positive real numbers.

*Change of variable.* — A change of variable yields ( $t \leftarrow at$ ,  $\tau \leftarrow a\tau$  and  $x(t) \leftarrow x(t/a)$ ).

$$(51) \quad x(t) = x_0 - \int_{t-\tau}^t h(x(\theta)) d\theta$$

Following [21], it is possible to rewrite this equation under the form

$$(52) \quad \begin{cases} \dot{x}(t) = -h(x(t)) + h(x(t - \tau)) \\ x(t) = \phi(t) \text{ for } t \in [-\tau, 0] \end{cases}$$

provided

$$\phi(0) + \int_{-\tau}^0 h(\phi(\theta)) d\theta = x_0$$

Let us note  $x_t: [-\tau, 0] \ni 0 \mapsto x_t(\theta) = x(t + \theta) \in \mathbb{R}$  and

$$(53) \quad f(x_t) \triangleq -h(x(t)) + h(x(t - \tau))$$

We now study the properties of solutions of equation (52).

*Existence and uniqueness of solutions.* — Let us show that  $f$  is a Lipschitz function. We define the following norm over the set of continuous functions mapping  $\phi: [-\tau, 0] \mapsto \mathbb{R}$

$$(54) \quad \|\phi\| = \int_{-\tau}^0 |\phi(\theta)| d\theta + |\phi(0)| + |\phi(-\tau)|$$

Since  $h$  is a Lipschitz function (its Lipschitz constant equals one), we deduce that  $f$  is also Lipschitz through the following simple calculations

$$\begin{aligned} \|f(x_t) - f(x'_t)\| &= |h(x(t)) - h(x(t'))| + |h(x(t - \tau)) - h(x(t' - \tau))| \\ &\quad + \int_{-\tau}^0 |h(x(\theta)) - h(x(\theta - \tau))| d\theta \\ &\leq |x(t) - x(t')| + |x(t - \tau) - x(t' - \tau)| + \int_{-\tau}^0 |x(\theta) - x(\theta - \tau)| d\theta \\ &\leq \|x_t - x'_t\| \end{aligned}$$

Then, uniqueness of solutions follows from [21, 2.3]. In particular, notice that, given  $\phi$  such as  $\phi \geq 1$ , the trajectory  $x(t) = \phi(0)$  is a solution. We conclude that, if the trajectory remains saturated longer than  $\tau$ , it remains saturated forever.

We now show that, for any given initial condition, the trajectory converges to a constant equilibrium point. We first show that the trajectory

is either after some times between 0 and 1 (which means that equation (53) is simply linear) or, permanently, above 1 (and thus always saturated). The proof consists in two cases depending on the initial condition. Convergence is proven by use of Lyapunov function.

We first show that if the trajectory enters the  $(0, 1)$  interval it remains there.

**Lemma 5.** — *Assume that there exists  $a > 0$  such that  $x(a) \in (0, 1)$ , then, for all  $t \geq a$ ,  $x(t) \in (0, 1)$*

*Proof.* — Assume that the trajectory exits  $(0, 1)$ . First assume the exit point is 1 and consider  $b$  such that  $x(b) = 1$  and, for all  $t \in (a, b)$ ,  $x(t) \in (0, 1)$ .

$$\dot{x}(t) \leq -x(t) + 1$$

Then, applying Gronwall's lemma one gets

$$x(t) \leq x(a)e^{a-t} + \int_a^t e^{\theta-t} d\theta$$

So,

$$x(t) \leq 1 - (1 - x(a))e^{a-t} < 1$$

In particular for,  $t = b$ ,

$$x(b) < 1$$

This contradiction shows that the trajectory can not exit the  $(0, 1)$  interval by passing through 1. Following along the same lines, one can show that there does not exist  $b > a$  such that  $x(b) = 0$ .  $\square$

Now, we exhibit a condition under which a trajectory, such that  $\phi(0) \geq 1$ , ends in the  $(0, 1)$  interval.

**Lemma 6.** — *Let  $\phi$  be an initial condition of equation (52) such that  $\phi(0) \geq 1$ . There exists  $a$  such that  $x(a) \in (0, 1)$  if and only if*

$$(55) \quad \int_{-\tau}^0 (1 - h(\phi(\theta))) d\theta > \phi(0) - 1$$

*Proof.* — Assume that, for all  $t \in [0, \tau]$ ,  $x(t) \geq 1$ . Thus  $h(x(t)) = 1$ . This assumption is consistent with  $\phi(0) \geq 1$ . Compute

$$\begin{aligned} x(\tau) &= x_0 - \int_0^\tau h(x(\theta))d\theta \\ &= \phi(0) - \int_0^\tau h(x(\theta))d\theta + \int_{-\tau}^0 h(\phi(\theta))d\theta \\ &= \phi(0) - \int_{-\tau}^0 1 - h(\phi(\theta))d\theta \end{aligned}$$

Referring to the inequality (55), we get  $x(\tau) < 1$ , which prevents  $x$  from remaining above 1 over the interval  $[0, \tau]$ . Therefore, there exists  $t_0 \in (0, \tau]$  such that  $x(t_0) < 1$ . Since  $x$  is a continuous function,  $x(0) \geq 1$  and  $x(t_0) < 1$  imply that there exists  $a \in (0, \tau]$  such that  $x(a) \in (0, 1)$ .

Conversely, let us assume that inequality (55) does not hold. Then

$$(56) \quad \int_{-\tau}^0 (1 - h(\phi(\theta)))d\theta \leq \phi(0) - 1$$

Assume that there exists  $b \in (0, \tau]$  such that  $x(b) < 1$ . We have

$$\begin{aligned} x(b) &= \phi(0) - \int_{-\tau}^{b-\tau} 1 - h(x(\theta))d\theta \\ &= \phi(0) + \int_{b-\tau}^0 1 - h(x(\theta))d\theta - \int_{-\tau}^0 1 - h(\phi(\theta))d\theta \end{aligned}$$

Applying inequality (56) one gets

$$x(b) \geq 1 + \int_{b-\tau}^0 1 - h(x(\theta))d\theta \geq 1$$

Again, this is in contradiction with our assumption, thus, for all  $b \in (0, \tau]$ ,  $x(b) \geq 1$ . This concludes the proof.  $\square$

At last we prove that for any initial condition the trajectory converges to an equilibrium value.

**Proposition 4.** — *For any initial condition  $\phi$ , the trajectory  $x$  of equation (53) asymptotically converges to  $\bar{x}$  when  $t$  goes to  $+\infty$ .*

1. *More precisely, if  $\phi(0) \in (0, 1)$ , then  $\bar{x} = x_0/(1 + \tau)$*

2. If  $\phi(0) \geq 1$

(a) If

$$\int_{-\tau}^0 (1 - h(\phi(\theta))) d\theta \geq \phi(0) - 1$$

then

$$\bar{x} = x_0 - \tau \geq 1$$

(b) else

$$\bar{x} = \frac{x_0}{1 + \tau}$$

$$\text{with } x_0 = \phi(0) + \int_{-\tau}^0 h(\phi(\theta)) d\theta$$

*Proof.* — According to Lemma 5, we know that in the (2.a) case, since  $x(t)$  always remains greater or equal to 1 during a period at least equal to  $\tau$ , the trajectory reaches a constant value  $\bar{x}$ . This value can be computed thanks to the integral expression (51). One easily gets  $\bar{x} \geq 1$ .

According to Lemma 6, we know that in the (2.b) case, one can find  $a$  such that  $x(a) \in (0, 1)$ . This proves that, for all  $t > a$ ,  $x(t) \in (0, 1)$ . Equation (53) is autonomous, therefore we can address this case together with case (1).

Assuming that  $\phi(0) \in (0, 1)$ , after some time, equation (55) reduces to

$$\dot{x} = -x(t) + x(t - \tau)$$

Using this last form, we can show that the trajectory eventually converges towards  $\bar{x} = x_0/(1 + \tau)$ . The proof relies on the following Lyapunov function candidate

$$V(\phi) = (\phi(0) - \bar{x})^2 + \int_{-\tau}^0 (\phi(\theta) - \bar{x})^2 d\theta$$

Simple calculation gives

$$\begin{aligned} \dot{V}(\phi) &= -2X(X - Y) + X^2 - Y^2 \\ &= -(X - Y)^2 \leq 0 \end{aligned}$$

where  $X = \phi(0) - \bar{x}$  and  $Y = \phi(-\tau) - \bar{x}$ . According to [21, Theorem 2.1],  $\bar{x}$  is stable. To show asymptotic stability, we use LaSalle's Theorem. We know that the trajectory eventually converges towards

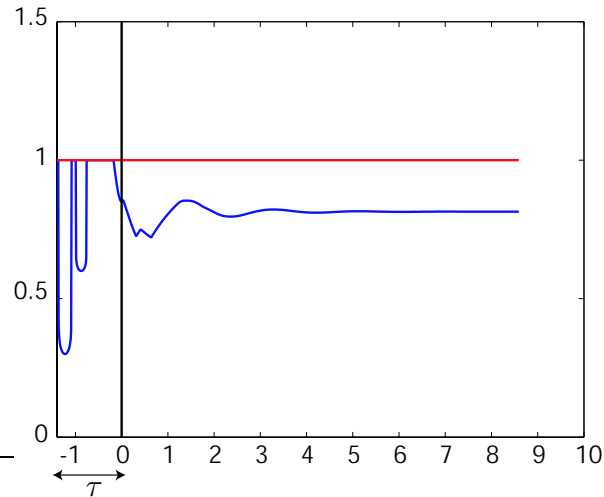


FIGURE 2.12. Case (1) :  $\phi(0) \in (0,1)$ . The trajectory converges towards a constant also comprised between 0 and 1.

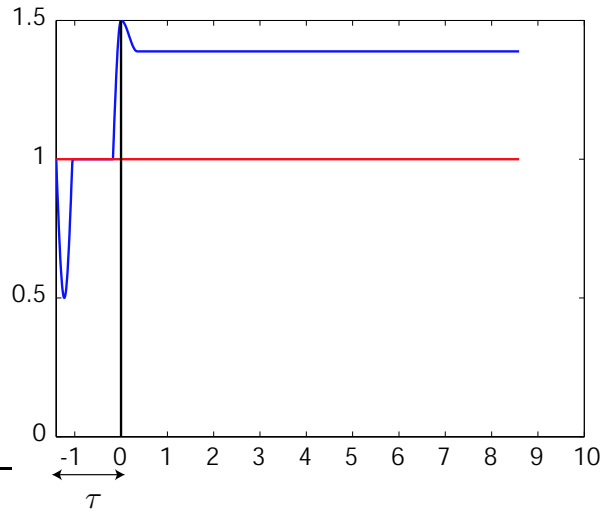
the largest invariant set included in  $\{\phi \mid \dot{V}(\phi) = 0\}$ , i.e. the set of constant trajectories. Moreover, the only constant consistent with the initial condition  $\phi$  is  $\bar{x}$ . We conclude that  $\bar{x}$  is asymptotically stable.  $\square$

We have proven that without gas expansion the well would not suffer from instability. The integral term in the equation (36) is thus necessary for proper modeling of the density-wave.

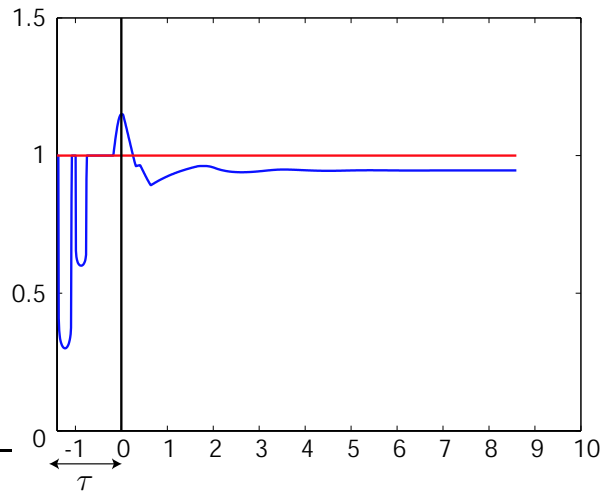
Further studies have been done on this subject. Based on the same Lyapunov approach, [30] has derived a sufficient condition for the complete linearized equation (43) to be stable. This result is in accordance with what is presented in paragraph 2.2.3. Moreover, this approach give some insight to a possible extension to nonlinear equation (37).

### 2.3. Global study of unstable phenomena

In this section we finally study the well as an interconnected system without neglecting neither the propagation phenomenon in the tubing (as was done in Section 2.1) nor the buffer effect of the casing (as was done in Section 2.2). We exhibit and justify the impact of design parameters



(a)  $\phi(0) \geq 1$ . Condition (55) is not satisfied. The trajectory converges towards a constant greater than 1.



(b)  $\phi(0) < 1$ . Condition (55) is satisfied. The trajectory converges towards a constant comprised between 0 and 1.

FIGURE 2.13. Cas 2. Depending on whether the Condition (55) is satisfied the trajectory converge between 0 and 1 or above 1.

such as well depth, tubing diameter, and the role of physical parameters such as reservoir pressure of Productivity Index.

Understanding the implications of choices made at the design-stage in the development of instability has concentrated a lot of research efforts. General stability criteria have been proposed. Some, such as [44], rely on steady state curves but most of the published work is based on a dynamical system study.

In [6], the key assumption is that stability is guaranteed if an increase of downhole tubing pressure causes a drop of mixture density and if the gas pipe depletes faster than the tubing pressure. Then, differential equations are used to derive a criterion taking the form of a set of inequalities. A more dynamical system oriented approach can be found in [8]. The analysis relies on Routh's criterion and a detailed study of the root locations of a third order transfer function when physical parameters of interest vary. In [4], a unified criteria based on previous studies of [8] and [6] is proposed. In all these works the oil column is considered homogeneous, which implicitly neglects the propagation phenomenon in the tubing. These models are mainly devoted to the study of casing-heading for which this simplifying assumption is particularly valid.

Our contribution here is to show that the well can be modeled as the feedback connection of a distributed parameter system (the tubing considered in Section 2.2) and a stable first order system (the casing as a buffer tank, considered in Section 2.1). This approach aims at encompassing both casing-heading and density-wave phenomena. The connection of casing and tubing subsystems is achieved through the injection valve, which is modeled with a saturation function. This seemingly cascaded system contains feedback loops at two different levels. The first loop appears in the tubing itself through the gravity terms in Bernoulli's law. The second loop takes place by means of the state dependent connecting term (injection valve) which serves as an input for the propagation equation. Stability of each subsystem is characterized. Additionally, input-output gains are computed and the small gain theorem allows us to conclude towards stability of the whole system when the asymptotic condition of large amount of injected gas holds. This analysis is in accordance to experimental observations. It stresses the contribution of each

subsystem design parameters and operating points to the stability of the global system.

In Section 2.3.1, we study the tubing subsystem and conclude on a sufficient condition for stability. In particular, we detail the role of various parameters in our proposed model and show the consistency with some state of the art wells production knowledge. In Section 2.3.2, we connect the casing dynamics to the tubing, and study the obtained interconnection's stability through the small gain theorem. We propose the interpretation of well-known phenomena at the light of our model. In conclusion, the density-wave phenomenon is interpreted as the stability loss due to the internal tubing feedback loop. Besides, the casing-heading phenomenon arises from the interconnection of the two systems.

The work in this section has appeared at the American Control Conference, in June 2006 under the title "Predicting instabilities in gas-lifted wells simulation" ([38]).

### 2.3.1. Tubing Analysis. —

*2.3.1.1. Equilibrium point and stability analysis.* — Remembering that the parameter  $u$  in equation (35) is proportional to the gas injection flow rate in the tubing  $q_g$ , one gets

$$(57) \quad \left\{ p_t(t, L) = p_L^* + \int_0^\delta k(\zeta)h \left( 1 - \frac{\bar{p}_r - p(t - \zeta, L)}{\lambda q_g(t - \zeta)} \right) d\zeta \right.$$

Given a constant input  $\bar{q}_g$ , the unsaturated equilibrium  $\bar{p}_t(L)$  can be computed through the integral equation (57).

$$\bar{p}_t(L) = p_L^* + \left( 1 - \frac{\bar{p}_r - \bar{p}_t(L)}{\lambda q_g} \right) \int_0^\tau k(\zeta) d\zeta$$

yielding

$$(58) \quad \bar{p}_t(L) = \frac{\lambda \bar{q}_g (p_L^* + \int_0^\tau k(\zeta) d\zeta) - \bar{p}_r \int_0^\tau k(\zeta) d\zeta}{\lambda \bar{q}_g - \int_0^\tau k(\zeta) d\zeta}$$

Linearization of the dynamics of (57) around the steady value of the input and state  $(\bar{q}_g, \bar{p}_t(L))$  yields

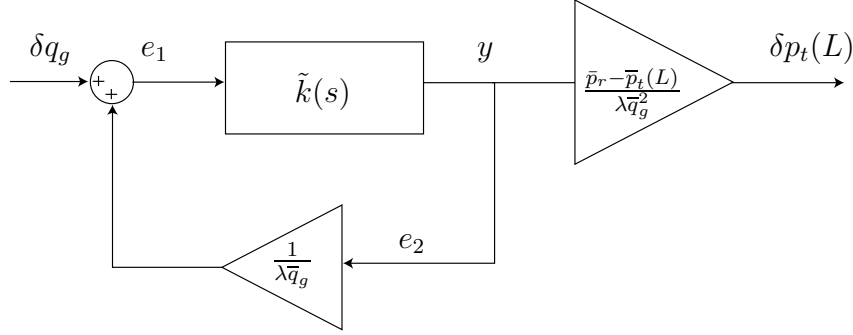


FIGURE 2.14. Block scheme of the tubing subsystem linearized around an equilibrium point. Gravitational effects of the non-homogeneous fluid column take the form of an inner positive feedback loop.

(59)

$$\delta p_t(t, L) = \frac{1}{\lambda \bar{q}_g} \int_0^\tau k(\zeta) \delta p_t(t - \zeta, L) d\zeta + \frac{\bar{p}_r - \bar{p}_t(L)}{\lambda \bar{q}_g^2} \int_0^\tau k(\zeta) \delta q_g(t - \zeta) d\zeta$$

Denoting  $\delta \tilde{p}_t(L)$  and  $\delta \tilde{q}_g$  the Laplace transforms of  $\delta p_t(L)$  and  $\delta q_g$  respectively, one gets

$$(60) \quad \delta \tilde{p}_t(s, L) = G(s) \delta \tilde{q}_g(s)$$

with

$$(61) \quad G(s) = \frac{\bar{p}_r - \bar{p}_t(L)}{\lambda \bar{q}_g^2} \frac{\tilde{k}(s)}{1 - \frac{\tilde{k}(s)}{\lambda \bar{q}_g}}, \quad \tilde{k}(s) = \int_0^\tau k(\zeta) e^{-s\zeta} d\zeta$$

Through this rewriting, the linearized dynamics of the tubing appears as a positive feedback connection (see Figure 2.14) which stands for the gravitational effects of the nonhomogeneous fluid column. To study its stability, we first note the finite gain stability of  $\tilde{k}(s)$  and then conclude using the small gain theorem.

In the following, we denote  $\|\cdot\|$  any  $\mathcal{L}_p$  norm.

**Proposition 5.** — *With the notations given in Figure 2.14, there exists a positive constant  $\gamma_k$  such that*

$$(62) \quad \|y\| \leq \gamma_k \|e_1\|$$

*Proof.* — We compute

$$\|k\|_{\mathcal{L}_1} = \frac{|k_1|\tau^2}{2} + |k_2|\tau < +\infty$$

Denoting  $\gamma_k = \|k\|_{\mathcal{L}_1}$  and referring to [14][Lemma A.6.5] we directly derive equation (62).  $\square$

**Proposition 6.** — *With the notations given in Figure 2.14, there exists a positive constant  $\bar{q}_g^{min}$  and  $\gamma' : [\bar{q}_g^{min}, +\infty[ \ni \bar{q}_g \mapsto \mathbb{R}^+ \setminus \{0\}$ , bounded and continuous, such that*

$$(63) \quad \|\delta p_t(L)\| \leq \gamma'(\bar{q}_g)\|\delta q_g\|$$

Moreover,  $\lim_{+\infty} \gamma' = 0$ .

*Proof.* — Recalling notations given in Figure 2.14, we get

$$e_1(t) = \delta q_g(t) + \frac{1}{\lambda \bar{q}_g} y(t)$$

Proposition 5 yields

$$(64) \quad \|e_1\| \leq \|\delta q_g\| + \frac{1}{\lambda \bar{q}_g} \gamma_k \|e_1\|$$

Define  $\bar{q}_g^{min} > \frac{\gamma_k}{\lambda}$ . For all  $\bar{q}_g > \bar{q}_g^{min}$ , we can write  $\|e_1\| \leq \frac{1}{1 - \frac{\gamma_k}{\lambda \bar{q}_g}} \|\delta q_g\|$  and thus,

$$\|p_t(L)\| \leq \frac{\bar{p}_r - \bar{p}_t(L)}{\lambda \bar{q}_g^2} \frac{\gamma_k}{1 - \frac{\gamma_k}{\lambda \bar{q}_g}} \|\delta q_g\|$$

Finally, replacing  $\bar{p}_t(L)$  by its expression (58) and noting that  $\gamma_k = -\int_0^\tau k(\zeta) d\zeta$  gives

$$\|p_t(L)\| \leq \left( \int_0^\tau -\lambda k \right) \frac{\bar{p}_r - p_t(L)^* - \int_0^\tau k}{(\lambda \bar{q}_g)^2 - \left( \int_0^\tau k \right)^2} \|\delta q_g\|$$

Therefore, we get the desired result with

$$(65) \quad \gamma'(\bar{q}_g) = \left( \int_0^\tau -\lambda k \right) \frac{\bar{p}_r - p_t(L)^* - \int_0^\tau k}{(\lambda \bar{q}_g)^2 - \left( \int_0^\tau k \right)^2}$$

And  $\lim_{+\infty} \gamma' = 0$ .  $\square$

*2.3.1.2. Conclusion and discussion on stability of the tubing.* — Clearly, the preceding derivation follows along the lines of the proof of the small-gain theorem (as exposed in [27]). If two systems are finite-gain stable and if the product of their gain is small enough (smaller than 1) the system resulting from their connection is also finite gain stable. Recalling that  $\gamma_k$  derives from the integration of equation (30), here, the condition that guarantees stability is

$$(66) \quad \frac{\gamma_k}{\lambda \bar{q}_g} = \frac{Lg}{RT\lambda \bar{q}_g} \left( RT\rho_l - \frac{1}{2}(\bar{p}_r + p_s) \right) < 1$$

From this, we can analyze the impact of several parameters on the behavior of the subsystem.

Increasing  $\bar{q}_g$  tends to lower the gain. Therefore, there exists a lower bound on gas injection rate that guarantees stability. This is consistent with the experimental conclusions found in [23]. These are based on OLGA<sup>®</sup>2000 simulations. In the same study, it also appears that an increase of reservoir pressure leads to more stability. Again, from equation (66), we conclude to the same result. We report in Figure 2.15, tests done with values for  $\bar{p}_r$  ranging from 150 to 220 bar. At  $P_r = 220$  bar, the system is eventually stable. We note that it is a marginal effect compared to an increase of the gas injection rate. This analysis provides some insights for middle to long-term aging phenomenon of reservoirs when pressure tends to decrease with time.

Further studies reveal that a decrease of  $\rho_l$  or  $L$  provides more stability. On the other hand, an increase of  $\lambda$  achieved through a decrease of  $PI$  tends to improve stability. These parameters are known for their stabilizing effects and can be taken into account at the design stage, e.g. to forecast instability issues.

We notice that the well-known fact that choking has a stabilizing effect is once again verified (see [16] and [23]): by increasing  $p_s$  we can let the gain in (66) be smaller than 1. This is one of the key idea behind the FCW controller (see Chapter 3 for more details). In fact, choking can be used in open loop or closed loop to reach unstable points (see [37]).

Quite surprisingly, parameters such as velocity and tubing diameter do not appear in equation (66). This is due to our simplifying assumptions. In fact, both impact on stability through the definition of flow regimes,

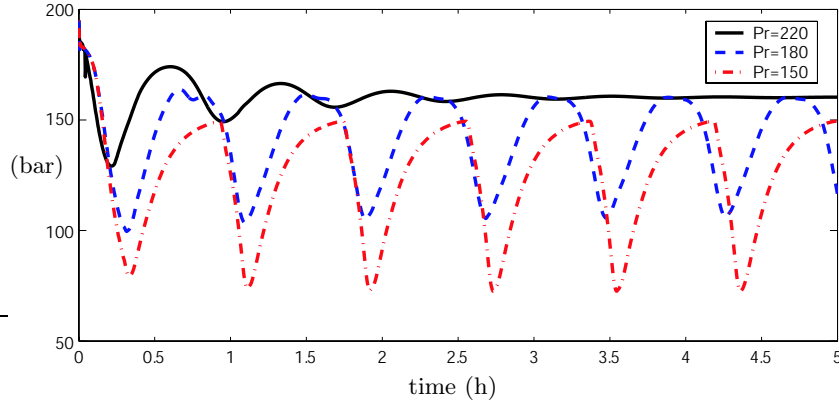


FIGURE 2.15. Simulation in OLGA<sup>®</sup>2000 of the impact of the pressure reservoir on the stability of the well.

e.g. bubbly or slug flow (see [12]). We have restricted our study to a single slip velocity law. Our model does not represent changes in flow regime and thus does not address hydrodynamic slug instability (see [12]). This could be a direction of future work.

Moreover, using the small gain theorem is a conservative approach. It does not provide an exact value for the turning point from stability to instability. A closer study of the location of the roots of the characteristic equation underlying (59) is needed. Such a study is performed in [39], dealing with the impact of the gas injection rate and quantitatively showing that below a computable limit the roots are located in the left half plane.

**2.3.2. Stability analysis with a connected casing.** — Casing and tubing, presented in Figure 1.2 are connected according to the scheme in Figure 2.17. While each of these blocks can independently be stable, the resulting connected system may be unstable. Therefore, even under the formal assumption that guarantees the absence of density-wave instability, casing-heading can still occur. Again, feedback connection plays a key role. For the casing, we use a simple first order model (the first equation of the 3D model exposed in (2) and perform an analysis. Among several conclusions, it appears that large amounts of gas prevent casing-heading instability.

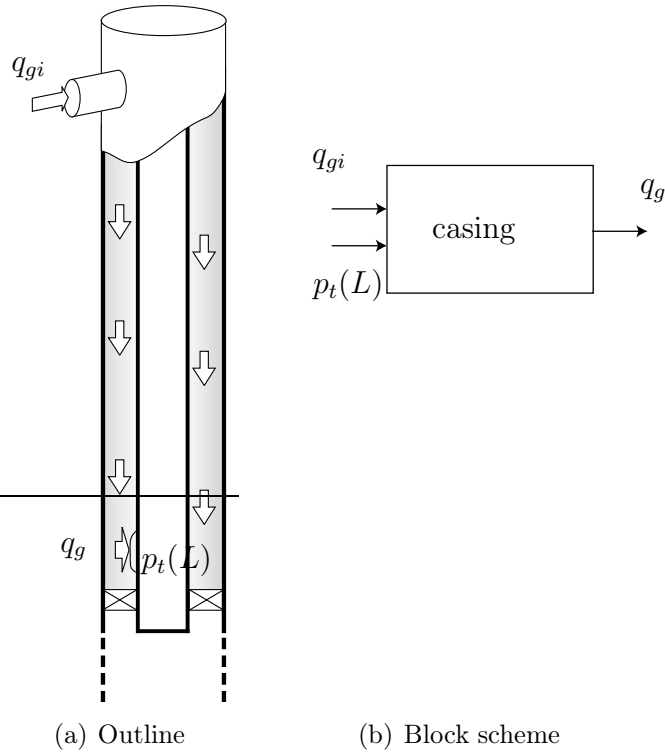


FIGURE 2.16. (a) Outline of the casing. (b) The inputs of the system are the gas mass injection rate  $q_{gi}$  and the boundary condition  $p_t(L)$  (the downhole pressure). The output is the gas rate entering the tubing:  $q_g$ .

*2.3.2.1. Casing model.* — A casing can be considered as an annular buffer filled with gas from a gas network (see Figure 2.16).

Assuming that the gas is ideal and that the column is at equilibrium, we get

$$(67) \quad \rho_c(0) \triangleq \alpha m_1 \text{ and } p_c(0) \triangleq \beta m_1$$

where  $\alpha$ ,  $\beta$  are defined by

$$(68) \quad \alpha RT = \frac{g}{S_c} \frac{1}{1 - \exp\left(-\frac{gL_c}{RT}\right)} = \beta$$

We consider as model the mass balance equation in the annulus volume

$$(69) \quad \begin{cases} \dot{m}_1 = q_{gi} - q_g(m_1, p_t(L)) \\ q_g(m_1, p_t(L)) = C_g \sqrt{\alpha m_1 \max(\beta m_1 - p_t(L), 0)} \end{cases}$$

*2.3.2.1.1. Stability analysis and equilibrium point definition.* — We assume normal flowing conditions, i.e. the pressure in the casing is sufficient to counteract  $\bar{p}_t(L)$  and to let the gas flow out. Given constant input values  $\bar{q}_{gi}$  and  $\bar{p}_t(L)$ , the equilibrium point is

$$(70) \quad \bar{m}_1 = \frac{1}{\beta} \left( \bar{p}_t(L) + \sqrt{\bar{p}_t(L)^2 + 4 \frac{\bar{q}_{gi}^2}{\alpha \beta C_g^2}} \right)$$

Linearization of equation (69) yields, for constant input  $q_{gi}$ ,

$$(71) \quad \begin{cases} \delta \dot{m}_1 = -\frac{\partial q_g}{\partial m_1}(\bar{q}_{gi}, \bar{p}_t(L)) \delta m_1 - \frac{\partial q_g}{\partial p_t(L)}(\bar{q}_{gi}, \bar{p}_t(L)) \delta p_t(L) \\ \delta q_g = \frac{\partial q_g}{\partial m_1}(\bar{q}_{gi}, \bar{p}_t(L)) \delta m_1 + \frac{\partial q_g}{\partial p_t(L)}(\bar{q}_{gi}, \bar{p}_t(L)) \delta p_t(L) \end{cases}$$

with

$$(72) \quad \frac{\partial q_g}{\partial m_1}(\bar{q}_{gi}, \bar{p}_t(L)) = \frac{C_g^2 \alpha}{2 \bar{q}_{gi}} \sqrt{\bar{p}_t(L)^2 + \frac{4 \beta \bar{q}_{gi}^2}{\alpha C_g^2}}$$

$$(73) \quad \frac{\partial q_g}{\partial p_t(L)}(\bar{q}_{gi}, \bar{p}_t(L)) = -\frac{C_g^2 \alpha}{4 \beta \bar{q}_{gi}} \left( \bar{p}_t(L) + \sqrt{\bar{p}_t(L)^2 + \frac{4 \beta \bar{q}_{gi}^2}{\alpha C_g^2}} \right)$$

**Proposition 7.** — For  $\bar{q}_{gi} > 0$  the equilibrium point of (71) is exponentially stable. Therefore, the linearized system (71) is finite gain stable. One can find  $(\gamma, \mu) : (\mathbb{R} \setminus \{0\})^2 \mapsto (\mathbb{R}^+ \setminus \{0\})^2$ , bounded and continuous, such that

$$(74) \quad \|\delta q_g\| \leq \gamma(\bar{q}_{gi}, \bar{p}_t(L)) \|p_t(L)\| + \mu(\bar{q}_{gi}, \bar{p}_t(L))$$

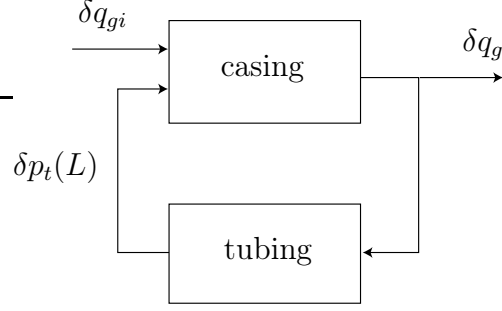


FIGURE 2.17. Block scheme of the interconnected systems linearized around an equilibrium point.

These functions are

$$(75) \quad \gamma = \frac{C_g^2 \alpha}{2\bar{q}_{gi}} \sqrt{\bar{p}_t(L)^2 + \frac{4\beta \bar{q}_{gi}^2}{\alpha C_g^2}}$$

$$(76) \quad \mu = m_1(0) \sqrt{\frac{C_g^2 \alpha}{8\beta \bar{q}_{gi}} \left( \bar{p}_t(L) + \sqrt{\bar{p}_t(L)^2 + \frac{4\beta \bar{q}_{gi}^2}{\alpha C_g^2}} \right)}$$

*Proof.* — By assumption, the equilibrium point is such that  $\bar{q}_{gi} > 0$ , then

$$-\frac{\partial q_g}{\partial m_1}(\bar{q}_{gi}, \bar{p}_t(L)) < 0$$

Using explicit formulas given in [27][Corollary 5.2] for linear systems, we can write (74) with

$$\begin{aligned} \gamma(\bar{q}_{gi}, \bar{q}_g) &= 2 \left| \frac{\partial q_g}{\partial p_t(L)}(\bar{q}_{gi}, \bar{p}_t(L)) \right| \\ \mu(\bar{q}_{gi}, \bar{q}_g) &= \frac{1}{\sqrt{2}} m_1(0) \sqrt{\frac{\partial q_g}{\partial m_1}(\bar{q}_{gi}, \bar{p}_t(L))} \end{aligned}$$

□

which concludes the proof.

### 2.3.3. Stability analysis of the connected system. —

2.3.3.1. *Stability criterion.* — We now consider the connected linearized system defined by

$$(77) \quad \left\{ \begin{array}{l} \delta \dot{m}_1 = -\frac{\partial q_g}{\partial m_1}(\bar{q}_{gi}, \bar{p}_t(L))\delta m_1 - \frac{\partial q_g}{\partial p_t(L)}(\bar{q}_{gi}, \bar{p}_t(L))\delta p_t(L) \\ \delta q_g = \frac{\partial q_g}{\partial m_1}(\bar{q}_{gi}, \bar{p}_t(L))\delta m_1 + \frac{\partial q_g}{\partial p_t(L)}(\bar{q}_{gi}, \bar{p}_t(L))\delta p_t(L) \\ \delta p_t(L)(t) = \int_0^\tau k(\zeta) \frac{1}{\lambda \bar{q}_g} \delta p_t(L)(t - \zeta) d\zeta \\ \quad + \int_0^\tau k(\zeta) \frac{\bar{p}_r - \bar{p}_t(L)}{\lambda q_g^2} \delta q_g(t - \zeta) d\zeta \end{array} \right.$$

In Proposition 6 and 7 respectively, we derived the gain of the tubing and casing subsystems. Gathering and connecting these requires to match their equilibrium points. This defines a constraint on  $\bar{p}_t(L)$  and  $\bar{q}_g$ . For  $\bar{q}_{gi} > 0$ , equilibria are defined by (78). New expressions for gains through the connections are given in (79), (80) and (81).

$$(78) \quad \left\{ \begin{array}{l} \bar{q}_g = \bar{q}_{gi} \\ \bar{p}_t(L) = \frac{\lambda \bar{q}_{gi} (p_t(L)^* + \int_0^\tau k(\zeta) d\zeta) - \bar{p}_r \int_0^\tau k(\zeta) d\zeta}{\lambda \bar{q}_{gi} - \int_0^\tau k(\zeta) d\zeta} \end{array} \right.$$

$$(79) \quad \hat{\gamma}(\bar{q}_{gi}) = \gamma(\bar{q}_{gi}, \bar{p}_t(L))$$

$$(80) \quad \hat{\mu}(\bar{q}_{gi}) = \mu(\bar{q}_{gi}, \bar{p}_t(L))$$

$$(81) \quad \hat{\gamma}'(\bar{q}_{gi}) = \gamma'(\bar{q}_g)$$

**Proposition 8.** — *There exists a positive constant  $\bar{q}_{gi}^{min}$  such that for all  $\bar{q}_{gi} > \bar{q}_{gi}^{min}$  system (77) is finite-gain stable.*

*Proof.* — From equations (63), (74) and (79), (80) and (81) we get

$$\begin{aligned} \|\delta q_g\| &\leq \hat{\gamma}(\bar{q}_{gi}) \|\delta p_t(L)\| + \hat{\mu}(\bar{q}_{gi}) \\ \|\delta p_t(L)\| &\leq \hat{\gamma}'(\bar{q}_{gi}) \|\delta q_g\| \end{aligned}$$

Notice that  $\lim_{+\infty} \hat{\gamma}' = 0$  and  $\lim_{+\infty} \hat{\gamma} > 0$ . Therefore, there exists  $\bar{q}_{gi}^{min}$  such that for all  $\bar{q}_{gi} > \bar{q}_{gi}^{min}$

$$(82) \quad \hat{\gamma}(\bar{q}_{gi}) \hat{\gamma}'(\bar{q}_{gi}) < 1$$

The small gain theorem implies that the connected system (77) is finite gain stable.  $\square$

Using the fact that

$$(83) \quad \int_0^\tau k(\zeta) d\zeta = Lg \left( \frac{p_s + \bar{p}_r}{2RT} - \rho_l \right)$$

We compute

$$(84) \quad \bar{p}_t(L) = \frac{\lambda \bar{q}_{gi} (p_s + Lg \frac{p_s + \bar{p}_r}{2RT}) - \bar{p}_r Lg (\frac{p_s + \bar{p}_r}{2RT} - \rho_l)}{\lambda \bar{q}_{gi} - Lg (\frac{p_s + \bar{p}_r}{2RT} - \rho_l)}$$

Therefore,

$$(85) \quad \hat{\gamma}' = \left( \frac{p_s + \bar{p}_r}{2RT} - \rho_l \right) \frac{\lambda Lg (p_s - \bar{p}_r + Lg \frac{p_s + \bar{p}_r}{2RT})}{(\lambda \bar{q}_{gi})^2 - (Lg)^2 (\frac{p_s + \bar{p}_r}{2RT} - \rho_l)^2}$$

and

$$(86) \quad \hat{\gamma}(\bar{q}_{gi}) = \frac{C_g^2 \alpha}{2 \bar{q}_{gi}} \sqrt{\bar{p}_t(L)^2 + \frac{4\beta \bar{q}_{gi}^2}{\alpha C_g^2}}$$

*2.3.3.2. Conclusion and discussion.* — From equations (82), (85), and (86), we can analyze the influence of several parameters on the interconnected system. The best known effect is the role of the  $C_g$  parameter. As reported in [23], it is necessary for stability to maintain the flow through the injection valve critical. This is guaranteed by a choice of a small diameter injection valve, which corresponds in our model to a small  $C_g$ . Indeed, reducing  $C_g$  lowers  $\hat{\gamma}$  in equation (86), and thus ultimately guarantees inequality (82) and provides stability. Other important parameters are  $\alpha$  and  $\beta$  (defined in equation (67)) through which  $S_c$ , the section of the casing, plays a key role. Increasing  $S_c$  decreases  $\alpha$  and  $\beta$ . Eventually,  $\hat{\gamma}$  provides stability through inequality (82). In physical terms, the stabilizing buffer effect is emphasized by increasing the volume, therefore a bigger section lowers the coupling effect.



## CHAPTER 3

### CONTROL SOLUTIONS

#### *SOLUTIONS DE CONTRÔLE*

*Les résultats du chapitre précédent ont permis de comprendre les mécanismes d'instabilité ainsi que le rôle des paramètres physiques. Partant de ce constat, deux solutions sont envisageables. Pour éliminer les instabilités on peut déduire des critères de stabilité établis un protocole de définition des conditions opératoires. On peut également développer une solution de contrôle permettant de stabiliser le puits même dans des conditions a priori instables. En vue de l'application industrielle nous ne considérons que la seconde solution. En effet le système physique est trop complexe et la connaissance quantitative qu'on en a est trop ténue pour envisager de pouvoir calculer précisément des conditions opératoires valides. En outre il est probable que l'optimum économique se situe dans une zone instable.*

*Dans la Section 3.1.2.2, nous rappelons certaines solutions proposées antérieurement dans la littérature. Elles forment deux catégories. Certaines proposent d'utiliser du matériel plus performant pour éviter le développement d'instabilité. D'autres utilisent une approche algorithmique. Ces dernières modifient automatiquement les consignes des vannes d'injection de gaz et/ou de production en fonction d'indicateurs, tels que la température en tête de puits, la pression...*

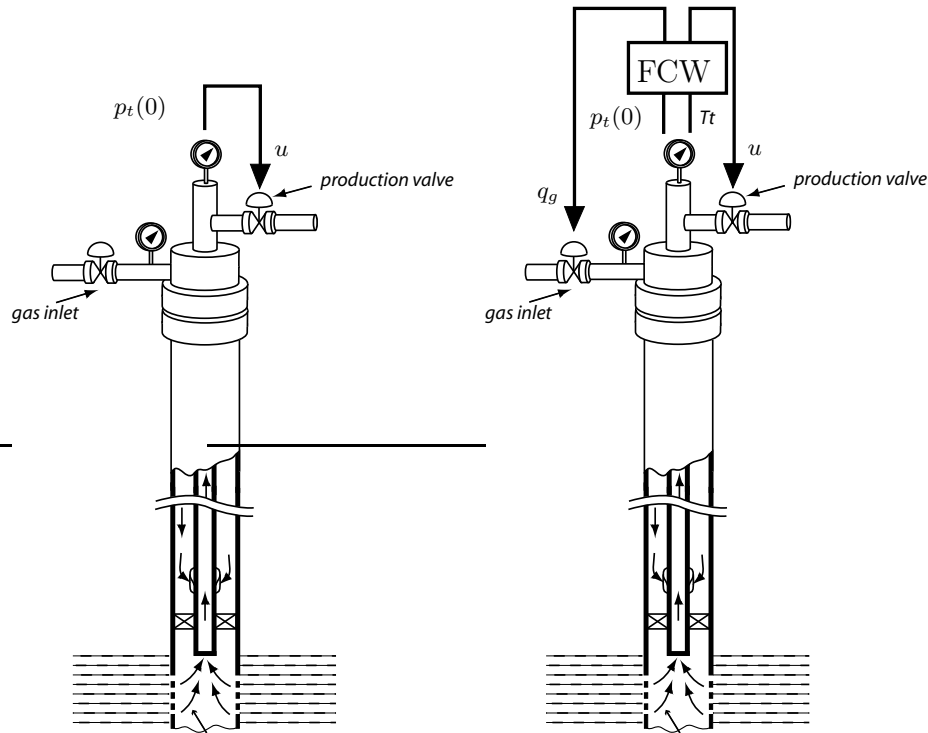
*Nous présentons ensuite une première solution de type boucle-ouverte. Ainsi dans la Section 3.2 nous supposons que le débit de gaz injecté au fond du puits est contrôlé. Nous proposons une loi de commande de débit, calculée à partir de la mesure de la pression de fond, qui permet de maintenir la fraction massique en gaz constante au fond du puits.*

*L'efficacité de cette solution est démontrée grâce à des simulations réalistes. Ceci souligne la pertinence du modèle à retards distribués présentés au Chapitre 2.*

*Nous présentons une solution plus réaliste vis à vis des contraintes opérationnelles à la Section 3.3. La faible disponibilité en gaz incite à préférer utiliser comme commande la vanne de production. En s'inspirant de l'analyse de stabilité présentée au Chapitre 2 nous démontrons la convergence du système bouclé avec un contrôleur de type Proportionnel-Intégral.*

*La loi de commande proposée utilise la mesure de la pression de fond. Ce capteur est très rarement disponible et en outre souvent sujet à des pannes. Nous montrons qu'il est possible de filtrer les mesures de pressions en tête de casing de façon à reconstruire la pression de fond. Cette solution est exposée à la Section 3.4 et illustrée par des résultats de simulation. L'efficacité de l'observateur de pression de fond est démontrée par les résultats de son application à un puits sur un site d'exploitation.*

In this chapter, we propose control solutions derived from the proposed modeling. First, in Section 3.1.2.2, we recall state-of-the-art control techniques for gas-lifted wells. Then, we address the control problem of stabilizing the tubing subsystem. A first open-loop solution is shown to be efficient in simulation (see Section 3.2). It stresses the relevance of the distributed parameters model proposed in Chapter 2. More realistic control solutions are addressed in Section 3.3. Following along the lines of the stability analysis of Chapter 2, we prove convergence of the closed loop system with a PI controller. At last, in Section 3.4, for sake of implementation, we filter measurements through an observer to reconstruct unavailable variables.



(a) Control of the tubing head pressure ( $p_t(0)$ ) by applying a PID controller on the production choke ( $u$ ).

(b) Sequential control based on temperature ( $T_t$ ) and pressure ( $p_t(0)$ ) measurements at the tubing head. Manipulated variables are the gas injection ( $q_g$ ) and the choke opening ( $u$ )

FIGURE 3.1. Some of the control solutions proposed in the literature.

### 3.1. State of the art

Results of the previous Chapter gives us clues to a better understanding of instability mechanisms and on the impact of physical parameters. However, while the proposed models are well suited for control design purpose, it seems quite hazardous to extrapolate quantitative stability criteria. Three phases (gas, oil, water) flow are too complex to be accurately modeled with our approach. Therefore, it is necessary to develop stabilizing solutions robust to changes of operating conditions.

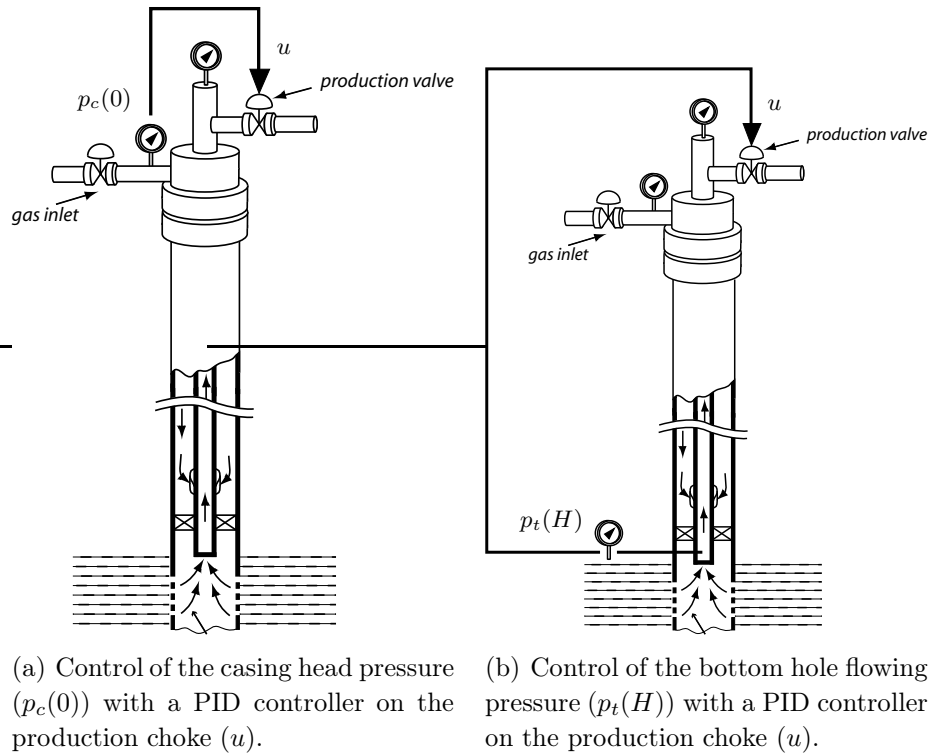


FIGURE 3.2. More control solutions proposed in the literature.

As described in Section 2.2 a hardware solution consists of using Venturi-Nozzle valve as injection valve. This let the injected flow rate be critical for pressure delta (i.e. the difference of pressure at the inlet and outlet of the valve) down to 10%. This solution is based on the idea that decoupling the casing from the tubing suppresses casing-heading instability. To suppress this coupling, one can also use feedback control.

Originally, the first proposed feedback controls aimed at getting rid of casing-heading. One method is exposed in [7] and in [9]. The idea is to control the tubing head pressure by applying a PID control on the production choke adjustments (see Figure 3.1(a)). In these publications, stability analysis is performed on the characteristic equation of the closed loop system. In [9], a root locus analysis is used for the design of the PID parameters. However, since no simulation nor actual test have been performed and because the model considered in [9] does not take into

account the propagation in the tubing, it is assumed homogeneous, we believe that more attention should be paid on other feedback methods. We now detail these approach in sections 3.1.1 and 3.1.2.

Publications [26], [15], [19] and [16] propose methods based on feedback control using production choke opening as input and sometimes also the gas injection rate.

**3.1.1. Steady state based feedback control.** — In [26], a system developed by TOTAL, the FCW (Full Control of Wells), is presented. This system schedules the opening of the production choke and the gas injection rate following a sequential logic algorithm which steers the system to a prescribed set-point (see Figure 3.1(b)). It is partly based on the facts that increasing the gas injection rate or decreasing the production choke opening tends to stabilize the well (see [16] or Section 2.3). Successful field results are exposed in [28], use of the FCW leads to a sharp increase in gas-lift efficiency with an increase in oil production and a decrease in gas injection. A tuning methodology for this algorithm is presented in [34].

**3.1.2. Dynamic feedback control.** —

*3.1.2.1. Use of casing head pressure measurements.* — In [16], casing head pressure measurements are used to stabilize casing-headings. Also based on the idea that casing heading can be simply suppressed by decoupling the annular dynamics from the pressure variations in the tubing, the control strategy assumes that the gas injection in the casing is constant. Therefore, controlling the the casing head pressure is sufficient to maintain the gas injection in the tubing constant (see Figure 3.2(a)). Two cascaded PID control loops are used. The inner one stabilizes the casing head pressure and the other one defines the casing head pressure set-point. This set-point is derived from the desired liquid production flow rate. This structure has been implemented and tested on the experimental gas-lift model in Rijswijk.

*3.1.2.2. Use of BHFP measurements.* — Engineers from the Norwegian oil company Norsk Hydro and from ABB present in [15] results obtained at the Brage field in the North Sea. Several pressures are measured, such

as casing head pressure, tubing head pressure, pressure downstream the production choke and bottom hole pressure. This last pressure seems to be the key measurement because the input from the operator to the well controller is reported to be “typically a set point for e.g. the downhole pressure” (see Figure 3.2(b)).

The use of the downhole pressure measurements can be somewhat difficult. Sensors located at such depth are often subject to damages or failures. Therefore, researchers from the Norwegian Institute of Technology have proposed in [19] a control solution based on the work presented in [25]. The idea is to use a state feedback control coupled with a state estimation. A Kalman filter is used to reconstruct the masses of oil and gas in the well from pressure measurements at the tubing head, casing head and bottom-hole. This strategy has been tested with OLGA<sup>®</sup>2000 and is proven to be robust to downhole measurements failures.

All these solutions aim at stabilizing casing headings. In [23] a control solution focused on the density-wave instability problem is mentioned. This phenomenon is reported to be alleviated by use of a PI structure controlling the downhole pressure with production choke opening as input.

### 3.2. Controlling the tubing dynamics using gas inlet as input

The solution proposed in this section uses the gas injection flow rate as an input. The goal is to underline the relevance of the modeling of Section 2.2.

**3.2.1. Control.** — In this section, we design control laws to steer system (35) to a predefined steady state.

*3.2.1.1. Control laws definition.* — We look for control laws  $u = \lambda q_g$  such that  $p_L$  converges to a chosen constant  $p_{\text{ref}} \in ]p_L^* + \int_0^\delta k(\tau)d\tau, p_L^* [$ . The corresponding steady state value of  $X$  defined in (34) is

$$(87) \quad X_{\text{ref}} = -\frac{p_L^* - p_{\text{ref}}}{\int_0^\delta k(\tau)d\tau} \in ]0, 1[$$

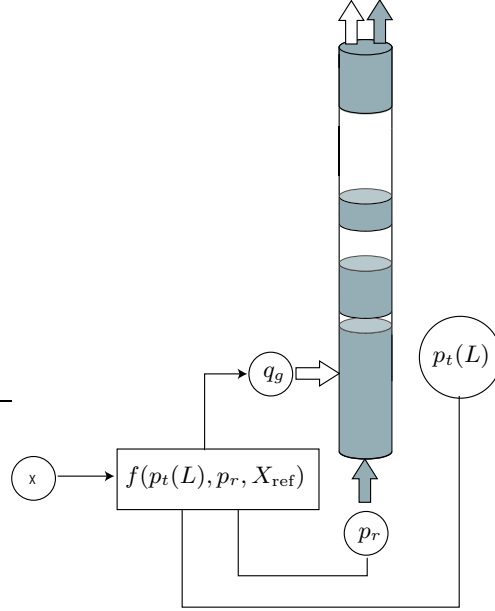


FIGURE 3.3. Control strategy using gas inlet as input. We feed the tubing with a computed gas flow rate  $q_g$  such that the gas mass fraction at the bottom of the tubing is equal to  $X_{ref}$ . This computation takes the bottom-hole pressure  $p_t(L)$  and the reservoir pressure  $p_r$  into account.

We note  $u_{ref}$  the value of  $u$  at steady state. It satisfies

$$(88) \quad X_{ref}(u_{ref}) = \frac{p_L^* - \bar{p}_r + u_{ref}}{u_{ref} - \int_0^\delta k(\tau) d\tau}$$

Our (closed-loop) control law is, simply,

$$(89) \quad u(t) = \frac{\bar{p}_r - p_L(t)}{1 - X_{ref}}$$

Figure 3.3 illustrates this strategy.

This control strategy feeds system (35), which has finite memory  $\delta$ , with a constant term. By direct computation, this straightforward approach provides convergence. We can state the following proposition.

**Proposition 9.** — *With control law (89),  $p_L$  which dynamics is defined by system (35) converges to  $p_{ref}$  in finite time  $\delta$  for any initial condition  $[-\delta, 0] \ni t \mapsto \phi(t) \in \mathbb{R}$ .*

Yet, the expression  $u$  defined in (89) does not take into account actuation saturations. Here, the most limiting factor in practice is a lower bound  $u_{\min} > 0$  on the control. In facts, some simulations show that this constraint is often reached with this naive approach. We now propose the saturated control law

$$(90) \quad \begin{cases} u = \frac{\bar{p}_r - p_L(t)}{1 - X_{\text{ref}}}, & \text{for } p_L < \bar{p}_r - u_{\min}(1 - X_{\text{ref}}) \\ u = u_{\min}, & \text{for } p_L \geq \bar{p}_r - u_{\min}(1 - X_{\text{ref}}) \end{cases}$$

**Proposition 10.** — Assume that

$$(91) \quad X_{\text{ref}} \geq \frac{p_L^* - \bar{p}_r + u_{\min}}{u_{\min} - \int_0^\delta k(\tau) d\tau}$$

With the (saturated) control law (90),  $p_L$  which dynamics is defined by system (35), converges to  $p_{\text{ref}}$  in finite time  $2\delta$  for any initial condition  $[-\delta, 0] \ni t \mapsto \phi(t) \in \mathbb{R}$ .

*Proof.* — We now show that, for  $t \geq \delta$ , the control law is unsaturated. Indeed, for  $t > 0$

$$h \left( 1 - \frac{\bar{p}_r - p_L(t)}{u(t)} \right) \geq X_{\text{ref}}$$

Therefore, for all  $t \in [\delta, +\infty[$ ,

$$p_L(t) \leq p_L^* + X_{\text{ref}} \int_0^\delta k(\tau) d\tau$$

Assuming (91), a simple computation yields

$$\forall t \geq \delta, p_L(t) \leq \bar{p}_r - u_{\min}(1 - X_{\text{ref}})$$

By equation (90), we get that, for all  $t \geq \delta$ ,  $u$  is simply defined by

$$u = \frac{\bar{p}_r - p_L(t)}{1 - X_{\text{ref}}}$$

The control is thus unsaturated and, by Proposition 9, we conclude that system (35) converges towards  $p_{\text{ref}}$  in  $2\delta$ .  $\square$

In practice, one must choose  $p_{\text{ref}}$  in accordance to the minimum value  $u_{\min}$  such that equation (88) holds. This choice implies that assumption (91) holds.

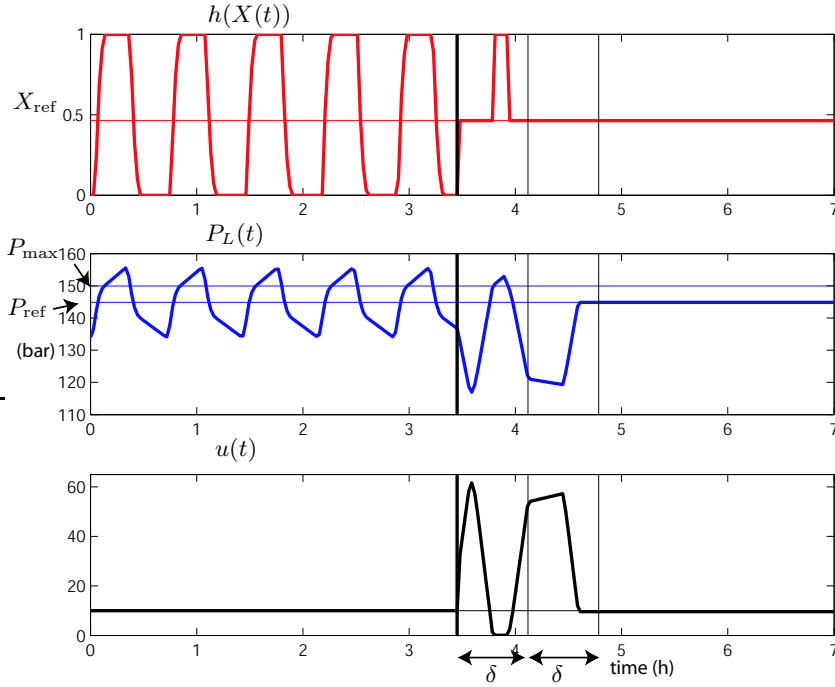


FIGURE 3.4. Stabilization of equation (35) using the saturated control law (90). Control is switched on after approximately 3.4 hours of open loop.  $p_L$  reaches  $p_{\text{ref}}$  and  $X$  reaches  $X_{\text{ref}}$  in finite time  $2\delta$ .

Indeed, if  $\bar{p}_r > p_L^* + \int_0^\delta k(\tau)d\tau$ , which simply means that the pressure at the bottom of pipe when it is full of gas is less than the reservoir pressure, then  $u_{\text{ref}} \mapsto X_{\text{ref}}(u_{\text{ref}})$ , given in (88), is increasing. Therefore, if  $u > u_{\text{min}}$

$$X > \frac{p_L^* - \bar{p}_r + u_{\text{min}}}{u_{\text{min}} - \int_0^\delta k(\tau)d\tau}$$

In short, assumption (91) states that one should not define  $p_{\text{ref}}$  outside the range of  $X$  that can be reached with  $u > u_{\text{min}}$ .

*3.2.1.2. Simulation.* — Figure 3.4 shows an example of stabilization with the saturated control law (90). Choosing  $u = 10$  bar and using equations (87) and (88) we compute the corresponding steady states  $p_{\text{ref}} = 145$  bar and  $X_{\text{ref}} = 0.464$ . We define  $u_{\text{min}} = 0.1$ . Assumption (91)

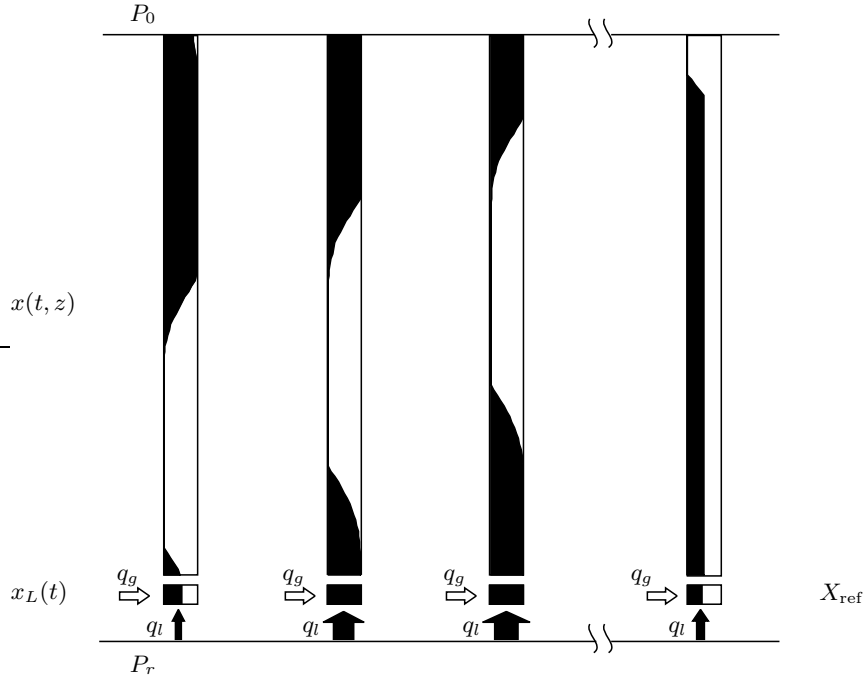


FIGURE 3.5. Comparison of open loop (3 schemes on the left) and closed loop behavior.

holds. Until  $t_c$  the system is left open loop. At  $t = t_c$ , the controller is turned on. From  $t_c$  to  $t_c + \delta$ , the gas mass fraction  $h(X(t))$  remains between  $X_{\text{ref}}$  and 1. Therefore, for  $t > t_c + \delta$ ,  $P_l(t)$  remains below  $P_{\text{max}} = \bar{p}_r - u_{\text{min}}(1 - X_{\text{ref}}) = 150$  bar and  $h(X(t)) = X_{\text{ref}}$ . Pressure  $p_L$  converges to  $p_{\text{ref}}$  in finite time.

An alternative view is given in Figure 3.5. Left three snapshots describe the open-loop behavior. Gas mass fraction profile ( $x(t, z)$ ) is represented in white (complementary black part stands for oil mass fraction). Boundary condition  $q_g$  is constant and  $q_l$  is defined by equation (31). Finally, the right scheme represents the transient obtained with closed loop control. The feeds keep the gas mass ratio constant at  $X_{\text{ref}}$ . During the transient,  $q_g$  is permanently adapted to counteract the effect of the state  $x(t, z)$ ,  $z \in [0, L]$ , onto  $q_l$ . This yields a constant  $X(t, L)$  which progressively steers the system to steady state through the transport equation.

3.2.1.3. *Stabilization of the well simulated in OLGA<sup>®</sup>2000.* — The closed loop control law can be tested in OLGA<sup>®</sup>2000. In Section 2.2.2.1, we assume the gas velocity to be constant, i.e. we neglect the impact of the gas mass fraction on the gas velocity. Therefore, when the gas mass flow rate is high enough, this assumption only results in a time scaling. But, when the gas inlet is too low, the well production eventually stops, which is not represented by the simple model. Therefore, we want the gas injection rate to remain above a minimum,  $q_g^{\min}$ , guaranteeing that an actual flow takes place in the pipe. This defines a lower bound for our control law. Following the same lines as in the section 3.2.1.1, we define the control  $q_g$ , corresponding to  $u$  (see equation (33)), to keep  $x^L$  at a

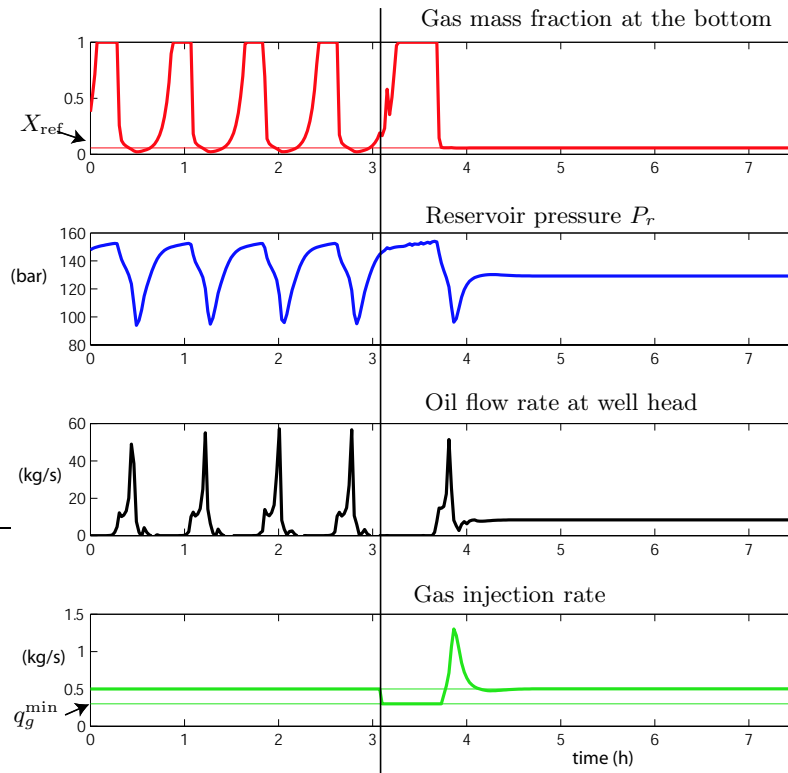


FIGURE 3.6. Stabilization of density wave instability simulated in OLGA<sup>®</sup>2000 (numerical set up given in Appendix A, Table 3).  $X_{\text{ref}} = 0.0568$  and  $q_g^{\min} = 0.3$ .

predefined constant,  $X_{ref}$ . Using  $x^L$  given in equation (32), our control law writes

$$q_g(t) = \max \left( \frac{X_{ref}}{1 - X_{ref}} IP(\bar{p}_r - p_L(t)), q_g^{\min} \right)$$

Figure 3.6 represents an example of stabilization of the density wave instability. We define  $q_g^{\min} = 0.3$  kg/s and  $X_{ref} = 0.0568$ . The controller is switched on at approximately  $t_c = 3.4$  hour and steers the well to the steady state corresponding to the initial gas injection rate. The period of the oscillations approximately equals the travel time  $\delta$ . One can see in Figure 3.6 that the well is stabilized in  $2\delta$ . As stated in Proposition 10,  $2\delta$  corresponds to the time needed by the well to forget its initial condition.

### 3.3. Controlling the tubing dynamics using the production choke as input

There exists a strong obstacle to the previously presented control technique. As discussed in Section 1.2.1.2, gas is allocated scarcely between the wells. Because the casing acts as a large buffer tank located at the input of the tubing subsystem, any control law using the gas inlet as input potentially demands large peaks during transients. To compensate the very slow casing dynamics, high gas flow rate variations must be considered. The induced variations need high gas availability. These requirements are incompatible with the above mentioned constraints. In practice, even for reasonably scaled transients, it is not uncommon to punctually need

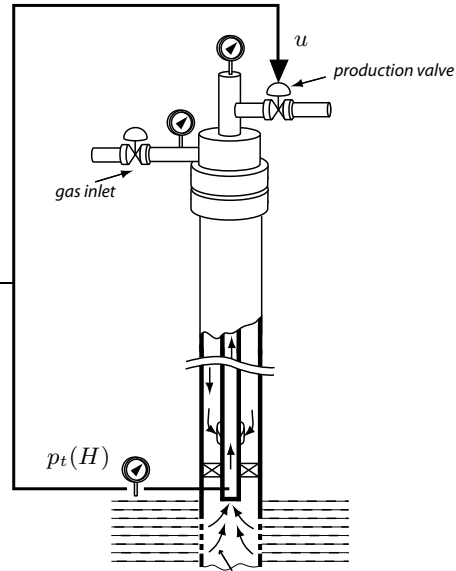


FIGURE 3.7. Control of the bottom hole flowing pressure ( $p_t(H)$ ) with a PID controller on the production choke ( $u$ ).



FIGURE 3.8. Block scheme of the OLGA<sup>®</sup>2000 simulation setup. First case (top) with a production choke, second case (bottom).

more than twice the nominal amount of gas. This issue prevents the gas inlet from being considered as a manipulated input (except for very low frequency signals).

Therefore, in this section, we propose a control strategy using the production choke as input (see Figure 3.7). The main advantage of this choice is that it has a direct impact on the dynamics, unfortunately it also has a counter part: the choke has a very small active range.

**3.3.1. Manipulated variable definition.** — In a first approximation, we model the production choke opening variations as tubing head pressure variations. Therefore, we investigate the role of the tubing well head pressure as input variable. With OLGA<sup>®</sup>2000 we consider two setups to simulate the flow in a single vertical pipe (see Figure 3.8). Oil is supplied by a reservoir and gas is injected at the bottom of the pipe. In the first setup, the pipe is equipped with a production choke that we progressively open. In the second setup, there is no production choke. Instead, the tubing is modeled as a pipe with a downstream pressure boundary condition. Gradually, we decrease this boundary pressure, simulating a reduction of the well head pressure. This section is part of a work that appeared in the International Symposium on Advanced Control of Chemical Processes, 2006 (see [35]).

Figure 3.10(a) shows the steady state well head pressure values as a function of the production choke opening. Classically, our focus is

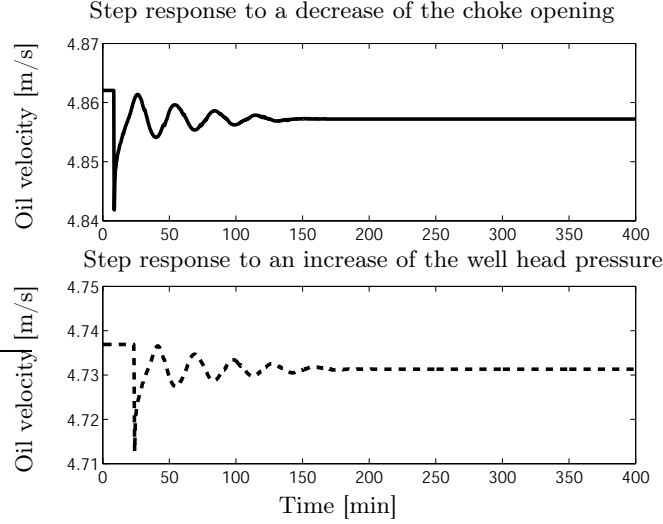


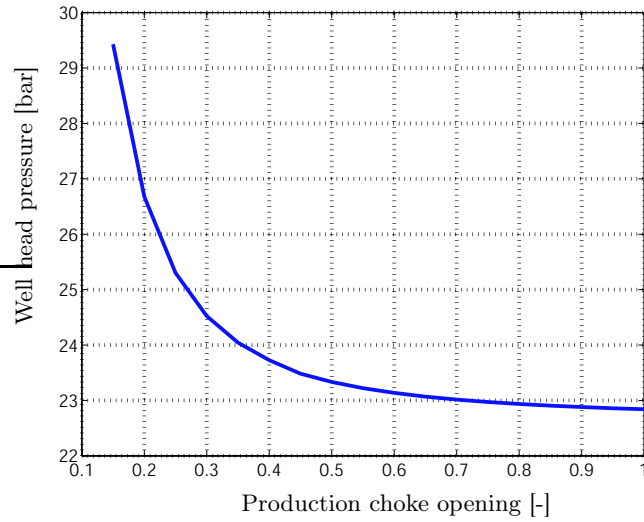
FIGURE 3.9. Comparison of the step responses to an increase of the well head pressure and to a decrease of the production choke opening.

on comparing the oil and gas velocities histories obtained from the two simulation setups. Figure 3.10(b) reports the static values of the oil and gas velocities as a function of the well head pressure. Over almost the whole well head pressure operating range (from 23 to 29 bar, i.e. from 0.2 to 1 choke opening), the curves coincide. It is only when the choke is almost closed that differences appear. Figure 3.9 shows the comparison of the step responses to an increase of the well head pressure and to a consistent decrease of the production choke opening, respectively. We notice similar undershoots of approximately 0.02 m/s. It takes between four and five noticeable oscillations for both systems to settle. This experiment suggests it is valid to consider  $p_t(0)$  as our input variable. From now on, we denote  $u \triangleq p_t(0)$ .

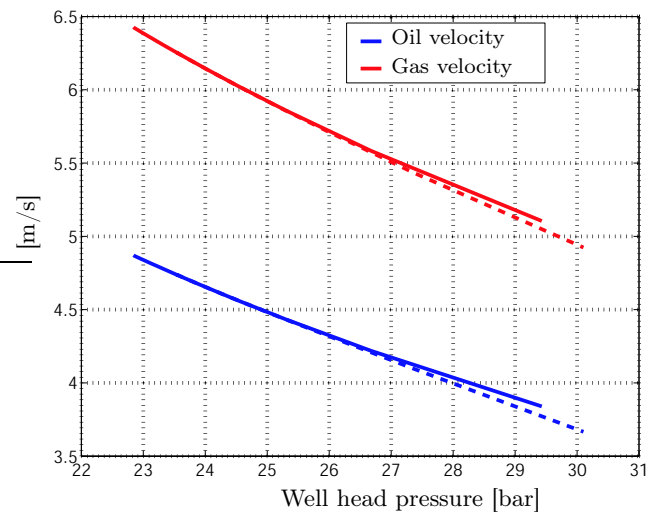
**3.3.2. Open loop stability analysis.** — Recall equation (35)

$$(92) \quad p_t(t, L) = p_t(0) + cst + \int_{t-\delta}^t k(t-\zeta)h \left( 1 - \frac{\bar{p}_r - p_t(\zeta, L)}{\lambda q_g(\zeta)} \right) d\zeta$$

We assume that the gas injection in the tubing is constant. Linearization yields



(a) Well head pressure as a function of the production choke opening.



(b) Comparison of the oil and gas velocities between the first and second cases (continuous and dashed line respectively).

FIGURE 3.10. Steady state comparison of the impact of variations of tubing head pressure and production choke opening.

$$(93) \quad \delta p_t(t, L) = \delta u + \int_0^\delta k(\zeta) \frac{\delta p_t(\zeta - \delta, L)}{\lambda q_g} d\zeta$$

In Laplace coordinates,

$$(94) \quad \delta \tilde{p}_t(s, L) = \frac{1}{1 - \frac{\tilde{k}(s)}{\lambda q_g}} \delta \tilde{u}(s)$$

Where  $\tilde{k}$ , the Laplace transform of  $k$ , writes

$$(95) \quad \tilde{k}(s) = k_2 \frac{1 - e^{-\delta s}}{s} + \frac{k_1}{\delta} \frac{1 - e^{-\delta s} - \delta s e^{-\delta s}}{s^2}$$

Using Nyquist criterion we know that the stability of the system which transfert writes as equation (95) is determined by the shape of the curve defined by  $-\tilde{k}(j\omega)/(\lambda q_g)$  for  $\omega \in [0, +\infty)$ . Since  $\tilde{k}(s)$  has no zero, if the Nyquist plot does not encircle  $-1$  the tubing dynamics is stable. We will not go through the complete stability analysis as it has already been performed in Section (2.2.3). We simply notice that the role of the gas injection  $q_g$  is played by as an homothety of the Nyquist plot. Besides, one should also notice that  $\tilde{k}(s, \alpha\delta) = \alpha \tilde{k}(\alpha s, \delta)$ , which means that an

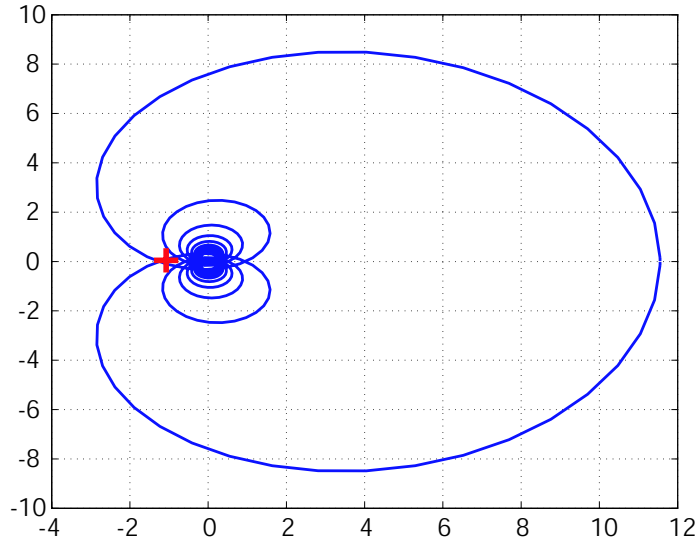


FIGURE 3.11. Nyquist plot corresponding to the linearization equation (35) for  $q_g=0.2\text{kg/s}$ . The tubing dynamics is unstable.

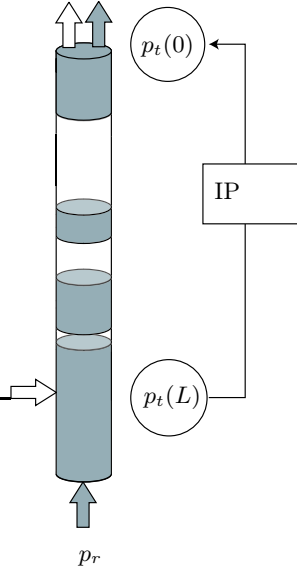


FIGURE 3.12. Control of the bottom hole pressure  $p_t(L)$  with the well head pressure  $p_t(0)$ .

increase of the delay also plays the role of an homothety. Figure 3.11 represents the Nyquist plot corresponding to the transfer function (95) for  $q_g = 0.2$  kg/s. One notice that the tubing dynamics is unstable but close to be stable, for  $q_g = 0.3$  kg/s it would be stable.

**3.3.3. Closed loop stability analysis.** — We will now show that, for all gas injection rate, the tubing dynamics can be stabilized either with a P controller or with an IP controller (see Figure 3.12). In the IP controller case, the reference is only taken into account in the integral term. It allows smooth responses when the reference is updated.

*3.3.3.1. P controller.* — Let us define the input  $u = p_t(0)$  as follows

$$u = u_0 - k_p(p_t(L) - p_t^{ref}(L))$$

The closed loop transfer writes

$$(96) \quad \delta \tilde{p}_t(s, L) = \frac{k_p / (1 + k_p)}{1 - \frac{\bar{k}(s)}{(1 + k_p)\lambda q_g}} \delta \tilde{p}_t^{ref}(s)$$

**Proposition 11.** — For all  $q_g > 0$  there exists  $k_p > 0$  such that the closed loop system defined by equation (96) is stable.

*Proof.* — Recalling computations done in Section 2.2.3, we know that there exist a minimum gas injection  $q_g^{min}$  such that for all  $q_g > q_g^{min}$ , the corresponding Nyquist plot does encircle -1. If  $q_g < q_g^{min}$  we just have to define  $k_p > \frac{q_g^{min}}{q_g} - 1$ .  $\square$

3.3.3.2. *Use of an IP controller.* — Let us define the input  $u = p_t(0)$  as follows

$$(97) \quad u = u_0 - k_p p_t(L) - \frac{k_p}{T_i} \int_0^t p_t(L) - p_t^{ref}(L)$$

with  $u_0$  defined such that  $p_t(0^+, 0) = p_t(0^-, 0)$ . It follows

$$u_0 = p_t(0, 0) + k_p p_t(0, L)$$

In Laplace coordinates,

$$\delta \tilde{u} = -k_p \left( 1 + \frac{1}{sT_i} \right) \delta \tilde{p}_t(L) + \frac{1}{sT_i} \delta \tilde{p}_t^{ref}(L)$$

The closed loop transfert writes

$$(98) \quad \begin{aligned} \delta \tilde{p}_t(L) &= \frac{k_p/T_i/s}{1 - \tilde{k}(s)/(\lambda q_g) + k_p \left( 1 + \frac{1}{sT_i} \right)} \delta \tilde{p}_t^{ref}(L) \\ &= \frac{1}{1 + T_i s \left( 1 + \frac{1}{k_p} \left( 1 - \frac{\tilde{k}(s)}{\lambda q_g} \right) \right)} \delta \tilde{p}_t^{ref}(L) \end{aligned}$$

**Proposition 12.** — For each  $q_g$  one can find  $k_p > 0$  and  $T_i > 0$  such that the system which transfer writes as equation (98) is stable.

*Proof.* — Let  $G$  be defined by

$$G(s) = T_i s \left( 1 + \frac{1}{k_p} \left( 1 - \frac{\tilde{k}(s)}{\lambda q_g} \right) \right)$$

Stability of the transfer (98) can be analyzed through the Nyquist plot of  $G(j\omega)$ . Its real and imaginary parts are

$$Re(G(j\omega)) = \frac{T_i}{k_p \lambda q_g} Im(\omega \tilde{k}(j\omega))$$

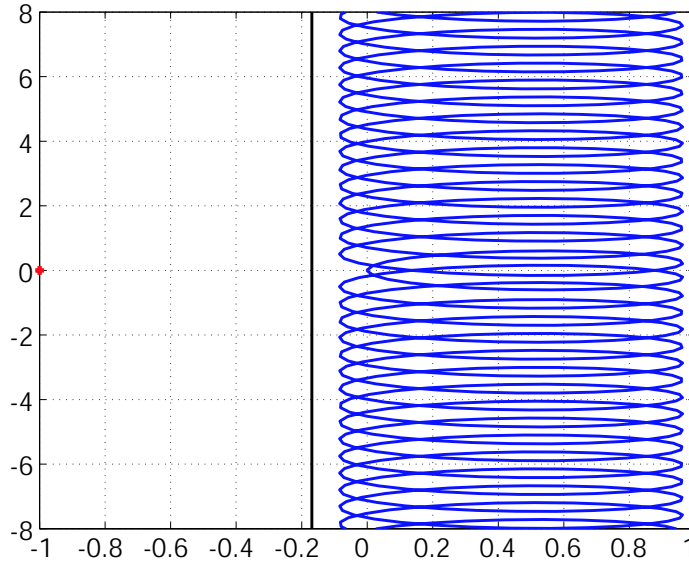


FIGURE 3.13. Nyquist plot of the closed loop tubing dynamics. The black line represents the lower boundary defined in equation (99).

and

$$\text{Im}(\omega\tilde{k}(j\omega)) = (k_1 + k_2) \cos(\omega\delta) - k_2 - k_1 \frac{\sin(\omega\delta)}{\omega\delta}$$

Remembering that  $k_1$  and  $k_2$  are both strictly negative, we get the following lower bound

$$(99) \quad \text{Re}(G(j\omega)) > 2k_1 \frac{T_i}{k_p \lambda q_g}$$

Therefore, choosing  $T_i > 0$  and  $k_p > 0$  such that the following inequality is verified guarantees the stability

$$\frac{T_i}{k_p} < -\frac{\lambda q_g}{2k_1}$$

□

### 3.4. Controlling the well dynamics using production choke as input

Up to this point we have shown that it is possible to control the tubing dynamics using the tubing head pressure as input and the bottom hole pressure as output (as summarized in Figure 3.7). Unfortunately there is often no sensor at the bottom of the well, and, when there are some, they are usually subject to recurrent failures. It is a common thought that we cannot rely on such measurements. Therefore we have to complement the analysis of the previous section with solutions to implementation issues. As shown in Figure 3.14 we propose to use the casing head pressure to estimate the bottom hole pressure.

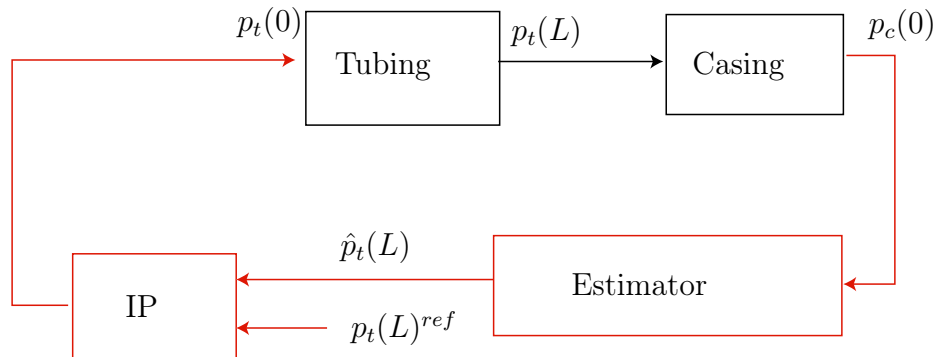


FIGURE 3.14. Scheme of the proposed control and estimation architecture.

**3.4.1. Bottom hole pressure estimation.** — The casing head pressure is related to the bottom hole pressure through the gas volume contained in the annular part. Given the input gas flow rate and the mass variation (given by the pressure variations), one can easily derive the output gas flow. The last step consists in computing the pressure downstream the gas injection valve, knowing the upstream pressure and the flow rate. This part presents the principles of an estimator software that has been deposited on the “Agence pour la Protection des Programmes” under the Inter Deposit Number

IDDN.FR.001.340008.000.R.P.2006.000.30400

3.4.1.1. *Estimator definition.* — We recall equation (69)

$$\begin{cases} \dot{m}_1 = q_{gi} - q_g(m_1, p_t(L)) \\ q_g(m_1, p_t(L)) = C_g \sqrt{\mu m_1 \max(\nu m_1 - p_t(L), 0)} \end{cases}$$

We just have to express  $m_1$  in term of  $p_c(0)$  through the ideal gas law

$$p_c(0) = \frac{RT_c}{V_c M} m_1 = \xi' m_1$$

Assuming that the bottom hole pressure is slowly varying compared to the casing dynamics, we estimate  $p_t(L)$  thanks to the following model

$$\begin{cases} \dot{p}_c(0) = \xi' \left( q_{gi} - C_g \sqrt{\mu' p_c(0) \max(\nu' p_c(0) - p_t(L), 0)} \right) \\ \dot{p}_t(L) = 0 \end{cases}$$

with  $\mu' = \frac{\mu}{\xi'}$  and  $\nu' = \frac{\nu}{\xi'}$ .

We define the following estimator

$$(100) \quad \begin{cases} \dot{\hat{p}}_c(0) = \xi' \left( q_{gi} - C_g \sqrt{\mu' p_c(0) \max(\nu' p_c(0) - \hat{p}_t(L), 0)} \right) - l_1 (\hat{p}_c(0) - p_c(0)) \\ \dot{\hat{p}}_t(L) = -l_2 (\hat{p}_c(0) - p_c(0)) \end{cases}$$

3.4.1.2. *Estimator physical interpretation.* — Linearization of equation (100) yield

$$\begin{pmatrix} \delta \dot{\hat{p}}_c(0) \\ \delta \dot{\hat{p}}_t(L) \end{pmatrix} = \begin{pmatrix} -r & t \\ 0 & 0 \end{pmatrix} \begin{pmatrix} \delta \hat{p}_c(0) \\ \delta \hat{p}_t(L) \end{pmatrix} - \begin{pmatrix} l_1 \\ l_2 \end{pmatrix} (\delta \hat{p}_c(0) - \delta p_c(0))$$

where  $r$  and  $t$  are two positive constants. Therefore, considering that this estimator is a filter which input is  $\delta p_c(0)$  and which output is  $\delta \hat{p}_t(L)$ , its transfer writes

$$(101) \quad \delta \hat{p}_t(s, L) = \frac{s + r}{\frac{s^2}{l_2} + \frac{l_1 s}{l_2} + t} \delta \hat{p}_c(s, 0)$$

Using a high gain  $l_2$ , this transfer reduces to

$$\frac{s + r}{t}$$

which means that this filter locally inverts the casing dynamics. Notice that this transfer is not causal (while transfert (101) is), which will lead to some implementation issues.

*3.4.1.3. Impact of modeling errors.* — Denote  $e_c = \hat{p}_c(0) - p_c(0)$  and  $e_t = \hat{p}_t(L) - p_t(L)$  the coordinates of the error vector between the real trajectory and the estimated one. The dynamics of the error writes

$$\begin{pmatrix} \dot{e}_c \\ \dot{e}_t \end{pmatrix} = \begin{pmatrix} -\xi'(q_g(p_c(0), \hat{p}_t(L)) - q_g(p_c(0), p_t(L))) - l_1 e_c \\ -l_2 e_c \end{pmatrix}$$

This means that the estimator dynamics converges towards a trajectory  $(\bar{p}_c(0), \bar{p}_t(L))$  which verifies

$$q_g(p_c(0), \hat{\bar{p}}_t(L)) = q_g(p_c(0), \bar{p}_t(L))$$

As  $q_g$  is a bijective function with respect to its second variable for  $p_t(L) < \nu' p_c(0)$  this defines, in this region,  $\bar{p}_t(L)$  as

$$\bar{p}_t(L) = p_t(L)$$

Now assume that the  $q_g$  function is not perfectly known and that the constant  $\nu'$  and  $\mu'$  are linear biased. We define

$$\hat{q}_g = C_g \sqrt{\hat{\mu}' p_c(0) \max(\hat{\nu}' p_c(0) - p_t(0))}$$

with  $\hat{\nu}' = (1 + \varepsilon)\nu$ ,  $\hat{\mu}' = (1 + \varepsilon)\mu$  and  $\varepsilon$  a small constant error. The trajectory  $(\bar{p}_c(0), \bar{p}_t(L))$  is now defined by

$$\hat{q}_g(p_c(0), \hat{\bar{p}}_t(L)) = q_g(p_c(0), \bar{p}_t(L))$$

Assuming that  $q_g$  and  $\hat{q}_g$  are not equal to zero, we get that

$$\hat{p}_t(L) = \frac{1}{1 + \varepsilon} p_t(L) - \frac{\varepsilon(2 + \varepsilon)}{1 + \varepsilon} p_c(0)$$

This means that the estimator probably reconstructs an affine biased value of  $\hat{p}_t(L)$ . This is not an issue. We do not need a precise value for  $p_t(L)$ , we just need to get enough information of the system behavior to be able to stabilize it. An affine biased reconstruction is enough.

We can easily get rid of the constants. As we define the reference for  $p_t(L)$  based on its estimation we do as if we knew the value of the biases.

Therefore in the definition of the IP controller (97) becomes

$$u = u_0 - k_p \frac{1}{1 + \varepsilon} p_t(L) + k_p \frac{\varepsilon(2 + \varepsilon)}{1 + \varepsilon} p_c(0) - \frac{k_p}{T_i} \frac{1}{1 + \varepsilon} \int_0^t p_t(L) - p_t^{ref}(L)$$

with

$$(102) \quad u_0 = p_t(0, 0) + k_p \frac{1}{1 + \varepsilon} p_t(0, L) - k_p \frac{\varepsilon(2 + \varepsilon)}{1 + \varepsilon} p_c(0, 0)$$

In practice the term  $\frac{\varepsilon(2+\varepsilon)}{1+\varepsilon}(p_c(0, t) - p_c(0, 0))$  is very close to 0 and does not perturb the convergence of the controller.

*3.4.1.4. Simulations results.* — Figure 3.15 shows simulations example of bottom hole estimation. The scenario is the following: at first the choke opening is set to 0.2, which correspond to a stable set point. The well tends to stabilize. Then, at time  $t=300$  min, the choke is opened up to 0.34. This corresponds to an unstable set point. In both cases the estimator correctly reconstructs the bottom hole pressure. Notice that, while convergence is almost instantaneous for  $\hat{p}_c(0)$ , it takes a bit more time for  $\hat{p}_t(L)$  to settle. Moreover the behavior of  $\hat{p}_t(L)$  is not as smooth as the one of the reconstructed casing head pressure. In this case, the convergence is perfect because we perfectly know the function  $q_g$ .

**3.4.2. Experimental results.** — Figure 3.16 shows experimental results obtained on a TOTAL operated well. The bottom hole pressure  $\hat{P}_t(L)$  is derived, thanks to the observer, from the casing head pressure measurements,  $P_c(0)$  and from the gas injection flow rate measurements,  $Q_g$ . The estimated pressure is compared with the tubing head pressure,  $P_t(0)$ , to validate the relevance of the approach. In Figure 3.16 the well is unstable. The oscillations are very regular and their period is close to the propagation time. The tubing head pressure is used to monitor the expulsions of the liquid slugs, which correspond to the pressure peaks. Each of these peak is followed by a drop of the estimated bottom hole pressure, this is relevant with the description of the density-wave phenomenon. The bottom hole pressure estimation behaves as predicted: it decreases when the tubing head pressure increases which corresponds to the arrival of the liquid-rich slug and then it increases as the tubing

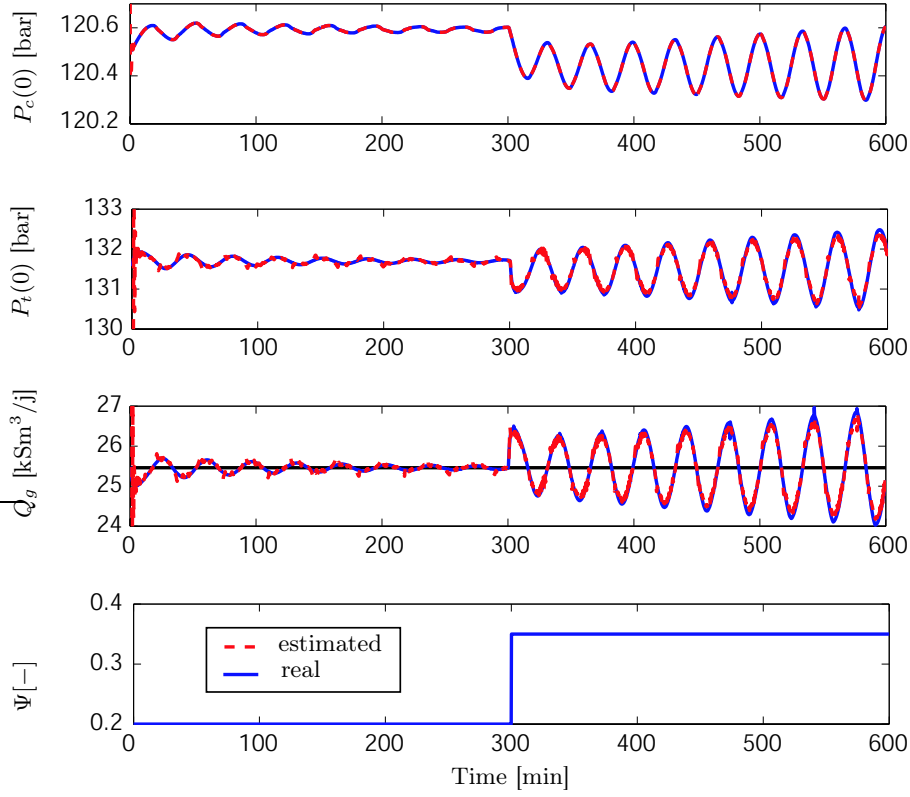


FIGURE 3.15. Estimation of the bottom hole pressure using the casing head pressure in OLGA<sup>®</sup>2000 simulation (numerical set up is given in Appendix A, Table 4). Solid blue (reference from OLGA<sup>®</sup>2000), dotted red estimation.

head pressure drops, at the end of the liquid-rich slug. Moreover the reconstructed values of  $\hat{P}_t$  are coherent with steady state computations.

**3.4.3. Controller results.** — Figure 3.17 shows simulations example of a closed loop stabilization. The scenario is the following: at first the choke opening is set to 0.2, which corresponds to a stable set point. The well tends to stabilize. Then, at a time less than  $t=100$  min, the controller is switched on. The reference for the pressure  $p_t(L)$  is set to 131.7 bar which corresponds to an unstable point. In both cases the estimator correctly reconstructs the bottom hole pressure. The well is stabilized.

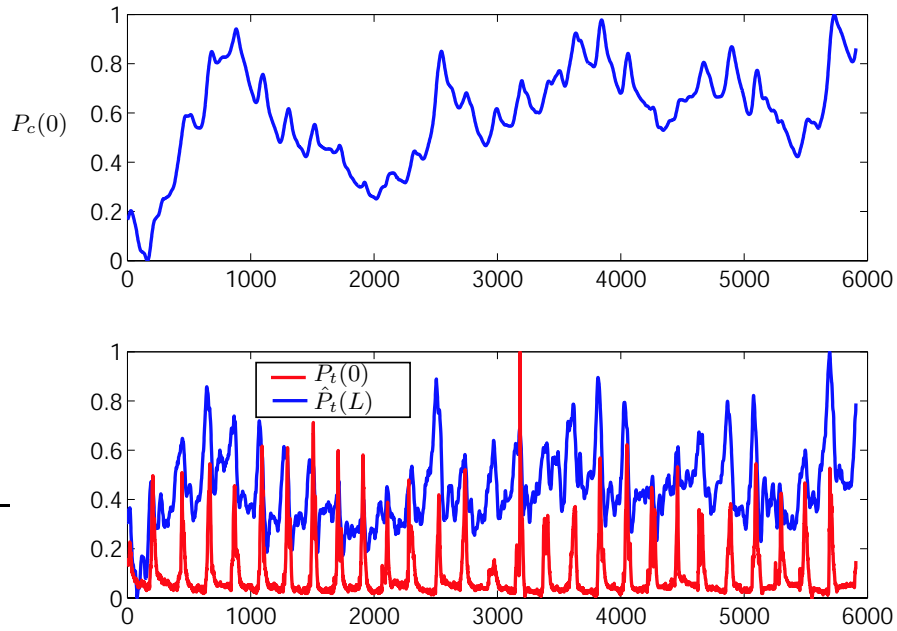


FIGURE 3.16. Experimental results on a TOTAL operated well over more than half a day. The bottom hole pressure,  $\hat{P}_t(L)$ , is reconstructed from the casing head pressure and from the gas injection flow rate measurements, respectively,  $P_c(0)$  and  $Q_g$ . The estimated pressure is compared with the tubing head pressure,  $P_t(0)$ , to highlight the relevance of the results (for confidentiality reasons, scales have been omitted).

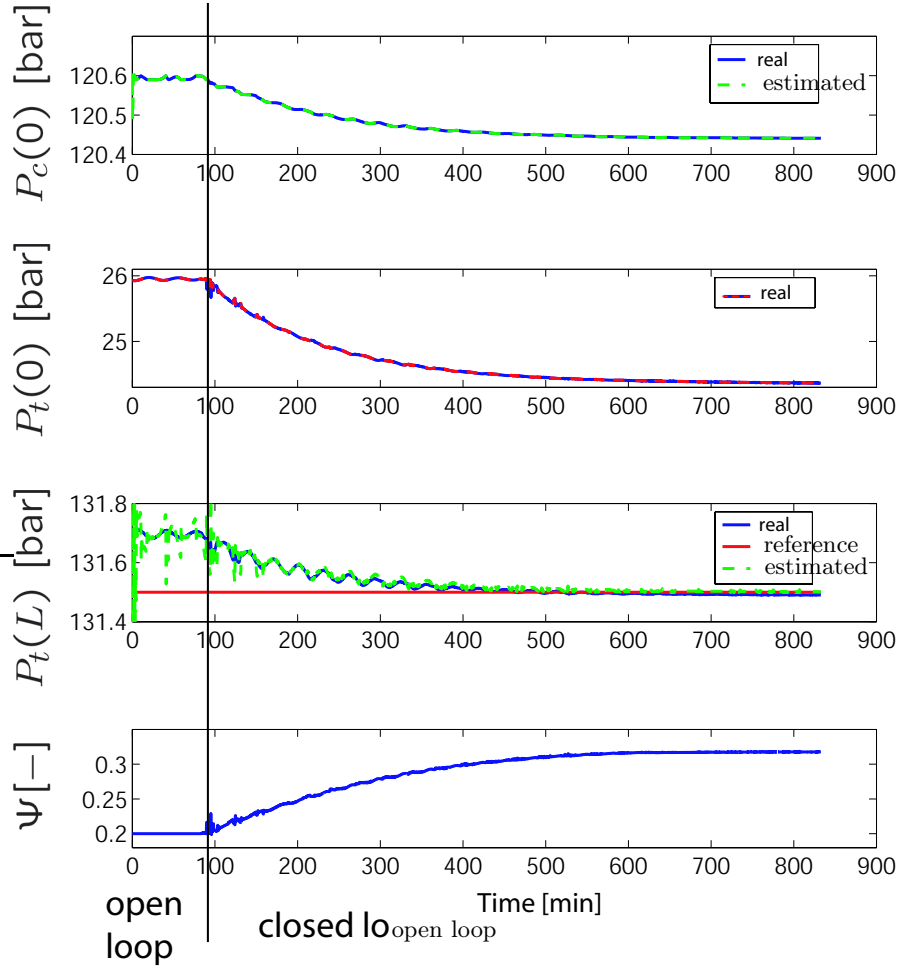


FIGURE 3.17. Closed loop stabilization example in OLGA<sup>®</sup>2000 simulation (numerical set up is given in Appendix A, Table 4). The choke opening  $\Psi$  is first set to 0.2 which corresponds to a stable equilibrium. The tubing pressure downstream the injection valve ( $P_t(L)$ ) is equal to 131.7 bar. The reference for  $P_t(L)$  is set to 131.5 bar. After approximately 100 min the controller is switched on. All pressures converge towards constant values. Notice that the estimator is well behaving: the estimation of  $P_t(0)$  and of the casing head pressure,  $P_c(0)$ , are relevant.

## CONCLUSION

*Dans ce mémoire consacré à l'étude des puits pétroliers activés en gas-lift nous avons cherché à apporter des solutions au problème pratique des instabilités d'écoulement fréquemment constaté sur les installations. Principalement, il a été constaté qu'en vieillissant les puits ont tendance à produire moins et moins bien. Leur production, constituée d'une succession de bouchons dont la répartition gaz/liquide est hautement fluctuante, est alors qualifiée d'instable. Ce type de comportements est préjudiciable. Il diminue la production moyenne du puits concerné, risque de se propager aux puits connectés sur les mêmes réseaux et également de créer des arrêts de production. Ces instabilités étant à la source de nombreux manques à produire, il est crucial de savoir les éviter, les supprimer ou du moins les gérer. C'est le thème principal de notre étude.*

*Dans une première approche nous ne nous autorisons pas d'autres actions sur le puits que le choix des conditions opératoires. Il s'agit de définir un critère garantissant la stabilité du système en boucle ouverte. Nous acceptons de sacrifier l'accès à certaines zones à fort rendement. Dans une seconde approche nous choisissons de nous placer délibérément dans ces zones en recourant à des contrôleurs en boucle fermée.*

*Dans l'étude en boucle ouverte nous proposons des modèles dont l'analyse nous permet de définir des critères de stabilité. Dans la littérature, la dynamique de l'écoulement est généralement négligée ce qui permet de réduire le système à un modèle à trois dimensions. Dans la thèse nous avons commencé par montrer que l'un des mécanismes d'instabilité,*

le casing-heading, pouvait effectivement être analysé de cette façon. La dynamique peut en fait se restreindre à deux dimensions et le phénomène s'interpréter comme un cycle limite dans un plan. Malheureusement cette approche ne couvre pas tous les cas pratiques. En effet un deuxième mécanisme, la density-wave, provient justement (comme nous l'avons démontré) de l'écoulement dans le puits et du retard lié à la propagation des effluents du réservoir à la surface. Une des contributions principales de cette thèse est de proposer un modèle à paramètres distribués qui permet de modéliser le puits et d'analyser le phénomène d'instabilité par l'étude des racines d'une équation du type

$$s = a + be^{-s\tau} + \frac{c}{s\tau}(1 - e^{-s\tau})$$

où  $\tau$  est le temps de propagation dans le puits. Il est possible d'unifier les deux approches. Nous proposons un modèle global, constitué du couplage de l'équation à paramètres distribués et d'un système dynamique du premier ordre. Nous faisons apparaître, dans le système physique, deux boucles de rétroaction (représentées sur la Figure 3.18) qui peuvent être positives. L'impact des principaux paramètres physiques sur la stabilité a été étudié et ainsi un certain nombre de règles opératoires empiriques ont pu être théoriquement validées. Les critères que nous proposons sont qualitatifs et non quantitatifs. En effet, les paramètres physiques du puits sont connus avec trop d'imprécision et varient tellement que ce critère n'aurait pas de sens.

Ce modèle nous sert de référence pour la conception de stratégies de contrôle en boucle fermée. Nous proposons une loi de commande. Les résultats obtenus en simulation sont probants. Les puits simulés en boucle fermée sont capables de produire de façon stable lorsque la vanne de production est très ouverte, ce qui est impossible en boucle ouverte. Les zones à haut rendement sont donc accessibles.

La pertinence de l'approche et des modèles proposés a été validée grâce aux résultats obtenus en simulation et surtout grâce aux résultats partiels obtenus sur site de production (présentés dans ce document). De nombreux problèmes d'implémentation doivent être résolus. En particulier, nous avons montré sur site qu'il était possible d'estimer la pression de fond en n'utilisant que des mesures obtenues à la surface.

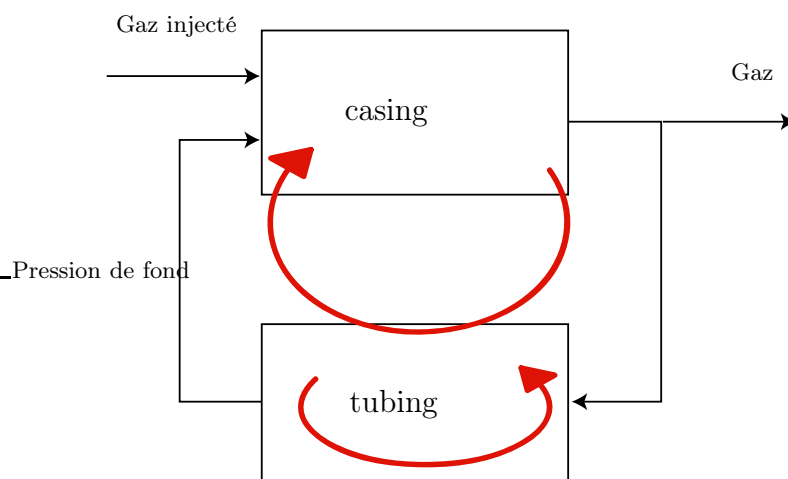


FIGURE 3.18. Représentation du puits sous forme d'un schéma bloc. Les instabilités correspondent aux boucles de rétroaction potentiellement positives représentées par les flèches rouges.

*Aujourd'hui, ces résultats nous ouvrent l'accès à des essais sur site de la loi de commande. Les résultats préliminaires sont très satisfaisants. Dans ce cadre d'industrialisation, un travail complémentaire d'analyse de robustesse est nécessaire, de façon à garantir l'efficacité dans le plus grand nombre de configurations possibles.*

This report is dedicated to the study of gas lift activated oil wells. We aimed at bringing solutions to the recurrent problem of flow instabilities. It has been noticed, in the literature, that, over time, wells tend to produce less in quantity and quality. Eventually, their production flow consists of a succession of slugs, whose gas/liquid ratio is highly fluctuating. This behavior should be avoided: it decreases the average production rate of the well, it might propagate to other connected wells and possibly cause production stops. These instabilities yield important production losses and it is interesting to know how to avoid them, get rid of them or at least how to handle them. This is the goal of our study.

In a first approach we decided not to consider any other actions besides choosing operating conditions. We defined a criterion which guarantees the open-loop system stability. This approach has a cost, because high return zone are most likely unreachable. In a second approach we chose to precisely pick operating conditions in the high return zone. The stabilization is achieved thanks to closed loop controller.

In the open-loop setup, we propose models from which stability criteria were derived. In the literature, the flow dynamics is often neglected. This allows to reduce the system dynamics to a three-dimensional model. In this report we first showed that one of the unstable mechanisms, the casing-heading, could be analyzed using this reduction. The phenomenon was interpreted as a limit cycle in the plane. Unfortunately, this approach does not address all issues. In the case of the second mechanism, the density-wave, the instability arises (as we have explained it) from the flow regime and from the propagation delay between the bottom of the well and the surface. Our main contribution is to interpret the system as a distributed parameters model and to analyse the density-wave thanks to the study of the roots of the equation

$$s = a + be^{-s\tau} + \frac{c}{s\tau}(1 - e^{-s\tau})$$

where  $\tau$  is the propagation time in the well. Finally, these two approaches can be combined. We proposed a global model, which consists in the coupling of the distributed parameters equation and a first order dynamical system. We highlighted the existence of two possibly positive feed-forward loops (represented on Figure 3.19). We studied the impact on the stability of the main physical parameters. Our results are in accordance with operating rules-of-the-thumb. We propose qualitative (and non quantitative) criteria. Deriving quantitative criteria from imprecise and possibly not up-to-date data records did not appear to us as a robust solution.

Rather, this model suggested a closed loop control strategy design. We proposed a control law. The results obtained in simulations stress the relevance of this approach. The closed loop simulated wells are able to produce steadily, even of large production choke openings. This is

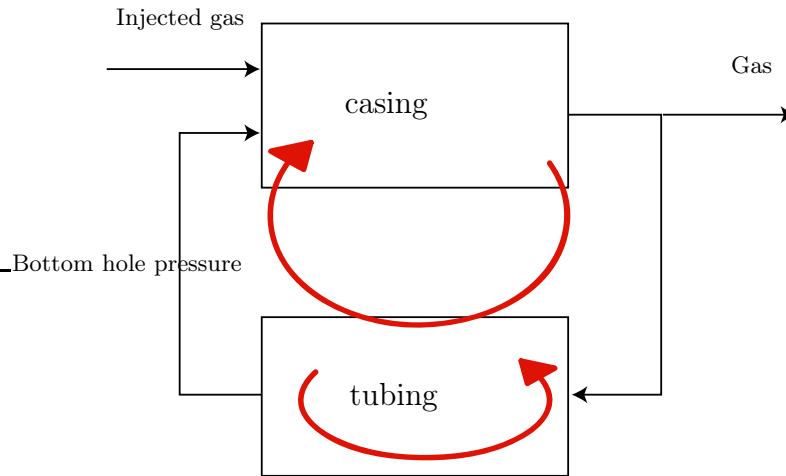


FIGURE 3.19. Block scheme the well as an interconnected system. The possibly positive feedback loops are in red.

not doable in open-loop. With feedback control, high return zones are reachable.

The relevance of the approach and of the proposed models has been validated thanks to simulations results and also mainly thanks to on-site results (presented in this document). Several implementations issues had to be solved. In particular, we showed, on site and in real time, how to reconstruct the bottom hole pressure measurements, using only surface measurements.

Now, this results give us access to broad field tests. Preliminary results are very promising. In the context of industrial use, a complementary study on the robustness of the solution is needed to guarantee the efficiency in the widest range of possible configurations.



# APPENDIX A

## OLGA<sup>®</sup>2000 SIMULATIONS SETTINGS

TABLE 1. Numerical set-up for Figure 1.3

Symb.	Description	Values	Units
$\phi$	injection valve orifice diameter	15.5/64	inch
$Q_{gi}$	gas injection flow rate	28-220	kSm <sup>3</sup> /j
$q_{gi}$	gas injection flow rate	0.01-7	kg/s
$PI$	Productivity Index	$10^{-5}$	
$p_r$	Reservoir pressure	150	bar

TABLE 2. Numerical set-up for Figure 2.2

Symb.	Description	Values	Units
$\phi$	injection valve orifice diameter	17.2/64	inch
$Q_{gi}$	gas injection flow rate	25	kSm <sup>3</sup> /j
$q_{gi}$	gas injection flow rate	0.2	kg/s
$PI$	Productivity Index	$10^{-6}$	
$p_r$	Reservoir pressure	180	bar

TABLE 3. Numerical set-up for Figure 2.9 and Figure 3.6

Symb.	Description	Values	Units
$\phi$	injection valve orifice diameter	12.8/64	inch
$Q_{gi}$	gas injection flow rate	62.5	kSm <sup>3</sup> /j
$q_{gi}$	gas injection flow rate	0.6	kg/s
$PI$	Productivity Index	$4^{-6}$	
$p_r$	Reservoir pressure	150	bar

TABLE 4. Numerical set-up for Figure 3.15 and Figure 3.17

Symb.	Description	Values	Units
$\phi$	injection valve orifice diameter	12.8/64	inch
$Q_{gi}$	gas injection flow rate	25	kSm <sup>3</sup> /j
$q_{gi}$	gas injection flow rate	0.2	kg/s
$PI$	Productivity Index	$10^{-5}$	
$p_r$	Reservoir pressure	150	bar
$\Psi$	Choke opening	0.2-0.317	-

Remark: The injection valve diameter is computed from OLGA<sup>®</sup>2000 simulations to fit the following rule of the thumb, based on two assumptions :

- if  $\phi = 8/64$  inch and if the flow is critical and if the upstream pressure is equal to 70 bar, then the flow rate will be 8 kSm<sup>3</sup>/j
- critical flow is obtained when the downstream pressure is less than half the upstream pressure.

$$(103) \quad Q_g = 2 * 8/70 \left( \frac{\phi}{8} \right)^2 \sqrt{P_t(L)(P_c(L) - P_t(L))}$$

# APPENDIX B

## NOMENCLATURE

Symb.	Description	Units
$a, b, c$	parameters of the distributed parameters equation	-
$C_g$	constant of the gas valve	S.I
$C_{pc}$	constant of the production choke	S.I
$g$	gravity constant	9.81 m/s <sup>2</sup>
$H$	reservoir depth	m
$L$	injection depth	m
$M$	molar mass of air	0.029 kg/mol
$m_1$	mass of gas in the casing	kg
$m_2$	mass of gas in the tubing	kg
$m_3$	mass of liquid in the tubing	kg
$p_c(L)$	pressure in the casing at the injection point	Pa
$p_r$	reservoir pressure	Pa
$\bar{p}_r$	appearing reservoir pressure	Pa
$p_s$	separator pressure	Pa
$p_t(0)$	pressure at the tubing wellhead	Pa
$p_t(H)$	pressure at the bottom-hole	Pa
$p_t(L)$	pressure in the tubing at the injection point	Pa
$p_t(L)^{ref}$	reference set point for the pressure in the tubing at the injection point	Pa

Symb.	Description	Units
$p_t(0)^{con}$	reference set point for the pressure in the tubing at the wellhead	Pa
$PI$	productivity index	$4e - 6$ kg/s/Pa
$q_g$	gas mass flow rate injected in the tubing	kg/s
$q_{gi}$	gas mass flow rate injected at the casing wellhead	kg/s
$q_g^{\min}$	saturation value of $q_g$	0.3 kg/s
$q_{lp}$	liquid mass flow rate produced at the wellhead	kg/s
$q_l$	liquid mass flow rate produced from the reservoir	kg/s
$q_{ls}$	liquid mass flow rate from the separator	kg/s
$R$	ideal gas constant	287 S.I.
$r_g(t, z)$	gas volume fraction	-
$r_l(t, z)$	oil volume fraction	-
$S_c$	equivalent section of the casing	m <sup>2</sup>
$S_t$	tubing section	m <sup>2</sup>
$T_t$	temperature of the tubing	293 K
$T_c$	temperature of the casing	293 K
$x(t, z)$	gas mass fraction	-
$x^L(t)$	gas mass fraction at $z = L$	-
$V_c$	casing volume	m <sup>3</sup>
$v_l(t, z)$	oil velocity	m/s
$v^\infty$	slip velocity constant	m/s
$v_g$	gas velocity	0.8 m/s
$\beta$	threshold parameter	0.03
$\delta$	tubing propagation time	s
$\Phi_l(t, z)$	oil mass flux	kg/s/m <sup>2</sup>
$\Phi_g(t, z)$	gas mass flux	kg/s/m <sup>2</sup>
$\Psi$	production choke opening	-
$\rho_c(H)$	gas density in the casing at the injection point	kg/m <sup>3</sup>
$\rho_g(t, z)$	gas density	kg/m <sup>3</sup>
$\rho_l$	density of oil	800 kg/m <sup>3</sup>

Symb.	Description	Units
$\rho_m(t, z)$	mixture density	kg/m <sup>3</sup>

Table 1: Nomenclature

All symbols in small letters have S.I. units.  $c$  indice denotes variables relating to the casing,  $t$  the tubing  $g$  the gas and  $l$  the oil, respectively.



## LIST OF FIGURES

1.1	Typical oil production process system (schematic borrowed from [29]). . . . .	14
1.2	Scheme of a gas-lift activated well. . . . .	17
1.3	Performance curve (liquid production $Q_{lp}$ with respect to gas injection flow rate $Q_{gi}$ ) derived from OLGA <sup>®</sup> 2000 simulations (numerical set up given in Appendix A, Table 1). The black star shows the optimum gas-lift injection $Q_{gi}^{opt}$ for given economic conditions. . . . .	20
1.4	Schematic of an onshore installation. Wells are linked together through three networks: the gas network, the production network and the reservoir . . . . .	22
1.5	Well instabilities example. Wellhead pressure, temperature and oil flow from the separator are represented. An almost periodic regime appears while oil production is intermittent. Scales are omitted for confidentiality reasons (courtesy of TOTAL). . . . .	23
2.1	Schematic of the well. Zones of consideration (well head zone, bottom hole zone) appear in gray. . . . .	28
2.2	Unstable well behavior, casing heading, obtained with $q_{gi} = 0.2\text{kg/s}$ simulated with OLGA <sup>®</sup> 2000 (numerical set up given	

	in Appendix A, 2). The four main stages of the phenomenon are highlighted. ....	29
2.3	Scheme of the well and notations used in equation (2) (the casing and the tubing part have been artificially separated to improve readability). ....	31
2.4	Unstable well behavior, casing heading, obtained with $q_{gi} = 0.2\text{kg/s}$ simulated with equation (2) ....	32
2.5	Performance curve corresponding to the model (2) with gas injection rate $q_g$ ranging from 0.01 to 7 kg/s and a liquid production from 3 to 17kg/s. Stable equilibrium points are represented in green and unstable in red. ....	34
2.6	Roots of model (2) are represented in the complex plane for gas injection ranging from 0.01 to 7 kg/s. Color axis goes from 0 to 100% of the gas injection range. ....	35
2.7	Limit cycle (in blue) and positive invariant set (rectangle $P_1P_2P_3P_4$ ) for the sample problem. Switching curves $\partial\mathcal{F}_g^o$ and $\partial\mathcal{F}_{gp}^o$ are represented. ....	44
2.8	Density wave occurring on a well. Casing-head and tubing-head pressures (respectively $p_c(0)$ and $p_t(0)$ ) are represented as well as oil flow from the separator ( $Q_{ls}$ ). Notice that the casinghead pressure is almost constant, which demonstrates that the gas injection is constant. Scales are omitted for confidentiality reasons (courtesy of TOTAL). ....	47
2.9	Density wave simulated with OLGA <sup>®</sup> 2000 (numerical set up is given in Appendix A, Table 3). ....	48
2.10	Scheme of the tubing. ....	49
2.11	Density wave simulated with equation (35). The reservoir pressure $P_r$ is 150 bar and $\lambda q_g$ is set at 10 bar. ....	54
2.12	Case (1) : $\phi(0) \in (0, 1)$ . The trajectory converges towards a constant also comprised between 0 and 1. ....	65
2.13	Cas 2. Depending on whether the Condition (55) is satisfied the trajectory converge between 0 and 1 or above 1. ....	66

2.14	Block scheme of the tubing subsystem linearized around an equilibrium point. Gravitational effects of the nonhomogeneous fluid column take the form of an inner positive feedback loop. ....	69
2.15	Simulation in OLGA <sup>®</sup> 2000 of the impact of the pressure reservoir on the stability of the well. ....	72
2.16	(a) Outline of the casing. (b) The inputs of the system are the gas mass injection rate $q_{gi}$ and the boundary condition $p_t(L)$ (the downhole pressure). The output is the gas rate entering the tubing: $q_g$ . ....	73
2.17	Block scheme of the interconnected systems linearized around an equilibrium point. ....	75
3.1	Some of the control solutions proposed in the literature. ....	81
3.2	More control solutions proposed in the literature. ....	82
3.3	Control strategy using gas inlet as input. We feed the tubing with a computed gas flow rate $q_g$ such that the gas mass fraction at the bottom of the tubing is equal to $X_{ref}$ . This computation takes the bottom-hole pressure $p_t(L)$ and the reservoir pressure $p_r$ into account. ....	85
3.4	Stabilization of equation (35) using the saturated control law (90). Control is switched on after approximatively 3.4 hours of open loop. $p_L$ reaches $p_{ref}$ and $X$ reaches $X_{ref}$ in finite time $2\delta$ . ....	87
3.5	Comparison of open loop (3 schemes on the left) and closed loop behavior. ....	88
3.6	Stabilization of density wave instability simulated in OLGA <sup>®</sup> 2000 (numerical set up given in Appendix A, Table 3). $X_{ref} = 0.0568$ and $q_g^{min} = 0.3$ . ....	89
3.7	Control of the bottom hole flowing pressure ( $p_t(H)$ ) with a PID controller on the production choke ( $u$ ). ....	90
3.8	Block scheme of the OLGA <sup>®</sup> 2000 simulation setup. First case (top) with a production choke, second case (bottom). ....	91

- 3.9 Comparison of the step responses to an increase of the well head pressure and to a decrease of the production choke opening. . . . . 92
- 3.10 Steady state comparison of the impact of variations of tubing head pressure and production choke opening. . . . . 93
- 3.11 Nyquist plot corresponding to the linearization equation (35) for  $q_g=0.2\text{kg/s}$ . The tubing dynamics is unstable. . . . . 94
- 3.12 Control of the bottom hole pressure  $p_t(L)$  with the well head pressure  $p_t(0)$ . . . . . 95
- 3.13 Nyquist plot of the closed loop tubing dynamics. The black line represents the lower boundary defined in equation (99). . . . . 97
- 3.14 Scheme of the proposed control and estimation architecture. . . . . 98
- 3.15 Estimation of the bottom hole pressure using the casing head pressure in OLGA<sup>®</sup>2000 simulation (numerical set up is given in Appendix A, Table 4). Solid blue (reference from OLGA<sup>®</sup>2000), dotted red estimation. . . . . 102
- 3.16 Experimental results on a TOTAL operated well over more than half a day. The bottom hole pressure,  $\hat{P}_t(L)$ , is reconstructed from the casing head pressure and from the gas injection flow rate measurements, respectively,  $P_c(0)$  and  $Q_g$ . The estimated pressure is compared with the tubing head pressure,  $P_t(0)$ , to highlight the relevance of the results (for confidentiality reasons, scales have been omitted). . . . . 103
- 3.17 Closed loop stabilization example in OLGA<sup>®</sup>2000 simulation (numerical set up is given in Appendix A, Table 4). The choke opening  $\Psi$  is first set to 0.2 which corresponds to a stable equilibrium. The tubing pressure downstream the injection valve ( $P_t(L)$ ) is equal to 131.7 bar. The reference for  $P_t(L)$  is set to 131.5 bar. After approximately 100 min the controller is switched on. All pressures converge towards constant values.

- Notice that the estimator is well behaving: the estimation of  $P_t(0)$  and of the casing head pressure,  $P_c(0)$ , are relevant. . . 104
- 3.18 Représentation du puits sous forme d'un schéma bloc. Les instabilités correspondent aux boucles de rétroaction potentiellement positives représentées par les flèches rouges. .... 107
- 3.19 Block scheme the well as an interconnected system. The possibly positive feedback loops are in red. .... 109



## BIBLIOGRAPHY

- [1]
- [2] “Standard handbook of petroleum and natural gas engineering,” W. C. Lyons, Ed. Gulf Professional Publishing, 1996.
- [3] O. M. Aamo, G. O. Eikrem, H. Siahhaan, and B. Foss, “Observer design for multiphase flow in vertical pipes with gas-lift - theory and experiments,” *Journal of Process Control*, vol. 15, pp. 247–257, 2005.
- [4] F. J. S. Alhanati, Z. Schmidt, D. R. Doty, and D. D. Lageref, “Continuous gas-lift instability: diagnosis, criteria, and solutions,” in *68th Annual Technical Conference and Exhibition*, no. SPE 26554, Houston, TX, October 1993.
- [5] H. Asheim, “Criteria for gas-lift stability,” *Journal of Petroleum Technology*, pp. 1452–1456, November 1988.
- [6] —, “Criteria for gas-lift stability,” *Journal of Petroleum Technology*, pp. 1452–1456, 1988.
- [7] E. F. Blick and L. Boone, “Stabilization of naturally flowing oil wells using feedback control,” in *Proc. of the 56th California Regional meeting of the Society of Petroleum Engineers*, no. SPE 15096, Oakland, California, 1986.

- [8] E. F. Blick, P. N. Enga, and P. C. Lin, "Theoretical stability analysis of flowing oil wells and gas-lift wells," *SPE Production Engineering*, pp. 508–514, 1988.
- [9] E. F. Blick and A. B. Nelson, "Root locus stability analysis of a flowing oilwell feedback controller," in *Proc. of the SPE Production Operations Symposium*, no. SPE 18874, Oklahoma City, Oklahoma, 1988.
- [10] F. Brauer and J. A. Nohel, *The qualitative theory of ordinary differential equations. An introduction*. Dover Publications, INC. , New York, 1989.
- [11] K. E. Brown, *Gas lift theory and practice*. Petroleum publishing CO., Tulsa, Oklahoma, 1973.
- [12] H. Cholet, *Well production. Practical handbook*. Editions TECHNIP, 2000.
- [13] A. J. Chorin and J. E. Marsden, *A mathematical introduction to fluid mechanics*. Springer-Verlag, 1990.
- [14] R. F. Curtain and H. J. Zwart, *An introduction to infinite-dimensional linear systems theory*, ser. Text in Applied Mathematics, 21. Springer-Verlag, 1995.
- [15] M. Dalsmo, E. Halvorsen, and O. Slupphaug, "Active feedback of unstable wells at the Brage field," in *SPE Annual technical Conference and Exhibition*, no. SPE 77650, 2002.
- [16] W. J. G. J. der Kinderen, C. L. Dunham, and H. N. J. Poullisse, "Real-time artificial lift optimisation," in *Proc. of the 8th Abu Dhabi International Petroleum Exhibition and Conference*, 1998.
- [17] E. Duret, "Dynamique et contrôle des écoulements polyphasiques," Ph.D. dissertation, École des Mines de Paris, 2005.
- [18] G. O. Eikrem, B. Foss, L. Imsland, B. Hu, and M. Golan, "Stabilization of gas-lifted wells," in *Proc. of the 15th IFAC World Congress*, 2002.

- [19] G. O. Eikrem, L. Imsland, and B. Foss, "Stabilization of gas-lifted wells based on state estimation," in *International Symposium on Advanced Control of Chemical Processes*, 2004.
- [20] J. Faustinelli, G. Bermúdez, and A. Cuauro, "A solution to instability problems in continuous gas-lift wells offshore lake Maracaibo," in *Latin American and Caribbean petroleum engineering conference, Caracas, Venezuela*, no. SPE 53959, 1999.
- [21] J. K. Hale and S. M. V. Lunel, *Introduction to functional differential equations*. Springer-Verlag, 1993.
- [22] I. A. Hiskens, "Stability of limit cycles in hybrid systems," in *Proc. of the 34th Hawaii International Conf. on System Sciences*, 2001.
- [23] B. Hu and M. Golan, "Gas-lift instability resulted production loss and its remedy by feedback control: dynamical simulation results," in *SPE International Improved Oil Recovery Conference in Asia Pacific*, no. SPE 84917, Kuala Lumpur, Malaysia, 2003.
- [24] L. S. Imsland, "Topics in nonlinear control - output feedback stabilization and control of positive systems," Ph.D. dissertation, Norwegian University of Science and Technology, Department of Engineering and Cybernetics, 2002.
- [25] L. S. Imsland, B. A. Foss, and G. O. Eikrem, "State feedback control of a class of positive systems: application to gas lift stabilization," in *Proc. of the 7th European Control Conf.*, 2003.
- [26] B. Jansen, M. Dalsmo, K. Havre, L. Nøkleberg, V. Kritiansen, and P. Lemétayer, "Automatic control of unstable gas-lifted wells," in *SPE Annual technical Conference and Exhibition*, no. SPE 56832, Houston, Texas, 1999.
- [27] H. K. Khalil, *Nonlinear Systems*. MacMillan, 1992.
- [28] P. Lemétayer and P. M. Miret, "Tool of the 90's to optimize gas-lift efficiency in the Gonelle field, Gabon," *SPE Annual technical*

- Conference and Exhibition.*, no. SPE number: 23089, September 1991.
- [29] W. C. Lyons and G. J. Plisga, *Standard handbook of petroleum and natural gas engineering*. Gulf Professional Publishing, 2005.
- [30] F. Mazenc, “A specific linear system with delays,” Private Communication, December 2005.
- [31] R. K. Miller and A. N. Michel, *Ordinary differential equations*. Academic Press, 1982.
- [32] Scandpower, *OLGA<sup>®</sup> 2000 User’s Manual*. Scandpower, 2004.
- [33] S. N. Simić, K. H. Johansson, J. Lygeros, and S. Sastry, “Hybrid limit cycles and hybrid Poincaré-Bendixon,” in *Proc. of the 15th IFAC World Congress*, 2002.
- [34] L. Sinègre, “Paramétrage de l’algorithme de contrôle fcv pour la conduite des puits activés en gas-lift,” École des Mines, Paris, option de fin d’étude, Tech. Rep., July 2000.
- [35] L. Sinègre, N. Petit, and P. Lemétayer, “Active control strategy for density-wave in gas-lifted wells,” in *Proc. of the International Symposium on Advanced Control of Chemical Processes*, 2006.
- [36] L. Sinègre, N. Petit, P. Lemétayer, P. Gervaud, and P. Ménégatti, “Casing heading phenomenon in gas lifted well as a limit cycle of a 2d model with switches,” in *Proc. of the 16th IFAC World Congress*, 2005.
- [37] —, “Contrôle des puits activés en gas-lift,” in *10th Congress of Société Française du Génie des Procédés*, 2005.
- [38] L. Sinègre, N. Petit, and P. Ménégatti, “Predicting instabilities in gas-lifted wells simulation,” in *Proc. of the 2006 American Control Conf.*
- [39] —, “Distributed delay model for density wave dynamics in gas lifted wells,” in *Proc. of the 44th IEEE Conf. on Decision and Control, to appear*, 2005.

- [40] G. Stépán, *Retarded dynamical systems: stability and characteristic functions*, ser. Pitman Research Notes in Math. Series. UK: Longman Scientific, 1989.
- [41] G. Takács, *Gas lift manual*. PennWell Corporation, 2005.
- [42] T. Tokar, Z. Schmidt, and C. Tuckness, “New gas lift valve design stabilizes injection rates : case studies,” in *SPE annual technical conference and exhibition*, no. SPE 36597, Denver, Colorado, 1996.
- [43] A. J. Torre, Z. Schmidt, R. N. Blais, D. R. Doty, and J. P. Brill, “Casing heading in flowing wells,” in *SPE Production Operations Symposium*, no. SPE 13801, Oklahoma City, Oklahoma, 1987.
- [44] Z. G. Xu and M. Golan, “Criteria for operation stability of gas lift,” *SPE paper*, no. 19362, 1989.
- [45] B. Yeten, L. J. Durlofsky, and A. Khalid, “Optimization of smart well control,” in *Proceedings of the SPE International Thermal Operations and Heavy Oil Symposium and International Horizontal Well Technology Conference*, no. SPE number 79031, Alberta, Canada, 2002.